Mitigation of Wind Turbine Induced Sub-Synchronous Oscillation by Implementation of Wide Area Monitoring and Control

C.A. van Vledder

Mitigation of Wind Turbine Induced Sub-Synchronous Oscillation by Implementation of Wide Area Monitoring and Control

by

C.A. van Vledder

to obtain the degree of Master of Science
at the Delft University of Technology &
at the Norwegian University of Science and Technology,
to be defended publicly on Monday November 7, 2022 at 10:00 AM.

Student number:	4609883	
Project duration:	January 10, 2022 – November 7, 2022	
Thesis committee:	dr. ir. J. Rueda Torres,	TU Delft, supervisor
	dr. ir. A. Stefanov,	TU Delft
	dr. ir. O. Anaya-Lara,	NTNU
	ir. B. Kruimer,	DNV

Cover photo by author, Wind Park Fryslân.
Consisting out of 89 type-4 Wind Turbines,
connected by a 55 km radial connection to the grid.

Abstract

Wind energy is a growing energy resource in the current energy transition. Massive new amounts are planned to be built in the face of the climate and energy crisis. The current state-of-the-art type-4 Wind Turbine (WT) uses a Full Rated Converter (FRC) to decouple the rotor speed from the grid frequency. In recent years this type of WT has been involved in so-called sub-synchronous events. The Grid Side Converter (GSC) of the FRC is very similar to other Inverter Based Generation (IBG) such as: Photovoltaic (PV), Battery Energy Storage System (BESS) and High Voltage Direct Current (HVDC)-links. As this research is focused on the GSC, it is very relevant to the integration of other Renewable Energy Resources (RES) as well.
This thesis investigates Sub-Sychronous Control Interaction (SSCI), a relatively new phenomenon. The GSC interacts with the grid, which can cause a Sub-Synchronous Oscillation (SSO), an oscillation below the system's fundamental frequency. This oscillation can lead to damage, increased components wear or triggering protection systems. After different facets of SSCI are discussed, a new solution is put forward in this thesis. By feeding wide area Phasor Measurement Unit (PMU)-based measurements into the control system of the WT, an algorithm is constructed to mitigate SSCI. This algorithm is tested on the ability to mitigate sub-synchronous event risks.

First, a WT model is selected in the DIgSILENT PowerFactory software to recreate sub-synchronous behaviour. This model is tested in the weak radial grid. The influence of the different control parameters on the sub-synchronous behaviour is investigated and comped to literature studies. Different tools are used for this research. PowerFactory is used for small signal analysis to obtain a linear dynamic model of the system. RMS-time simulations are used to test the oscillatory behaviour of the system. These results are further analysed using eigen-analysis on the linear model and Fourier and Prony analysis on the time simulations.
Then, the same WT-model is implemented in a modified IEEE-39 bus system to see the behaviour of SSO propagation in a transmission network. The results are compared to an analytical method to determine voltage oscillations based on mode shapes. However, as SSCI has a fundamentally different driving force, this method is not valid in this case. In the same transmission network, the influence of grid operations is tested. Different variations are tested: the connection point, power output of the WT, grid loading and disconnection of nearby connections. As all these features can vary during normal operation, it is vital to understand better which circumstances increase the risk of SSO event.

At last, using the knowledge obtained, a new control algorithm is proposed. This algorithm uses wide-area voltage angle measurements. These measurements can be provided by PMUs. A remote signal is fed into the control system. Minimal modifications are made to the control system for this. Additional damping is performed on the local voltage reference angle depending on the movement of the remote signal. This prevents the initialisation of SSCI. This implementation of a Wide Area Monitoring and Control (WAMC) is tested using eigen-analysis and time simulations and shows promising results.

The results of this thesis research are also modelled in the NextGen GridOps Framework of DNV. The framework aims to stimulate a fast deployment of the finding of this thesis research in the field. This is accomplished by sharing knowledge in an accessible, structured environment. This allows taking the findings into consideration for solving the complex problems encountered by transmission and distribution system operators.

Acknowledgements

This thesis is the final work in my journey through European Wind Energy Master (EWEM). EWEM has given me the opportunity to study and live abroad for two semesters in Copenhagen and Trondheim. Both times it has enabled me to make many new friends and learn about Scandinavian culture. The past two years have been a fantastic experience. I would like to thank everyone involved who made this master program possible.

The work presented results from a collaboration between Delft University of Technology and the Norwegian University of Science and Technology. Both universities are part of the EWEM program. As an industry partner, DNV is also part of the collaboration. Knowledge about the topic of this thesis and obtained during this thesis research is shared within the NextGen GridOps Framework.

I would like to express my gratitude to my supervisors. First of all, Dr. Jose Rueda Torres and Dr. Alex Stefanov for their daily guidance during my thesis from TU Delft. Dr. Olimpo Anaya-Lara for his enthusiastic supervision from NTNU. At last, I also like to thank Bas Kruimer and Coen Berenschot for allowing me to work within DNV on my thesis research.

Finally, I would like to thank my friends who have always helped me to get the necessary distractions to keep me mentally and physically healthy along the way. Furthermore, they always supported me and kept me motivated. Last but not least, my family for always supporting me in following my curiosities. Especially to my dad, who has always set a perfect example of this, thank you!

Cees van Vledder, *Delft, October 2022*

Contents

List of Figures

List of Tables

List of Acronyms

1 Introduction

1.1. Problem Formulation

The electrical power grid has become an increasingly essential part of daily society since the first electrical power systems were introduced [1]. Therefore, reliable operation is one of the critical aspects of any future development in the power system. Currently, the power system is undergoing a major shift in how it is operated by installing more Power Electronic Interfaced Generation (PEIG) RES. This leads to a reduction of inertia in the grid, a reduction in controllability of power generation, and introduces new dynamics in the power systems [2]. Moreover, another part of this major shift is the increasing electrification of processes previously powered by gas or other fossil fuels [3–5]. This leads to a new philosophy in how the power flows from generators to loads. Power generation will become less centralised and more distributed [6]. New PEIG can also introduce new controller systems. These can have unexpected interactions with other components or controllers in the grid. When these interactions occur at low frequencies, this is referred to as SSCI [7]. All these aspects should be carefully monitored and investigated during the grid transformation.

One of these new dynamic behaviours is a SSO, an oscillation below the system frequency. SSOs have occurred on multiple occasions where Wind Power Plant (WPP) have played a key role in the occurrence of the phenomena [8–16]. The impact ranges between increased wear of components to large blackouts [16]. As wind energy and other PEIG will become more dominant in future power systems, it is important to understand SSOs and develop ways to quickly identify and mitigate them [7, 17]. A scientific gap exists in all the circumstances which play a key role in the emergence of SSOs.

On the observation side of the grid, many developments have taken place to improve the observability [18]. Most grid operators use Supervisory Control and Data Acquisition (SCADA) to monitor the power system [19]. SCADA is an ageing monitoring system with relative low refresh rates of 2-3 seconds. Control of the power system is mostly done manually from a central control room. This makes it impossible to react to the increasing fast dynamics and limits the considered safe operation zones. Furthermore, the low refresh rate and inaccurate time stamping of measurements make it difficult to do postmortem analysis after cascading events. Events which mostly occur within sub-seconds are virtually impossible to observe.

PMU based WAMC can significantly improve the power system's observability and controllability. PMUs are fast and usually synchronised measuring devices in the power system with measurement rates of up to 250 Hz [20]. Although the first PMU systems were developed in the late '80s, the usage is quite limited at the moment in most power systems. They are mostly used as a secondary system next to existing SCADA systems. The potential of implementing automatic digital control systems fed by wide area PMU data could lead to improved system operation and decrease the risk of SSO.

Currently, a gap exists in the infrastructure to transfer the vast amount of data PMUs are providing [21]. Additionally, processing this data into useful information for (automatic) controllers is an active research area. To summarise, the push for RES in the power system leads to new, fast and yet not fully understood dynamic behaviours. Current observation methods of the power grid are not suitable for observing these phenomena. SSCI is one of these phenomena, and only a little research has been done on the subject. Furthermore, new PMU technology has been around for a long time, but the real time usage of data is only very limited. It seems there is much potential in implementing digital monitoring and control systems using PMU data.

1.2. Research Goal

The goal of this research thesis is twofold: finding the way different control parameters and network operating conditions influence the dynamics (in terms of frequency and damping ratio) of SSOs, and ascertaining if PMU signals can be deployed for wide area damping.
Furthermore, the obtained knowledge needs to be effectively shared within the DNV NextGen Grid-Ops Knowledge Framework. The NextGen Grid-Ops Knowledge Framework aims to collect and share a wide range of knowledge in order to build the future electrical grid. An overview of this implementation is given in appendix A.

1.3. Research Questions

In order to achieve the goal set out in the previous section, the thesis involves two aspects with related research questions:
Aspect 1: identification of a suitable model for investigation of type-4 WT induced SSO.

1. Which control- and grid parameters influence the frequency and damping ratio of SSOs?
2. How to effectively recognise the propagation of SSO through an AC transmission network?

Aspect 2: feasibility of wide area damping to mitigate SSO.

3. How to design a wide area controller to effectively out perform damping control that is exclusively based on local signals?
4. What is the effect of the implementation of WAMC based on PMU on SSO using minimal modifications?

1.4. Methodological Approach

In order to reach the research goals, different steps are identified.

1. Literature review to identify important conditions contributing to significant SSO events.
2. Selection of a suitable WT model to use for simulations in PowerFactory.
3. Modify the reference model based on to simulate and observe SSO events similar to incidents described in recent literature.
4. Investigate control and grid parameters affecting SSOs.
5. Implement virtual PMU devices in the system.
6. Implement and tune control schemes to mitigate the previously created SSO events.
7. Evaluate the performance of the control schemes by different use cases.
8. Sketch theoretical future implementation of the findings in the DNV NextGen GridOps Framework.

1.5. Thesis Outline

Chapter 2: Literature review
A description of the operation principles of the electrical power grid is given. This will touch upon the history and current transition of the grid. Challenges of this transition are addressed with particular attention to SSO events and observability of the grid. Examples of events and solutions will support this.

Chapter 3: Modelling & Methods
The used software, DIgSILENT PowerFactory, for this research is introduced. The model structure

and simulation tools are explained. Hereafter, other theories and analysis methods are discussed to examine the results further. At last, the models used are introduced. These are models for a type-4 WT, a weak radial grid and the Institute of Electrical and Electronics Engineers (IEEE)-39 bus system. The behaviour of the base settings of these models is discussed.

Chapter 4: Modelling of Weak Radial Connection
The influence of different parameters on sub-synchronous modes is investigated. Six control parameters and one grid parameter are varied. Also, the effect of participation factors is investigated. In this chapter, small signal analysis is used and verified by Prony analysis on time simulation output.

Chapter 5: Sub-Synchronous Oscillation in the IEEE-39 Bus System
The SSOs are simulated in the IEEE-39 bus system. In this system, the propagation of voltage magnitude oscillations and voltage angle oscillations are observed. These results are compared to a method described in [22]. Participation factors are used to explain the difference in the results obtained. In this chapter, small signal analysis, Fourier analysis and Prony analysis are used.

Chapter 6: Influence of Grid Operation on Sub-Synchronous Oscillations
This chapter investigates the grid operation influence on the sub-synchronous frequency and damping. The WPP model is connected to different buses in the system. For each connection point, the loading of the network and power output of WPP varies. Additionally, the influence of disconnected lines close to the connection point is investigated.

Chapter 7: Implementation of Wide Area Monitoring and Control
In this chapter, an implementation of wide area measurements into the control system of the WPP model is introduced. The philosophy of this control scheme is explained. Simulations are performed to compare the frequency and damping to a standard WPP control model.

Chapter 8: Conclusions & Future Work
The conclusions are discussed in this chapter. This is done by a reflection on the research goals. Furthermore, answers are formulated and supported by the results of the previous chapters. At last, possible future research is described. These proposals are based on interesting phenomena observed or assumptions made in this research and do not fall within the scope of this thesis.

2
Literature Review

In this chapter different topics relevant to this research within the electrical power systems are introduced. First classical electrical power systems are introduced. In a classical power system most power is generated by Synchronous Generator (SG)s. This is followed by introducing new generation type to the system. It will be discussed what type of challenges the new PEIG systems introduce the electrical power system. After this, the use of Wide Area Monitoring and Control (WAMC) is introduced and discussed. The chapter in finalised by discussing different type of sub-synchronous behaviour related to WTs.

2.1. Basics Notions of Power System Analysis

In this section the fundamentals of the classical approach of power system analysis concisely overviewed.

2.1.1. Conventional Electrical Power System

The first electrical power systems were developed around 1870. During the first years Alternating Current (AC) and Direct Current (DC) were strong competitors [23]. However, AC systems quickly dominated after transformers were introduced, allowing for higher voltages and larger transmission distances. Also, three phases in the power grids were introduced. When the phases are balanced, equal voltage and current flows through each phase with 120° phase difference. The main advantage of three phases is the constant instant power and, thus, torque on electrical three phase electrical machines. This dramatically reduces internal vibrations and wear.

During these early developments, separate electrical grids were introduced as a local service. Each grid used its own voltages and frequencies. As the grids expanded and started to overlap, standardisation became increasingly important. Nowadays, most systems are either operated at 50 Hz or at 60 Hz, depending on the continent. Most countries or even whole continents have a single synchronous area.

2.1.2. Rational Behind Balancing Problem

The frequency of the grid system should be operated within strict limits. In a classical power system, the frequency is directly coupled to the synchronous machines and thus to rotational mass. The rotational speed of the machines is balanced by the mechanical input power and the electrical output power. Keeping the system frequency within limits is therefore a balancing act between the generated power and consumption of electrical power. The dynamics of the machines can be described with the following equations [24].

$$T_a = T_m - T_e = J\frac{\partial \omega}{\partial t} \tag{2.1}$$

In this equation T_m and T_e represent the mechanical shaft torque and the electrical torque, respectively. T_a is the resulting torque which accelerates the machine. J is the total inertia of the machine and ω is the rotational speed. The total inertia of the machine can be compared to the rated power of the machine. This gives a value H with units of time as is described in equation 2.2. A large time constant indicates that the frequency will respond more slowly to a power imbalance in the grid.

$$\mathrm{H} = \frac{1}{2}\frac{J\omega_{0m}^2}{VA_{base}} \tag{2.2}$$

By defining a rotor angle δ, which is the angle of the rotor relative to a rotating reference frame rotating the system frequency ω_0, the equations can be rewritten in per unit (p.u.) values. This means the values are weighted to some nominal value. Often this is related to the ratings of a machine or grid element.

$$P_a = \frac{2\mathrm{H}}{\omega_0}\frac{\partial^2\delta}{\partial t^2} \tag{2.3}$$

In this differential equation P_a in p.u. is the resulting acceleration. H has units of seconds, ω_0 in rad/s, δ in rad and t in seconds. It can be seen that if the electrical demand is lower than the mechanical input, the machine will speed up and vice versa. In a classical synchronous generator based system, all generators will be synchronised to the same system frequency. This means that an overall lack of electrical energy generation compared to electrical demand will lead to a decreasing frequency. More rotating mass in the system will lead to a lower Rate of Change of Frequency (RoCoF) of the system as more energy is stored as rotational energy. This will lead to slower frequency dynamics, thus more time for controllers to react and increase the stability margins. In section 2.2.1, it will be further discussed how current developments are decreasing the Total System Inertia (TSI), which leads to faster frequency dynamics. Also, it is discussed how this is dealt with now and in the future.

2.1.3. Voltage Phasor Angles and Power Flow

Power grids are often represented as single line diagrams. The single lines represent the three phases of power lines connecting different buses. The lines can be modelled to have an impedance. This can represent line resistance and inductance. Buses can be connected to other buses by line connections or transformers. They can also be directly connected to loads and generators. Each bus has its own voltage. When the system is in equilibrium, power flows from generators through the lines to the loads. For power to flow, a current from one bus to another needs to flow through a line. A voltage difference between two buses can create this current. This is shown in equation 2.4.

$$\tilde{I}_{1,2} = \frac{\tilde{V}_2 - \tilde{V}_1}{\tilde{Z}_{1,2}} \tag{2.4}$$

Where $\tilde{V}_1$ and $\tilde{V}_2$ are the phasor voltages on the two buses between which current $\tilde{I}_{1,2}$ flows. $\tilde{Z}_{1,2}$ is the complex impedance of the line connecting the two buses.

Phasors are used to simplify calculations. A phasor is a vector starting at the origin of the complex plane and has an amplitude A and an angle θ. In mathematical format, this can be represented as $Ae^{j\theta}$. The phasor is used to represent a sinusoidal function which also has an amplitude and angle. This gives the following expression for a voltage phasor.

$$\tilde{V} = Ve^{j\theta} = Ve^{j(\omega_0 t+\phi)} \tag{2.5}$$

In this equation, only one phasor is used to represent a three phase system. An assumption is made that all phases are symmetrically and separated by 120°. In this report, a convention is used in which a phasor is represented by a $\tilde{V}$ while its amplitude is represented as V. The angle of a voltage is represented by θ.

In the format of equation 2.5 the phasor will be rotating at the system frequency. In equation 2.4, it can be seen that only the bus voltage relative to other bus voltages is essential. Since the system frequency is a global variable in the system, the ωt term can be removed from all phasors resulting in stationary phasors when the system is in equilibrium. One bus will be chosen as the slack bus, with a zero angle to which all other buses will have a relative angle.

In the same manner as the voltage, also the current can be represented as a phasor. The transported power can be calculated using the following equation:

$$\tilde{S} = \tilde{V}\,\tilde{I}^* = P + jQ \tag{2.6}$$

In this equation $\tilde{S}$ is the complex apparent power, P and Q are the real power and reactive power, respectively.
In practical power grids, the power flow is strongly dependent on the voltage phase difference between buses rather than the voltage amplitude difference. This is because a power line is usually more inductive than resistive (the imaginary part of the impedance is larger than the real part). When only a small voltage angle difference between two buses is present, the difference between the phasors $\tilde{V}_2 - \tilde{V}_1$ can be represented as another phase which is perpendicular to both of them. In equation 2.4, it can be seen that this leads to the current phasor which will close to parallel to the voltages for a primarily imaginary impedance. From equation 2.6, it is shown that this leads to a primarily real power flow. Since the impedance in the power system is small, a small phase difference can result in significant power flows.
In stable conditions, power will flow to a lagging bus. When this derivation is combined with the power balancing of SG in sections 2.1.2, it can be seen that if a SG is slowing down due to a lack of mechanical input power, it will start lagging. Thus the electrical power output will also decrease. In some cases, this can create slow inter area oscillations. Within the continental European synchronous area, different oscillation modes have been identified in [25, 26]. In these inter area oscillations, SG groups are essentially exchanging energy by slightly speeding up and down opposite to other SG groups.

2.2. Stability Challenges in Future Grids

In future power electrical systems, more distributed RES will be integrated into the grid. This means the system will be operating closer to stability limits. A system's stability is its ability to operate at a desirable equilibrium operation point after a disturbance has affected the system. In the following sections, both frequency stability and voltage stability challenges are discussed. The frequency stability is challenged by the increasing decoupling of the inertia of the grid. The voltage stability is challenged by the integration of PEIG.

2.2.1. Decoupled Renewable Energy Resources

In order to achieve the goals of the Paris Agreement [27] power grids are planning on increasingly integrating new decoupled RES such as PV and WT [17]. Decoupled electrical generators have no inertia which is coupled to the system frequency.
Specifically, these types of RES are challenging because they have no inertia and have an output power with little controllability. The principles of type-3 and type-4 WTs are discussed in more detail in appendix B. Other RES such as hydro power, biomass or nuclear power are less difficult to integrate since they are usually connected through synchronous generators. Therefore, these types of RES contribute to the TSI and have very predictable dynamics. However, only these green energy sources will not be able to provide enough electrical energy everywhere.
When less inertia is present in the power grid, a mismatch in power generation and demand will lead to a higher initial RoCoF. As a result there is less time to act with control action before the frequency is outside desired or safe boundaries. This is already a significant problem in small islanded grids. In [28–32] solutions are proposed by introducing synthetic inertia to both PV system, HVDC links and in WTs. This is done by releasing stored energy in those systems during a frequency event. For PV and HVDC systems, this energy is stored in the capacitance of the DC links. The control systems can detect a frequency event and lower the voltage in the DC links. For decoupled WTs, the energy stored in the rotation of the blades can also be used to create synthetic inertia. When a frequency event occurs, the control systems of the WTs will increase the torque of generators to increase the power output to stabilise the grid. This can only be done for a short amount of time since it will lead to a reduction in the speed of the blades. Subsequently, this pushes the WT away from the optimal operating point to extract maximum energy.

2.2.2. Voltage Stability in the Future Power System

Besides system frequency stability of future power systems, the voltage stability will decrease as more PEIG local generation is introduced to the grid. In contrast to frequency, the voltage is a local variable in the grid. Because more loads and generation are connected to distribution grids maintaining a stable voltage is increasingly difficult. For synchronous generators, it is relatively easy to keep a stable voltage and inject reactive power into the grid in case of under voltage [24]. As synchronous generators are decommissioned, this control mechanism becomes less available. Therefore, grid codes for PEIG are becoming more strict on voltage regulation. Especially, Fault Ride Through (FRT) is has been a challenge for Power Electronic (PE) [33]. FRT is the capability of the system to maintain the voltage during fault by injecting reactive power to the grid. This prevents other cascading effects, such as further disconnection of loads and generators by protection mechanisms. Uncontrolled disconnection can lead to a power imbalance in the electrical system.

2.3. Wide Area Monitoring and Control

Introducing WAMCto the power grid is often referred to as the implementation of PMUs to various location in the system to improve the observability and controlability of the system. Control action can be executed automatically. If PMUs are only used to monitor the system it is referred to as Wide Area Monitoring (WAM). The time synchronisation of measurements of PMUs by GPS makes it possible to compare data of different location. This enables to determine voltage phasors, as described in equation 2.5, at different locations in a network and compare the relative phases. In combination with a high measurement rate, enables a whole variety of new application which are not possible with any other type of measurement devices. In the following section, different examples of the usefulness of PMU data is described. PMUs are further elaborated on in appendix B.

2.3.1. Application of Wide Area Monitoring and Control

Implementing PMUs in the power grid significantly improves the observability of the system. The observability of the system is a measure of how fast and how accurate the current state can be determined. Observability is critical in grids with relatively low stability. Possible unstable operation points can quickly be recognised. Europe has a relatively stable grid. This could be why relatively few PMUs have been installed in both transmission and distribution grids in Europe. In the power grids of China and the USA, thousands of PMUs are already installed. However, in these two areas, the data generated by the PMUs is barely used in real time. There exists a significant gap in the potential of the generated data and the possibilities to transform it into helpful information. To implement automatic control algorithms, the data latency should be lower than two electrical cycles [34]. In a 50 Hz system, this is 40 ms. If these automatic control algorithms use data originating from a larger area, this is referred to as WAMC. In the next section, some examples will be given on events where PMU data plays or could have played a key role during events.

Reconnection of the European Synchronous Area after separation

On the evening of the 4th of November in 2006, the European Synchronous Area was divided into three separate areas. The event was caused by a poorly planned disconnection of a 380 kV connection in the North-West of Germany [35]. The line was disconnected to let a cruise ship safely pass the lines. Due to some last minute changes in the time schedule, surrounding grid operators were unaware of the situation, which led to the overloading of nearby connections. Automatic protection action led to a cascading effect to protect against the overloading of lines. The European Synchronous Area was divided into three separate areas, and many people in the North-West of Europe were left in the dark. Because of the power imbalance within each area, the frequency in each area either rose or dropped significantly. After the frequencies in all the areas were stabilised, several unsuccessful reclosing attempts were performed. It took quite a while for the Transmission System Operator (TSO)s to become aware of the separation of the grid and the difference in system frequencies [19]. Reclosing action without similar frequencies and phases on both ends of a line is a dangerous action. The line will probably be overloaded before the system can be synchronised. This again leads to immediate disconnection. In the short time frame the connection is made, strong currents can cause damage or oscillations can be initiated on both sides of the line, leading to additional problems. When the TSOs finally became aware of the situation, coordinated actions could be undertaken to synchronise the different areas once again and attempt proper reclosing.

WAM data (unavailable to the TSOs) clearly showed the situation in the different areas. This shows clearly how valuable this information could be. Currently, still, no European wide monitoring system is available for TSO operators. Although the PMU technology has been around since the late 80s, no significant progress has been made in continental Europe. This can be explained by the high investment cost and the highly meshed and reliable European grid, which can make them seem unnecessary.

However, with the integration of more RES, the stability of the grid will become increasingly unpredictable. Improved visibility of the grid will be essential to respond quickly to instabilities.

On the 8th of January 2021, the European Synchronous Area was split again following an unexpected bus bar disconnection in Ernestiovo, Croatia [36]. The disconnection of the bus bar was essentially due to an extraordinary power flow from the South-East towards North-West Europe. This power flow was divided over multiple connections in the area. From PMU recordings, it is visible that the phase voltage between the South-East area and Swiss was close to 90 degrees. This information was not available TSOs since they only relied on SCADA based ENTSO-E Awareness System (EAS), which does not provide phase information. The first disconnected bus bar led to a cascading effect which separated South-Eastern Europe from the synchronous area. However, after the separation, the EAS was able to notify the TSOs on the separation. EAS has been operational since 2013 and was definitely valuable in this instance. EAS is a platform that allows TSOs to receive information about the operations of other TSOs.
Like in 2006, the frequency in both areas first had to be stabilised. Once this was established, a resynchronisation plan was devised by the three TSOs, who controlled the area around the separation line. First, the frequency difference between the areas should be lower than 100 mHz. Then three strong connections would be made, the first of which would use a synchro-check device. A synchro-check device is a device that checks the phases and frequency difference before the connection is reclosed. Usually, this is no problem since a connection would be in the same synchronous area. Therefore, these devices are not very common in European synchronous area. The reconnection of the two areas was successful in one attempt, just over an hour after the system was separated [36]. Overall it was concluded that the event was handled much more efficiently than the separation in 2006. This was partly due to lessons learned then and the improved availability of operational data between TSOs.

Iceland
In 2007 PMUs were installed in the grid of Iceland. The Icelandic grid consists of a relatively weak 132 kV ring connection around the island. Iceland has two main load points, one in the west around Reykjavik and one in the East where an 800 MW aluminium factory is located with a similar size hydropower plant [37]. Both load points have a local strong 220 kV grid backbone. Because the two load points are connected through a weak link, an event in one part of the system could lead to a difference in frequency acceleration between the two parts of the network. A quick response is required to prevent the voltage angle from becoming sufficiently large to overload and trip the connection between the two areas. A manual response will not be quick enough to prevent separation. After observing and analysing the PMU data during several events, a protection scheme was designed. The protection scheme is activated by a combination of the relative frequency difference and the voltage angle difference between the areas. The scheme will disconnect generation units on the accelerating of the two areas until no relative acceleration is present between the two areas. In [38], it is stated that disturbances that previously led to a grid separation are now automatically well handled without separation.

Conclusions from PMU use cases
Comparing the European case to the Icelandic case, it is clear that the PMU integration in Iceland is more developed than on the European continent. The use of PMU and automatic protective control action has proven effective on the Icelandic grid. Since the European grid is strongly meshed compared to the Icelandic grid, it is challenging to introduce effective algorithms. Moreover, the European grid is usually operating at very safe operational points. However, significant events such as the grid separations mentioned lead to unexpected behaviour and SCADA is ineffective in giving a proper view on the system during such events. PMUs can give this visibility. However, more effort is needed to transform the fast amount of PMU data into useful information for grid operators or automatic control systems.

2.4. Sub-Synchronous Oscillations

This section will introduce and discuss different types of SSOs. SSOs are now classified on which circumstances play a role leading up to the event. Recently a reclassification has been proposed, which will be used in this section [7]. An overview of this proposed reclassification is shown in figure 2.1.

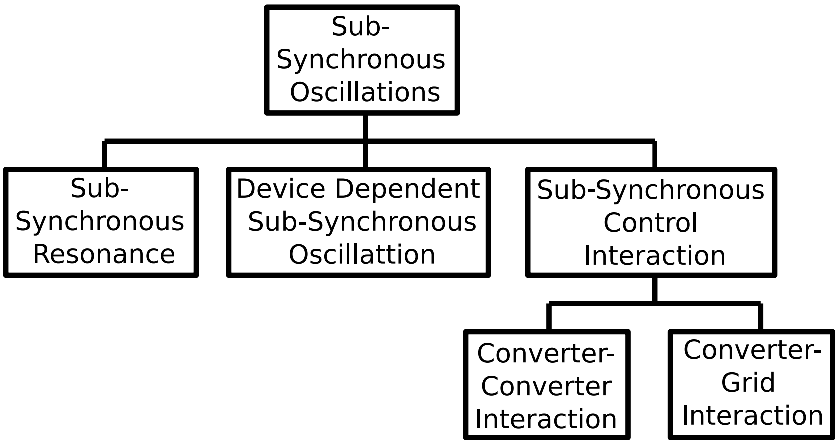

Figure 2.1: Proposed reclassification according to [7]. More subcategories are defined for Sub-Synchronous Resonance and Device Dependent Sub-Synchronous Oscillation.

Year	Area	Type	Impact	References
2009	Texas, USA	SSR	Damaged WTs by over voltage and high current	[8, 39]
multiple events in 2010	Hebei, China	SSR	Tripping of WT protection systems	[9]
2011	Minnesota, USA	SSR	Failed commissioning test of compensator capacitors	[10]
58 events in 2012 & 2013	Hebei, China	SSR	Tripping of WT protection systems	[11, 12]
2015	Xinjiang, China	SSCI	Loss of generation of 1280 MW by 3 synchronous generators	[13, 15, 40]
3 events in 2017	Texas, USA	SSR	Tripping of WT and other generator units	[14]
2017	Xinjiang, China	SSCI	Grudaully tripping of wind farm	[13, 15]
2019	England, UK	SSCI	Disconnection of 1.1 million customers	[16]

Table 2.1: List of SSO events where WPPs play a key role [7].

Three different categories of SSOs will be discussed in the following sections. These categories are Sub-Sychronous Resonance (SSR), Sub-Synchronous Control Interaction (SSCI) and device dependent sub-synchronous oscillations. The first two will be discussed with some SSOs events as an example. A list of reported SSO events in which WPPs had a significant role is shown in table 2.1. These events show how this phenomenon is already causing instabilities in electrical grids. Recent studies propose different ways to mitigate SSOs. These range from active damping control to switch action to changing the grid topology to remove oscillation modes.

2.4.1. Sub-Synchronous Resonance

The first sub-synchronous event leading to damage to the power grid occurred in Mohave, Nevada, in 1970. During this event, the shaft of a generator was damaged due to sustained SSO [41]. The generator was connected by a Fixed Series Capacitors (FSC) powerline during the event. One other non compensated power line was also connected to connect the generator to the grid. However, this connection went out of service. The capacitance of the FSC can store energy in the electric field between the plates. Also, the inductance of any power line stores energy in its magnetic field as current flows. These two components can exchange energy, and thus resonance occurs. The resonance frequency of this type of LC resonance is shown in the following equation.

$$f_r = \frac{1}{2\pi\sqrt{LC}} \tag{2.7}$$

Where f_r is the resonance frequency and L and C are the line inductance and series capacitance, respectively. In real world systems, it is found that this resonance frequency is mainly in a sub-synchronous range between 5-45 Hz [42, 43]. This resonance frequency alone does not explain the excitation of Sub-Sychronous Resonance (SSR) as the line resistance should dampen any sustained oscillation. The induction generator has an essential role in amplifying oscillations. An induction generator is the type of generator used in type-3 WTs.

In [44] the Induction Generator Effect (IGE) is described which explains the excitation of SSR. Using the following induction generator equations 2.8 and 2.9, it can be shown that the generator has a negative resistance for frequency below the system frequency. These formulas are used to determine the resistance of the generator as a function of the slip. The slip is the relative speed difference between the magnetic field and the rotor speed.

$$R_g = \frac{R_r}{s} \tag{2.8}$$

$$s = \frac{f_n - f_0}{f_n} \tag{2.9}$$

Where R_g and R_r are the generator resistance and rotor resistance, respectively. s is the slip and f_n and f_0 are the sub-synchronous frequency and system frequency. Since f_n is by definition smaller than f_0, it is shown that the generator has a negative resistance for sub-synchronous frequencies. This means the real part of the impedance on this frequency can be negative when no significant additional resistance is present in the grid. This results in an effective negative resistance for sub-synchronous frequencies and thus results in amplification.

2.4.2. Sub-Synchronous Resonance Events

Texas, USA

The events in Texas of 2009 are the most referenced SSO events of sub-synchronous events with WT interaction. It was the first time a SSO occurred due to SSR with FSC. The events have been well documented, including important new insight [8, 39]. The event started when a faulted line was unexpectedly taken out of service. This led to a situation in which two type-3 WPP were radially connected to the core of the grid by a compensated line. In less than half a second, voltages of three times the nominal voltage were measured. These extreme voltages were caused by sub-synchronous waveforms with a significant amplitude. This SSO could grow due to the negative resistance of the Doubly Fed Induction Generator (DFIG). When the WTs experienced a 1.5 p.u. voltage, they would have had extensive damage and enter a crowbar state. In a crowbar state, a short circuit is created to protect the electrical components.

In [39] several recommendations are given for preventing future events. These include limiting the compensation level and preventing radial topologies. In addition, using a more complex Thyristor-controlled Series Capacitors (TCSC) instead of capacitor based compensators or installing SSR filters. It is also mentioned to explore the possibilities of changing the controllers of the WTs.

Minnesota, USA

In [10] the events during a commissioning test of a newly installed FSC are described. The FSC was installed in the middle of a 90 kilometer 345 kV line. In years before an increasing amount of new WTs was installed on one end of the line. By installing the FSC, more capacity would be available to transport the energy to the load centres. During the tests, one line would be disconnected before bypassing the FSC. The connected wind generation at the time of the test was very low and a small amount of power was transferred. Before the FSC was bypassed, SSO occurred in the system. Due to overvoltage, a flash-over occurred and the system tripped.

To prevent future damages, a microprocessor was developed to detect SSO in a range of 5-25 Hz. The microprocessor used 3 phase voltage and current measurements at up 96 measurements per cycle. The microprocessor was first tested using Real Time Digital Simulation (RTDS) and could accurately detect SSO events. The microprocessor could then be programmed to take automatic control actions, such as bypassing the FSC to prevent a sustained SSR.

Hebei, China

In the Hebei province in the North-East of China, the first SSR events were reported at the end of 2012. By the end of 2013, a total of 58 events were reported [12]. In the previous years, many new

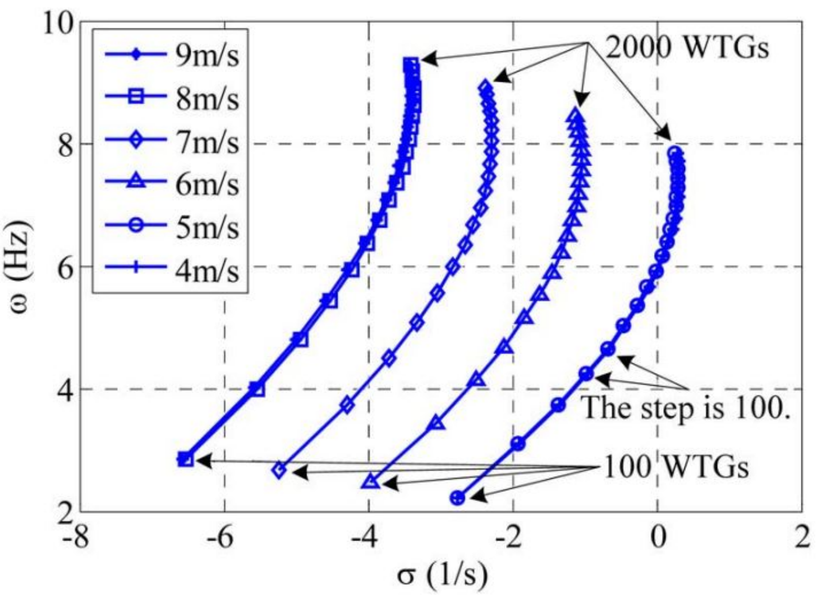

Figure 2.2: Eigenvalue analysis of simulations of the Hebei area [11]. σ is the real part of the eigenvalue and ω is the imaginary part of the eigenvalue.

WPPs were commissioned. Also, FSC were installed in the 500 kV high voltage lines to transmit large amounts of energy over longer distances to big load centres in the East en South East of China.

An analysis of all events showed that certain factors play an essential role. Four FSCs are present in the area. During all events, all four FSCs were activated. During some of the events, operators were able to bypass at least one of these FSCs. In all cases, these control actions lead to a quick disappearance of the SSR. During most of the events, a relatively low wind speed was powering the WTs and seems to be an important factor SSR events.

Further research on the factors leading up to the events was performed in [11]. In this research, simulations were performed on a simplified grid. In this model, the type-3 WTs were aggregated in one generator unit with similar control systems as the individual WTs for the Rotor Side Converter (RSC) and GSC. The number of WTs and the wind speed was varied and eigenvalue analyses was performed. It was found that for low wind speeds (thus low rotor speeds) and a range of the number of active WTs the real part of the eigenvalues became larger than zero. This indicates no damping at that resonance frequency and the danger of undamped oscillations exists. The results of this eigenvalue analysis as a function of wind speed and the number of active WTs are shown in figure 2.2.

Additionally, the control parameters were investigated for their influence on the eigenvalues. It was found that the gain factor for the RSC current tracking control, stator reactive power control, DC voltage control, and stator voltage control strongly influence the eigenvalues.

2.4.3. Sub-Synchronous Control Interaction

Sub-Synchronous Control Interaction is a relatively new type of sub-synchronous interaction. It is a new phenomenon caused by interaction between mostly Voltage Source Converter (VSC) which are increasingly integrated into the grid [45, 46]. VSCs are AC to DC converters which have significant advantages over previous Line Commutated Converters (LCC) technologies [47]. VSC are now increasingly used in, for example, type-4 WTs, HVDC links, BESS and PV systems. A more detailed description of how a VSC works and is controlled is given in appendix B. In multiple papers, the emerging challenges of integrating DC systems to the existing AC infrastructure are brought to the attention [48, 49]. One of these problems is the unprecedented, and therefore unknown, interactions between the converters and the grid and interactions among converters [49–51]. These two problems are also categorised in [7] and are shown in figure 2.1 as a sub-synchronous challenge.

In [50], it is argued that the control systems of VSCs are mainly designed as if they are connected to

an infinite grid. Of course, this is not true as it can be connected to relatively weak grids or grids with many different VSCs. In these cases, this assumption is not applicable.
As described in appendix B multiple control parameters are used in the control system of the inverter. In [40, 52], the influence of the four parameters in the current controller is investigated. It is found that these parameters have a significant influence on the frequency and damping of the sub-synchronous mode in a small network. This work is used to verify the models described in chapter 3.
Besides the current controller, the Phaso Locked Loop (PLL) can affect SSOs. The function and operation of a PLL is further elaborated on in appendix B. How the PLL influences sub-synchronous behaviour is introduced in [13]. A theory is introduced on how oscillation frequencies which are prone to SSO are amplified by type-4 WTs and influenced by the PLL. This is done by introducing a disturbance current sine wave from the grid to the GSC with amplitude δ and frequency ω_s. This leads to a voltage perturbation in each phase, as shown in equation 2.10 for phase A.

$$\Delta u_a = \omega_s L_g \delta \cos\left(\omega_s t + \frac{\pi}{2}\right) \tag{2.10}$$

The work shows how the voltage perturbation influences the angle θ of the PLL. In appendix B it is explained how the PLL is essential for proper operation of a VSC. How the angle difference $\Delta\theta$ affects the VSC further investigated. This results in a response perturbation of the VSC as shown in equation 2.11.

$$\begin{aligned}\Delta u_{as} = \overbrace{\frac{K_1}{2}\cos\left(\omega_s t + \gamma_1\right)}^{\text{First term}} &+ \frac{K_2}{2}\cos\left(\left(2\omega_0 - \omega_s\right)t + \gamma_2\right) \\ + \frac{K_2}{2}\cos\left(\left(3\omega_0 - 2\omega_s\right)t + \gamma_3\right) &+ \frac{K_3}{2}\cos\left(\left(\omega_0 - 2\omega_s\right)t + \gamma_4\right) \\ + \frac{K_2}{2}\cos\left(\left(4\omega_0 - 3\omega_s\right)t + \gamma_5\right) &+ \frac{K_3}{2}\cos\left(\left(2\omega_0 - 3\omega_s\right)t + \gamma_6\right)\end{aligned} \tag{2.11}$$

It can be seen that only the first term gives a response at the same frequency as the original perturbed signal. Therefore, only the first component can contribute to an amplification of the perturbation when the phase difference between Δu_a and Δu_{as} is less than $\frac{\pi}{2}$. In this case, the summation of Δu_a and Δu_{as} will have a larger amplitude than the original perturbation Δu_a. Therefore, a criteria value Q for instability is introduced as shown in equation 2.12.

$$Q = \sin\left(\gamma_1\right) > 0 \tag{2.12}$$

Both K_1 and γ_1 are ultimately a function of the control parameters of both the PLL and the GSC. This explains how the control parameters of a wind turbine can influence the sub-synchronous mode behaviour.
The criterion in equation 2.12 is then validated by simulations. Significant power oscillations are found with a frequency predicted by the criteria of Q. At last, the influence of different control parameters is investigated.
In [50] interaction between the control systems of multiple VSC in an AC network is addressed. In the last years, this has had an increasing interest. HVDC connections are now also part of the European Network of Transmisssion System Operators for Electricity (ENTSO-E) grid codes. In the research, two VSC are modelled as two Single Input Single Output (SISO), which are connected by grid impedances in a π-model. This effectively creates one Multiple Input Multiple Output (MIMO) system. From this, normal stability criteria such as Nyquist criteria or a Bode plot of the closed loop system can be tested. This means the parameters of the AC network can easily be tested on their influence on the system stability. The Short Circuit Ratio (SCR) is tested and it is found that a decrease leads to a shift of resonance frequency. The decrease of SCR will also lead to a smaller phase margin and become unstable at some point.

2.4.4. Sub-Synchronous Oscillation Events with Wind Turbine Interaction

In this section, the events mentioned in table 2.1 will be discussed further. Attention will be given to what lessons were learned in that area to prevent future events.

Xinjiang, China

In 2015 an SSO event occurred in the Xinjiang region in China without the presence of FSC. At the time, it was the first event without the presence of a FSC. By that time SSR by FSC and DFIG WTs was a relatively well understood phenomena. This event triggered new research on the influence of control systems of WTs on SSO events. What was even more exceptional about these events was that type-4 WTs were involved in contrast to the type-3 WTs. Also, the 300 WTs in the area were producing at almost maximum capacity, which is also in stark contrast compared to previous events where the turbines were producing minimum power at the time [13].

In 2017 a new event occurred in the same area without the presence of FSC. However, during this event type-3 WTs and a Static Compensator (STATCOM) were involved [15]. A STATCOM is a Flexible AC Transmission Systems (FACTS) device that can regulate a network's reactive power.

Because these events were very different in nature compared to previous events, new research was focused on the control systems of the different components. In [13] it was concluded that for type-4 WTs the PLL of the GSC has a big impact on sustained oscillations. This was done using small signal analysis. It was found that the gain factors of the PLL have a large influence on the amplifications at multiple frequencies at a fixed distance from multiples of the primary frequency. Also, in [15], further analysis in the controllers of the type-3 WTs and the STATCOMs showed that some sub-synchronous frequencies were prone to amplification. The analyses found that 37.4 Hz was most susceptible to this. From measurements during the events in 2017, it was found that an initial voltage oscillation at 37.5 Hz started the event. The initial cause of the oscillation was not found. However, it did show that proper tuning of controllers and interactions between them is necessary to prevent amplification at specific frequencies.

Hornsea One, United Kingdom

On the 9th of August 2019, a significant frequency event occurred in the grid of the United Kingdom. An SSO event caused by SSCI of the offshore Hornsea One wind park led to the power output drop of this wind park. This lead to cascading problems in the network. Due to a frequency drop to 48.8 Hz, load shedding schemes were initiated, leaving 1.1 million customers in the dark [16].

The sequence of events started after a lightning strike in the network and multiple generator units disconnected. Also, in the offshore Hornsea One WPP rapidly deloaded from 799 MW to 62 MW contributing to a total loss of generation of 1878 MW [7]. Leading up to the lightning strike already, a 10 Hz voltage oscillation was present which was not significantly damped. After the lightning strike, the grid was further weakened due to the line temporarily being taken out of service. This led to a further amplification of the oscillation by the controllers of the WPP. In [7] this type of SSCI is distinguished as Converter Grid Interaction (CGI). Soon after this incident, the control parameters were updated by the WPP manufacturer, which could have damped the SSO.

Because of the significant generation loss resulting in a frequency drop to 48.8 Hz, about 1.1 million customers were disconnected within 20 seconds to balance demand and generation. The operators could stabilise the grid at 50 Hz in the following minutes. From that moment, Distribution System Operator (DSO) were instructed to reconnect loads to the grid gradually. About 45 minutes after the initial lightning strike, all loads were connected again.

2.5. Conclusion

In this chapter different topics related to a stable operation of the electrical power system are introduced. Control system which are based on SG dominated system are not suitable systems with a high penetration of PEIG. WAMC can over solution to this problem. On of the emerging problematic phenomanon are SSO.

Since 2011 multiple SSO events have occurred in which WPPs played a significant role. Because the installation of new WT systems is still increasing, this type of event will also pose an increased risk for future power systems. This literature review discusses two types of SSO events. SSR is a problem which can mostly be solved by avoiding grid topologies with radial FSC connections to WPPs. SSCI is a more difficult challenge. In type-4 WTs, HVDC systems and PV systems VSC are used as a coupling between the DC and AC parts. As more generation and transmission is shifting towards using VSCs instead of classical synchronous generators and AC transmission systems, new phenomena are introduced in the grid. Only a little research has been performed on this phenomenon and no general solution is present to prevent or dampen SSCIs and especially CGI. Therefore, this project will focus on mitigating CGI by providing wide area PMU data. Damping schemes can be implemented by identifying sub-synchronous modes and relaying this information to the control system.

3

Modelling & Methods

In this chapter, the models and methods used are introduced. In the first section, the modelling software DIgSILENT PowerFactory is introduced. The structure of the software will be explained, followed by the tools provided. The following section explains different methods for further analysis of the results from DIgSILENT PowerFactory. At last, the modelling steps are introduced. In these steps, two grid models are used. These grid models will be introduced as a base model. Of these base models, the basic behaviour is shown. In different parts of the research, modifications to these base models are made to evaluate their response behaviour.

3.1. Modelling in DIgSILENT PowerFactory

For this research, DIgSILENT PowerFactory 2022 SP1 is used. This will be referred to as PowerFactory. PowerFactory offers many tools to perform different kinds of analysis on electricity grids and the physical and control interaction of different elements in the grid. For this research, three tools are used: Load Flow Calculation, RMS/EMT simulation and Modal/Eigenvalue Analysis. The two latter ones are used to analyse how the system behaves dynamically. In the following section, first the structure of a PowerFactory model is explained. This is followed by explainin different tools available in the PowerFactory software.

3.1.1. PowerFactory modelling structure

Before performing static or dynamic analysis on a network, a model must be defined within the PowerFactory software. The structure of such a model will be explained in this section. A schematic overview of a PowerFactory model is shown in figure 3.1 and is further elaborated below.

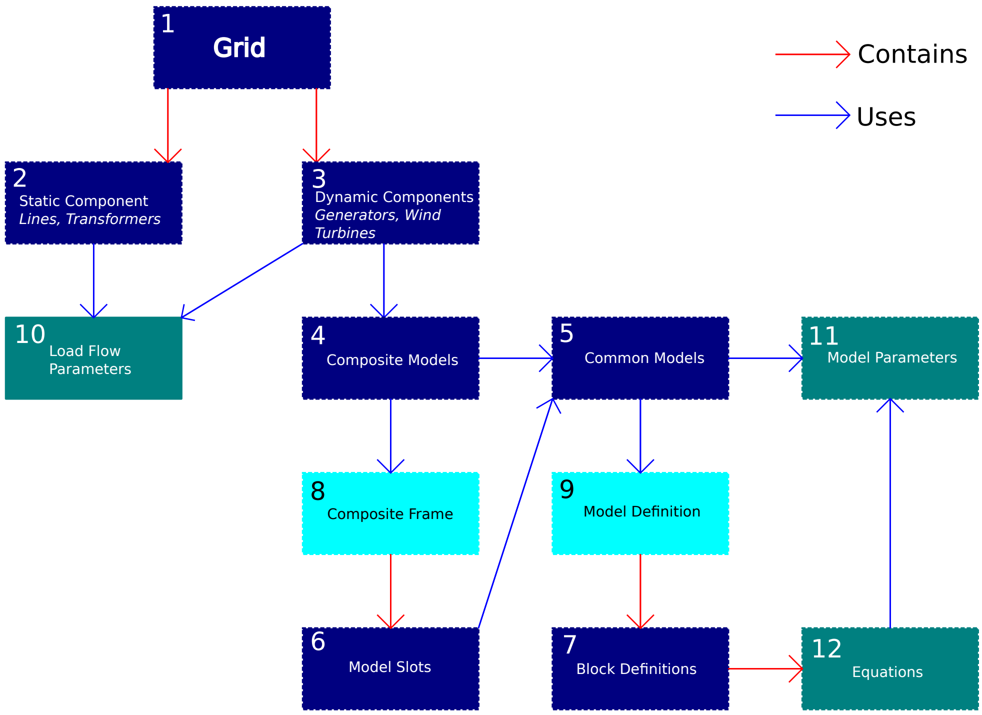

Figure 3.1: Schematic structure of a PowerFactory model.

1. **Grid:** This is the model's top layer, which defines the connection between the different components. It is often represented as a single line diagram. This means buses are connected by a line or a transformer element shown as a single line rather than all three phases of this connection. Components in the grid can be sub-categorised as static components (2) and dynamic components (3).

2. **Static Components:** These components do not have a dynamic model and have static parameters, which are called load flow parameters (10). Examples of static components are loads, transformers and lines.

3. **Dynamic Components:** These components have a composite model (4), which defines their dynamic behaviour. An example of a dynamic component is a generator.

4. **Composite Model:** Each dynamic component (3) has its own composite model. Different composite models can have the same composite frame (8), which is a framework for different dynamic components in the model. The composite frame defines what kind of common models (5) can be used by the composite model.

5. **Common Model:** This models one part of all the dynamics, which can be a physical component or a control system. For example, in a generator, the torsional shaft dynamics can be modelled separately from the voltage or torque control. The model is defined by both the model definition (9) and the model parameters (11).

6. **Model Slots:** The composite frame (8) defines a frame with model slots. The model slots are filled with common models (5).

7. **Block Definition:** These components are found in the model definitions (9). Usually, these blocks perform an elementary function on one or more incoming signals and outputs one or more processed signals. An example of multiple input and output can be a Park transformation. Inside the block definition, equations (12) are defined, which define the exact behaviour.

8. **Composite Frame:** This framework defines how different dynamic models within a grid component interact with each other. In the case of a generator, this can be different dynamics, such as shaft torsion and inertia interacting with different control models. These will both be modelled in a common model (5). The composite frame defines model slots (6) which will be filled with the common models. The model slots are connected so signals between the different common models can be fed from one common model to another.

9. **Model Definition:** The model definition is a block diagram in which a specific dynamic is defined. Input signals are fed into different blocks that models interactions. The block definitions (7) usually contain elementary functions such as differentiators, integrators or time delays.

10. **Load Flow Parameters:** The load flow parameters are the most basic parameters. For components such as lines or transformers, these are the impedances of these components. These parameters are the set points for voltages or power consumed or generated for generators or loads. These parameters are used in a load flow analysis and can also be used as a reference signal of the dynamic model.

11. **Model Parameters:** The parameters are defined for each common model (5) and used in the bottom layer of the equations (12). Because they are defined for each common model, a dynamic component can have the same model definition while using different parameters. For example, in a generator, the torsional interaction of the shaft can be modelled in the same way while using a different shaft stiffness for the different generators.

12. **Equations:** The equation define the exact behaviour of block definitions (7). It is possible to work with differential equations when defining these equations. In these equations, state variables and internal variables are used. Also, model parameters are used in these equations, which can change the behaviour of the dynamic system.

3.1.2. Load Flow Calculation

Load flow calculation is a simple method to calculate power flow through the network. The impedances of different lines and transformers are considered, as well as the power set points of loads and generators. A Newton-Raphson iterative algorithm finds the voltage at each bus and power flow. As long as the grid is set up properly, a solution can be found in a few number of steps. This method allows for a quick network evaluation before further tests are performed. The results of this analysis do not consider any dynamics of the system and only represent an equilibrium based on the generators and loads. The results include voltage levels and angles for each bus as well as power flows between different connections. This will show where in the network the loading of lines is highest and show where voltage magnitude problems are present.
In this research, the Load Flow Calculation is used during each model setup to ensure no extreme operational scenario is used during further system analysis.

3.1.3. RMS/EMT simulation

RMS/EMT simulations are two types of time simulations available in PowerFactory that include the system's dynamic models. In this research only RMS simulations are used. RMS simulations are also often referred to as Phasor-Domain Transient (PDT) simulations [53]. This simulations uses voltage phasors to simulate the transient behaviour in the grid seen from the rotating reference frame. This implies the phasors are not rotating at the fundamental frequency of the grid. They move only relative to the reference bus. Phasor equations as described in equations 2.4 and 2.6 are used to simulate the dynamic behaviour.
Electromagnetic Transient (EMT) simulations on the other hand uses actual differential equations for capacitive and inductive components. The real voltages for all three phases are calculated. Thus this includes the fundamental frequency of the grid.
Using the RMS simulations, different signals and variables are monitored during the simulation. This makes it possible to evaluate the system's dynamics in great detail. During a time simulation, events such as load steps or a short circuit can be defined. Transient behaviour of the system can be observed during and after an event. This can show if and how much the system is damped. During the transient period, the system will transfer to a new equilibrium. During this transient period, different variables

could swing outside of their designed range. RMS simulations offer an excellent insight to show the exact dynamics of the system.
Before the time simulation can be executed, first, the system needs to be initialised. This means all dynamic variables in the system should be given an initial value. The initialisation step ensures the simulation starts in an equilibrium of the system. Some variables will be given a predefined initial value, and others will be determined such that time derivatives will be zero. If the model is set up correctly, no variables should change values at the beginning of the simulations. If the system is not in an equilibrium state at the start of an event, it is challenging to replicate transient behaviour since actually to transient events will be interfering with one another.
In this research, RMS simulations are used to dive into the dynamics of the model. Also, time simulation can be used to verify the results from the Modal/Eigenvalue Analysis by performing a Prony analysis and Fourier analysis on the time signals.

3.1.4. Modal/Eigenvalue Analysis

Modal/Eigenvalue Analysis is a powerful tool for finding different oscillation modes of a system. To understand what this type of analysis is used for, some knowledge about a linear state space model must be explained.

$$\frac{d}{dt}\mathbf{x} = \mathbf{Ax} + \mathbf{Bu} \tag{3.1}$$

$$\mathbf{y} = \mathbf{Cx} \tag{3.2}$$

In equations 3.1 and 3.2 an abstract form of a dynamic system is shown. In these equations, vector **x** represents the state of the system. It contains all state variables, which could be the excitation voltage or speed of the generator. For a whole system, all state variables are collected in this vector **x**. **u** is a vector which gives control signals from outside to the system. Matrix **A** and **B** form the connection between the system's current state and control signals to its derivative. Each row in matrix **A** defines how much influence a state variable has on another state variable. Matrix **B** does the same for control signals. Equation 3.2 gives an observability vector **y** of the system. When looking at a system from the outside, not all state variables will be observable, and some state variables will only be visible as a superposition of each other. Matrix **C** connects the actual system **x** to the observability vector **y**. **y** and **x** do not have to be the same length as not all state variables are necessarily directly observable.
In a linear dynamic model, the eigenvectors and corresponding eigenvalues represent oscillation modes of the system. Important to realise is that both the eigenvectors and the eigenvalues can have complex values. There are as many eigenvalues as state variables in the system. This represented in equation 3.3.

$$\mathbf{A}\boldsymbol{\phi}_i = \lambda_i\boldsymbol{\phi}_i \tag{3.3}$$

In this equation, $\boldsymbol{\phi}_i$ is the (right) eigenvector i containing a complex value corresponding to the phase and magnitude of each state variable. This phase can determine which components in the system are oscillating together or in opposite directions. This is an important signature of a mode. λ_i is the (complex) eigenvalue which can be represented as $\sigma + j\omega$. In this form, σ represents the damping and ω the frequency of the mode. A complex eigenvalue will always have conjugate pairs which form one oscillation in the system because **A** is not a complex matrix. From this, the damping and frequency properties of the eigenvalue can be shown. If the system is excited by an external input and all modes are excited equally, the system will respond as in equation 3.4.

$$y(t) = \sum_{i=1}^{n} \mathbf{A}_i e^{(\sigma_i + j\omega_i)t} \tag{3.4}$$

When only one conjugate eigenvalue pair is considered (let it be $\sigma + i\omega$ and $\sigma - i\omega$), only the time dependent part of the summation can be considered. Since A_i is not time dependent, it can be left out for simplicity. In equation 3.5 this response is rewritten to an exponential function multiplied with a cosine function.

$$\begin{aligned} y^*(t) &= e^{(\sigma+j\omega)} + e^{(\sigma-j\omega)} \\ &= e^{\sigma t}\left(e^{j\omega t} + e^{-j\omega t}\right) \\ &= 2e^{\sigma t}\cos\omega t \end{aligned} \tag{3.5}$$

In this form, it can be easily seen that σ represents a damping term while ω is the oscillation frequency. From this, it is obvious that a mode is only stable if it holds that $\omega < 0$. This will be an important property to keep in mind for this research. The damping ratio ζ is defined below.

$$\zeta = \frac{-\sigma}{\sqrt{\sigma^2 + \omega^2}} \tag{3.6}$$

The damping ratio relates the damping and frequency of the mode. This is useful because it tells about how many swings an oscillation can grow. This is important because observing this growth takes at least two swings.

The model defined in PowerFactory will not necessarily be a linear dynamic system. Therefore, the Modal/Eigenvalue analysis returns a linearisation of the system in a specific state. This is done by an iterative algorithm which will calculate how small changes in state variables influences other state variables (therefore, it is also referred to as small signal analysis). This will allow for building a matrix **A**, which can then be used to determine the eigenvalues and eigenvectors. The linearisation is dependent on the current state of the system. The linearisation can be performed at any time within a time simulation. In order to obtain reproducible results, it is good practice to only perform this analysis in an equilibrium state.

3.2. Analysing Results from PowerFactory

In this section, some mathematical tools used in this research will be further explained. These tools are used to perform further analysis on the results from PowerFactory. Understanding how these tools operate and what they can and cannot be used for is essential.

3.2.1. Particaption Factors

The participation factor measures the participation of a state variable in a mode. Equation 3.7 gives the definition of the participation factor p_{ik}.

$$p_{ik} = \boldsymbol{\phi}_{ki}\boldsymbol{\psi}_{ik} \tag{3.7}$$

In this equation, $\boldsymbol{\phi}$ is the matrix with right eigenvectors and $\boldsymbol{\psi}$ the left eigenvector matrix. The participation factor is a real number p_{ik}, which tells how much a state variable i contributes to an oscillation mode k. Because the left and right eigenvectors have complementary units, these are cancelled for the participation factor. Thus, the participation factors have no units and are therefore weighted equally. This enables it to be used as another tool to identify which state variable in the system could be worth implementing additional damping on. This can either be done by tuning current or new control systems.

3.2.2. Observability in bus voltages

This research aims to include PMU measurements from different buses into the control systems of WTs to mitigate SSO. Therefore it is essential to determine at which buses the SSO are observable. The geometric observability measures are only available for state variables and not for the algebraic quantities of bus voltages magnitudes V_i and bus voltage angles θ_i at bus i. In [22] a method is proposed determine the sensitivity of both V_i and θ_i to a change in rotor angle δ_j of SG j. This method is further referred to as Vanfretties method.
Since the rotor angle is a state variable of the system, it will be part of the mode eigenvector. These values can be translated into a change in voltage magnitude V_i and voltage angle θ_i on each bus. This can be used as a measure of observability for a sub-synchronous mode. In [22], the following matrices are derived to find ΔV_i and $\Delta\theta_i$.

$$\begin{bmatrix} \Delta V_1 \\ \vdots \\ \Delta V_n \end{bmatrix} = \begin{bmatrix} \left.\left(\frac{\partial V_1}{\partial \delta_1}\right)\right|_{eq,0} & \cdots & \left.\left(\frac{\partial V_1}{\partial \delta_N}\right)\right|_{eq,0} \\ \vdots & \ddots & \vdots \\ \left.\left(\frac{\partial V_n}{\partial \delta_1}\right)\right|_{eq,0} & \cdots & \left.\left(\frac{\partial V_n}{\partial \delta_N}\right)\right|_{eq,0} \end{bmatrix} \begin{bmatrix} \Delta \delta_1 \\ \vdots \\ \Delta \delta_N \end{bmatrix} \tag{3.8}$$

This can be written as multiplication of matrix $\mathbf{C}_{V\delta}$ and vector $\Delta\boldsymbol{\delta}$ to obtain vector $\Delta\mathbf{V}$. Matrix $\mathbf{C}_{V\delta}$ has a size of nxN, where n is the number of buses and N is the number of SGs in the system.

$$\Delta\mathbf{V} = \mathbf{C}_{V\delta}\ \Delta\boldsymbol{\delta} \tag{3.9}$$

In matrix $\mathbf{C}_{V\delta}$ each element contains a partial derivative of the voltage magnitude in bus i for a rotor angle change in SG j. This derivative is defined for the equilibrium derived from load flow calculations. Similarly, a matrix $\mathbf{C}_{\theta\delta}$ is defined as follows.

$$\Delta\boldsymbol{\theta} = \mathbf{C}_{\theta\delta}\ \Delta\boldsymbol{\delta} \tag{3.10}$$

The elements of $\mathbf{C}_{\theta\delta}$ have a similar form as in equation 3.8 as $\left.\left(\frac{\partial\theta_i}{\partial\delta_j}\right)\right|_{eq,0}$. $\Delta\boldsymbol{\delta}$ are the mode shapes which are present in the eigenvector of each mode.
To calculate the derivative elements, the following derivations are made [22]. It starts with extending the normal network admittance matrix. The normal admittance matrix of a network with n buses will have the following form.

$$\mathbf{I}_n = \mathbf{Y}_{nn}\mathbf{V}_n \tag{3.11}$$

In this equation, $\mathbf{I}_n$ is a vector representing the current injected into the network at each bus. $\mathbf{Y}_{nn}$ is a square matrix representing the network's admittance. $\mathbf{V}_n$ is a vector containing the bus voltages. The extended admittance matrix equation will have the following form.

$$\begin{bmatrix}\mathbf{0}\\ \mathbf{I}_N\end{bmatrix} = \begin{bmatrix}\mathbf{Y}_{nn} & \mathbf{Y}_{nN}\\ \mathbf{Y}_{nN}^T & \mathbf{Y}_{NN}\end{bmatrix}\begin{bmatrix}\mathbf{V}_n\\ \mathbf{E}'_N\end{bmatrix} \tag{3.12}$$

In this equation $\mathbf{Y}_{nN}$ is a matrix which connects the network to the excitation voltages of the SGs $\mathbf{E}'_N$. N is the number of SG in the network. The extension is accomplished by using the transient reactance X'_j on the elements, which corresponds to the bus to which a generator is connected. $\mathbf{V}_n$ are the bus voltages calculated in a load flow calculation. $\mathbf{I}_N$ is the current flowing into the network from the generators. All other buses will have no current flowing in because all loads are already included in $\mathbf{Y}_{nn}$. The property is represented by the $\mathbf{0}$ vector of length n in the current vector. From this property, the following can be derived.

$$\mathbf{V}_n = -\mathbf{Y}_{nn}^{-1}\mathbf{Y}_{nN}\mathbf{E}'_N \tag{3.13}$$

Which can partly be put in a new matrix $\tilde{\boldsymbol{\kappa}}$

$$\tilde{\boldsymbol{\kappa}} = -\mathbf{Y}_{nn}^{-1}\mathbf{Y}_{nN} = \boldsymbol{\kappa}\angle\boldsymbol{\gamma} \tag{3.14}$$

This new matrix $\tilde{\boldsymbol{\kappa}}$ connects the bus voltages to the internal excitation voltages of the SGs. The complex elements of $\tilde{\boldsymbol{\kappa}}$ can also represented as the magnitude $\boldsymbol{\kappa}$ with phase $\boldsymbol{\gamma}$.
These variable are then used to calculate the derivatives in matrices $\mathbf{C}_{V\delta}$ and $\mathbf{C}_{\theta\delta}$ from equations 3.8 and 3.10.

$$\frac{\partial V_i}{\partial\delta_j} = \frac{1}{|\tilde{V}_i|}\sum_{\substack{p=1\\ p\neq j}}^{N}\kappa_{ij}\kappa_{ip}E'_jE'_p\sin\left(\delta_j+\gamma_{ij}-\delta_p-\gamma_{ip}\right) \tag{3.15}$$

$$\frac{\partial\theta_i}{\partial\delta_j} = \frac{1}{|\tilde{V}_i|^2}\sum_{q=1}^{N}\kappa_{ij}\kappa_{iq}E'_jE'_q\cos\left(\delta_j+\gamma_{ij}-\delta_q-\gamma_{iq}\right) \tag{3.16}$$

where

$$|\tilde{V}_i| = \sqrt{\left(\sum_{j=1}^{N}\tilde{\kappa}_{ij}\tilde{E}'_j\right)^2} \tag{3.17}$$

Thus, in equation equation 3.15 and 3.16 the sensitivities of the voltages magnitude and angle at bus j with respect to rotor angle of SG j are calculated respectively.

3.2.3. Prony Analysis

Prony analysis is a method to extract information about an oscillation from a time signal. This is done by fitting a function of a damped oscillation on the time signal. This is the following function.

$$y(t) = \sum_{i=1}^{n} A_i e^{(\sigma_i + j\omega_i)t + \phi_i} \tag{3.18}$$

This function is very similar to equation 3.4. A parameter ϕ_i is added to compensate for any phase the time signal might have. Parameters A_i, σ_i, ω_i and ϕ_i will be found by fitting the function on the time signal.

If n is set to 2, a conjugate eigenvalue pair of $\sigma \pm j\omega$ will result from a damped cosine signal. This can be explained following the derivation of equation 3.5. A damping ratio ζ can then be determined using equation 3.6. This result can be used to verify the results following from a state space model.

It is essential to use a proper window to fit the function on. An oscillation usually does not grow infinitely but stabilises to a sustained oscillation. To determine a proper damping ratio, a window of the time signal needs to be selected in which the oscillation is growing.

3.2.4. Method overview

An overview of all methods used in this research is shown in figure 3.2. It is shown which methods are used within PowerFactory and which methods use the results but are executed outside of PowerFactory. It also gives an overview of the results obtained from each method.

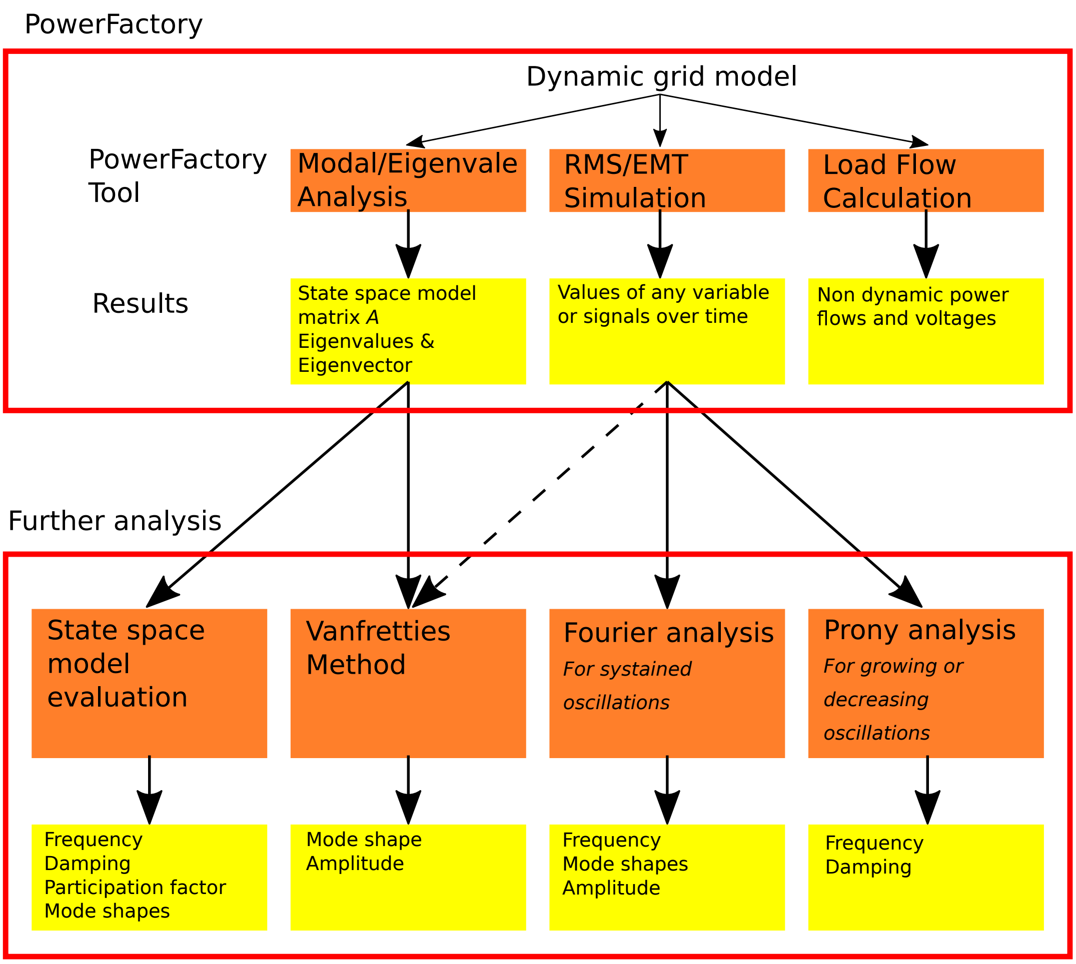

Figure 3.2: Overview of methods used in this research. For each method, the results which can be expected are shown. It is depicted which tools in PowerFactory are used.

3.3. Modelling steps

This research defines three modelling steps to properly investigate and mitigate wind turbine induced SSOs in a grid. These steps are as follows:

- **Wind Power Plant on a weak radial connection to the grid:**
  The literature shows weak grids are more prone to SSOs. Therefore, a small weak grid is ideal to find and verify sub-synchronous behaviour. Also, the sensitivity of the sub-synchronous modes to different control parameters can be tested and compared to literature. This model will be used in chapter 4.

- **WPP in the IEEE 39 bus system:**
  The IEEE 39 bus system is a reference system which is often used to test new grid elements. It has well known characteristics which make it ideal for research. In this step, the WPP model from the previous step will be implemented in the grid without further modification to the control systems. The observability of SSO modes will be tested and influence of grid operation will be tested using this model. This model is used in chapters 5 and 6.

- **Implemting WAMC in the IEEE 39 bus system:**
  Using the results of the previous steps, a WAMC system is implemented in the IEEE 39 bus system. The effects on damping of SSO modes is tested.

3.3.1. Weak radial grid

First, a small grid is modelled to study sub-synchronous modes, which can be compared to literature [40, 52]. In this grid, a WPP with a capacity of 1050 MW is connected with a weak radial connection to the grid. This is shown in figure 3.3.

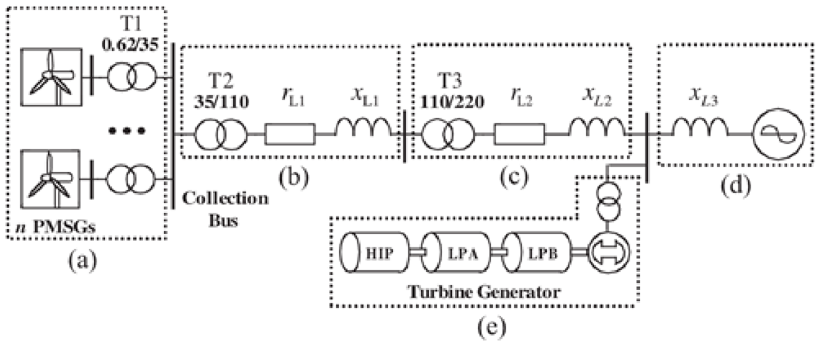

Figure 3.3: Weak grid model of multiple type-4 WT (a) connected by a weak link (b,c) to an external grid (d). At the connection point of the grid also, a synchronous generator is connected (e).

The wind turbine model used in the simulation is a template from the DIgSILENT Library: DIgSILENT FullyRatedConv WTG 6.0MW 50Hz [54]. This template is chosen because it has a similar grid following control structure as literature [40, 52]. Also other emerging PEIG often have the same similar control systems [45, 46]. The Fully Rated Converter WTG model definition is further elaborated in appendix C. This model only models the GSC of the type-4 WT. For this application this is sufficient since the RSC is decoupled by the DC-link [49].
The impedance parameters of the network are shown in table 3.1. The SCR of this network is calculated using equation 3.19 [42] and is found to be 1.34 based on 700 wind turbines of 1.5 MW each. In the model used in this research 175, 6 MW wind turbines are used. Since the output of the WPP is an aggregated result in both simulations, this difference can be ignored. Different voltage levels are present in the system. Each wind turbine has an output voltage of 620 V. Each wind turbine has its own transformer (T1), stepping up the voltage to 35 kV. At this voltage level, the power from all wind turbines is collected and sent to the next step up transformer (T2), which transforms it to 110 kV. A short line connects it to the last step up transformer (T3) for the voltage to be raised to 220 kV. A long line

connects the turbines to an infinite grid at this voltage level. This model is a realistic representation of how a remote WPP would be connected to the grid.

$$\text{SCR} = \frac{\left(\frac{S_B}{\Sigma_i x_i}\right)}{nS_{PMSG}} \tag{3.19}$$

Component	Resistance (p.u.)	Reactance(p.u.)
Line 1	0.02	0.12
Line 2	0.05	0.65
Line 3	0	0.08
Transformer 1	0	0.06
Transformer 2	0	0.07
Transformer 3	0	0.15

Table 3.1: Impedance of different components within the weak grid. Values in p.u. are based on S_B = 1500 MVA.

In the experiments on the sensitivity of different control parameters, six control parameters were varied as well as the inductance of the connection. The nominal values of these control parameters are shown in table 3.2. The inductance will be varied by changing the length of line 2, which has the most significant inductance.
Only one parameter will be varied at a time. This means the influence of only one parameter at a time can be investigated around the same nominal operation point.
The nominal control parameters are related to values which are used in literature modelling [13, 55–58]. However, no consistent set of parameters is mentioned in different literature. Therefore, a set of nominal control parameters is chosen that fall in the range of possible values. The nominal parameters are chosen such that the nominal sub-synchronous mode is close to unstable. This enables minimal modification to create an unstable system on which further analysis can be performed. Furthermore, the power output is set to 5% of the rated power output. This is the same setting used in [40].

Model	Name	Symbol	Value	Notes
Current Controller	Proportional gain Active current	$K_{d,p}$	0.2	
Current Controller	Integrational gain Active current	$K_{d,i}$	40	In PowerFactory model, this parameter is defined as a time constant T_d (see appendix C).
Current Controller	Proportional gain Reactive current	$K_{q,p}$	0.2	
Current Controller	Integrational gain Reactive current	$K_{q,i}$	40	In PowerFactory model, this parameter is defined as a time constant T_q (see appendix C).
PLL	Proportional gain	$K_{PLL,p}$	3	
PLL	Integration gain	$K_{PLL,i}$	100	

Table 3.2: Overview of nominal control parameters which are researched on their influence on sub-synchronous modes in a weak system. The values represent the base values of each variable.

In this section, the results of different simulations of this base weak grid will be discussed. In the next chapter, other results will be discussed when these six control parameters and line inductance are varied. It is important to know the characteristics of the base system in order to understand what changes by varying the control parameters.

In figure 3.4 the results of a eigenvalue analysis performed using the base values defined in 3.2 are shown. All normal eigenvalues are coloured blue, and the two eigenvalues which form the sub-synchronous mode are shown in red. This mode will be referred to as the sub-synchronous mode. This mode has a sub-synchronous frequency of ω = 85.5 rad/s or f = 13.6 Hz. The damping is σ = -2.34 s^{-1} which gives this mode a damping ratio of ζ = 0.027.

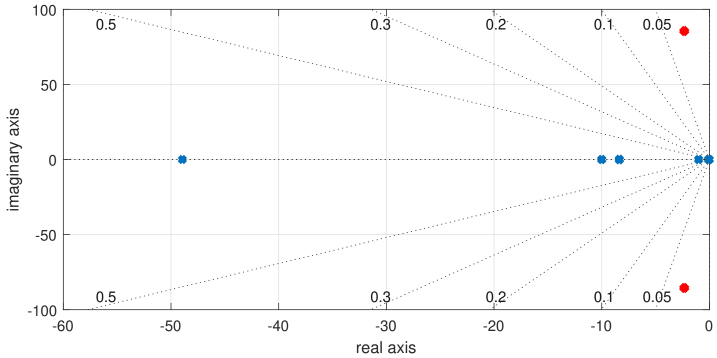

Figure 3.4: Eigenvalues of the base weak grid. All normal eigenvalues are in blue, and the two red eigenvalues form the sub-synchronous mode. The diagonal lines show a constant damping ratio ζ

Model	State Variable	Value	Notes
Current Controller	x_d	0.34	State variable of the PI controller
Current Controller	x_q	0.36	State variable of the PI controller
PQ Controller	$x_{p,ctrl}$	0.02	State variable of the PI controller
PQ Controller	$x_{q,ctrl}$	0.02	State variable of the PI controller
PLL	x_1	0.00	State variable of the PI controller [59]
PLL	x_2	0.26	State variable of the integrator [59]

Table 3.3: State variables which have relevant or significant participation factors.

The PI state variables all operate in the same way as described by equations C.1 - C.3 in appendix C. The state variable x_2 of the PLL is used in the integrator to convert the frequency ω, which results from the PI controller to an angle θ. This PI controller is shown in figure B.6 in appendix B.
Only 6 of the 20 participation factors of the state variables are shown in table 3.3. These participation factors are either selected because they have a value which is not close to zero or are interesting for this research.
The results in table 3.3 show that the current controller has the highest participation factor for both the d-axis and q-axis. The outer control loop or PQ controller has a significant lower participation factor. The slower characteristics of this controller could explain this. The PI controller of the PLL has no participation, while the integrator has a significant participation factor but is smaller than the current controller. It is important to realise that x_2 is placed directly behind the PI controller of the PLL with state variable x_1. Therefore, x_1 is still shown in these results. Because x_1 has a zero value and x_2 does not, it is suspected that the proportional gain is more important in this sub-synchronous mode. The proportional gain influences x_2 but not x_1.

3.3.2. IEEE-39 Bus System

The IEEE-39 bus system is a model often used in research and publications [60]. It is based on the grid of New England in the northeast of the USA. The model is further elaborated on in appendix C and [60]. An schematic overview of the modified network is shown in figure 3.5. In this figure a WPP is connected to bus 12. This is research the WPP can be connected to bus 12, 16, 23, 26 and 38.

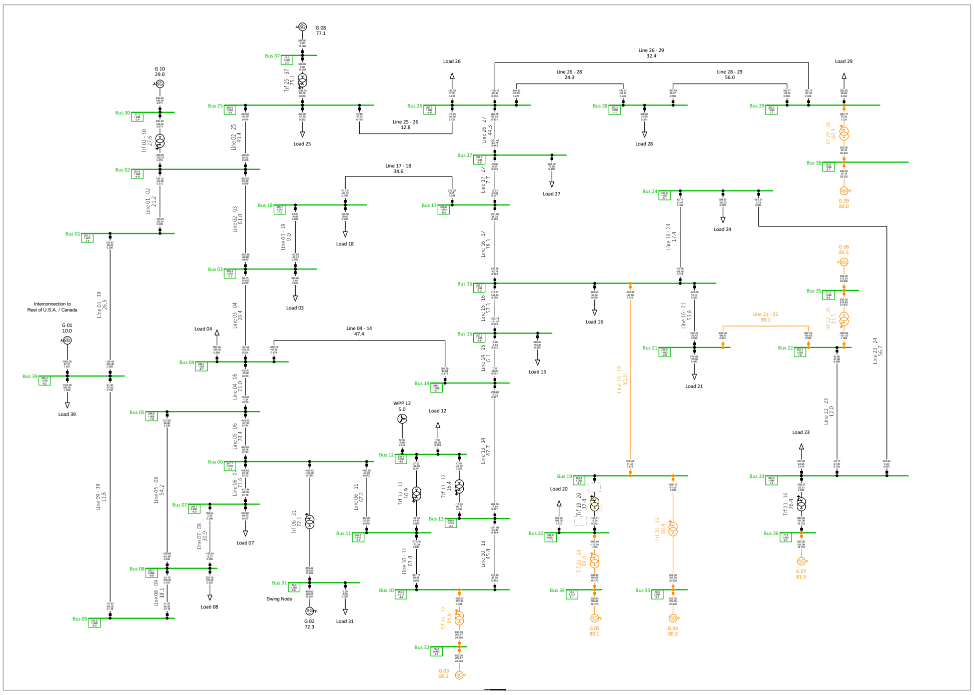

Figure 3.5: Overview modified IEEE-39 bus system. At bus 12 a WPP is connected to the grid.

In this step, the same WT model will be implemented in the network as used in the previous step. The observability of sub-synchronous modes will be tested in this step. This is done to determine at which buses PMUs would be most suitable to observe and relay measurements to the control systems of the WTs.

It is important to realise that the IEEE 39 bus system has many more state variables than the radial weak grid. This is because every SG has a dynamic model which adds a couple of state variables each. In total, this system has 166 state variables without the WPP connected compared to only 20 state variables in the radial weak grid. The SG will introduce inter area oscillations to the system. These are oscillations of generators or groups of generators whose rotational speeds oscillate against each other. This is a well known feature of the IEEE 39 bus system and is therefore often used to test Power System Stabilizer (PSS) [61, 62]. In order to separate these oscillation modes from sub-synchronous oscillations introduced by the WPP an analysis of the eigenvalues is performed without any WPP connected. These results are shown in figure 3.6.

In the results, a group of eigenvalues is visible in the upper and lower right corner, which all have a damping factor $\zeta < 0.1$. These are the inter area oscillations of different generator groups oscillating against each other. The mode plot on the right shows the generator speeds of the mode, which are marked in red in the eigenvalue plot on the left. From this mode plot, it can be seen that for this mode, generators 4 and 5 oscillate together against generators 6 and 7. This mode is taken as an example. Other inter area modes have similar characteristics of one or more generators being opposite to another group of generators.

Although the mechanism behind these inter area oscillations is entirely different compared to sub-synchronous oscillations, it is vital to know where these oscillations are present in the system. Otherwise, these can easily be confused with one another. These are shown to get to know the base characteristics of the network before introducing sub-synchronous modes induced by a WPP.

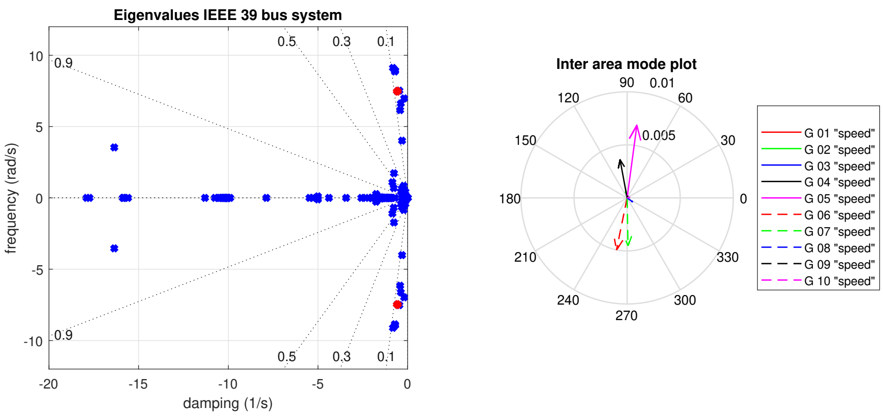

Figure 3.6: Eigenvalues of normal IEEE 39 bus system (left) and a mode plot of the generator speed of one of the modes (right).

4

Modelling of Weak Radial Connection

This chapter discusses the influence of six different parameters in the control system of a type-4 wind turbine on the eigenvalue of the sub-synchronous mode. In addition, the influence of the line reactance or short circuit ratio is discussed. These results are compared to literature. The current controller and short circuit ratio results are compared to the results presented in [40]. The results for the PLL are compared to [55]. Also, the participation factors of important state variables in the model are presented. These results are used to contribute to answering research question 1 of this thesis research.
The weak radial grid is the most simple model which can be used to simulate sub-synchronous oscillations. This step in this research is to compare the model's behaviour to literature. This is done to ensure the model is suitable for simulating sub-synchronous oscillations in further steps. Additionally, it gives some useful hand on experience and insight into the behaviour. An overview of the method used to obtain the results presented in this chapter is shown in figure 4.1.

4.1. Influence of Current Controller

As described in the previous chapter, the current controller consist of two PI-controllers for the d- and q-axis. Therefore, the current controller has four parameters. A proportional gain and integration gain. The proportional gains have a nominal value of 0.2 and are varied from 0.04 to 0.40. The integration gains have a nominal value of 40 and are varied from 20 to 100. The influence on the eigenvalue of the sub-synchronous mode is shown in figure 4.2.

It is shown that the influence of the parameters on both axes have very similar behaviour. The proportional gains have little influence on the frequency of the mode. An increasing proportional gain increases the stability as the eigenvalue moves further to the left-hand plane. Small proportional gains even lead to an unstable system.
The integration gains both influence the damping and frequency of the sub-synchronous mode. Increasing the integration gain leads to both a higher frequency and damping.
These results can be compared to [40]. The first thing to note is that the results presented here have a significantly lower oscillation frequency ranging between 10.7 to 19.1 Hz. In literature, the frequencies range between 20 and 44 Hz. This could be explained if the nominal values of the parameters are significantly different. Also, the damping is much more sensitive to the influence of the control parameters found in this research.
The general direction for the d-axis parameters is similar to the literature. The results for the q-axis a different from literature. In literature, frequency increases for an increasing proportional gain. Furthermore, the system would become less stable when the integration gain increases. These differences could also be caused if the nominal parameter values are very different.
In figure 4.3 the change in the participation factors when the different control parameters are varied.
A significant decrease in participation is visible as the proportional gain increases for one of the axes in the current controller. The decreases are partially compensated by an increasing participation in the other axis and "x2" of the PLL.
The participation of the PQ controller on both axes does not change significantly due to the varying proportional gains. The integration gains have to opposite effect on the current controller and PLL as

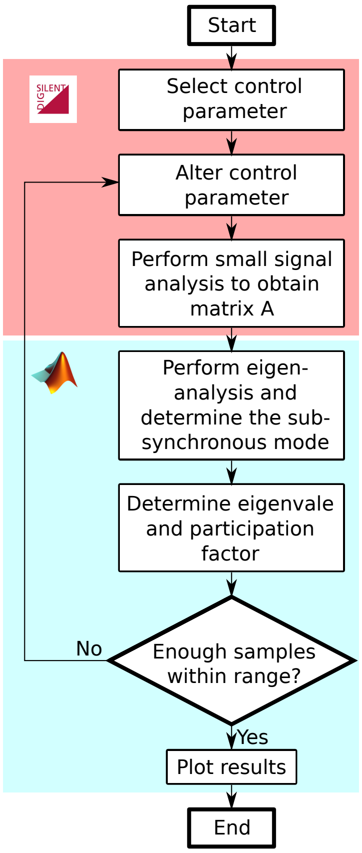

Figure 4.1: Flow diagram of used methods to obtain the results for this chapter.

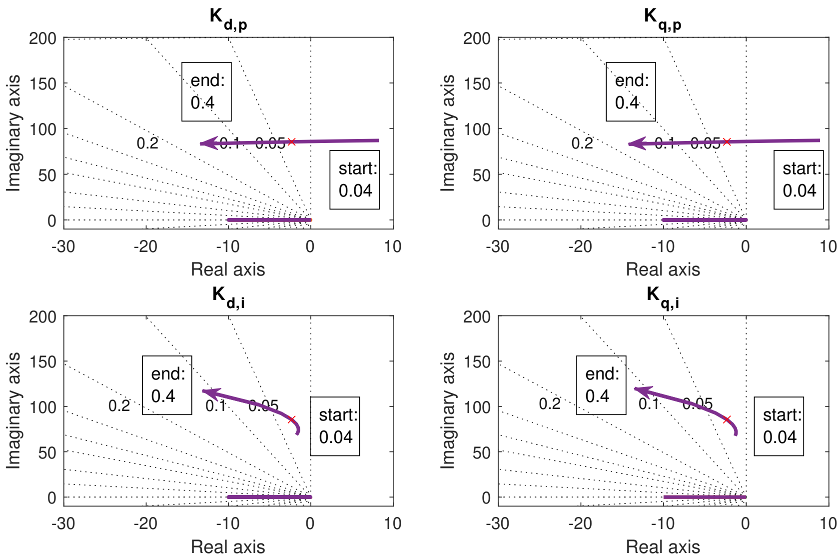

Figure 4.2: Eigenvalue mobility for varying the control parameters of the current controller. The parameters for the d-axis are shown on the left and the right for the q-axis. Arrows indicate the direction of increasing the parameter. The red cross indicates the nominal eigenvalue.

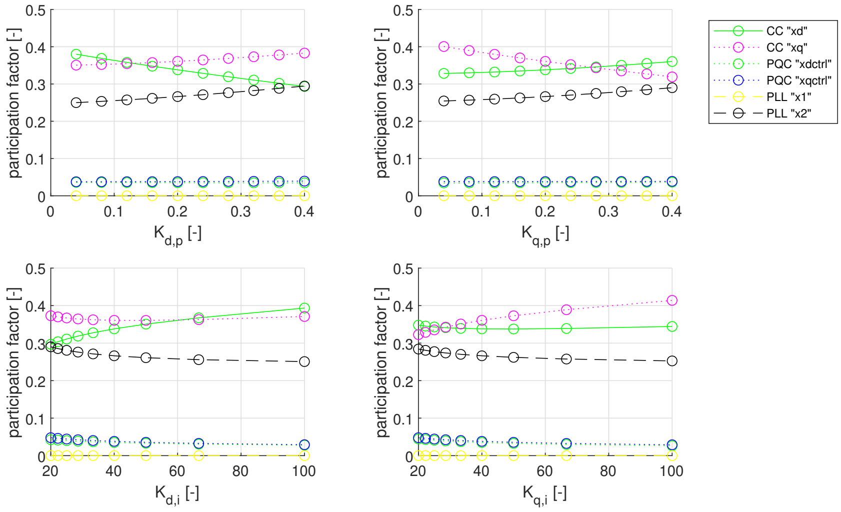

Figure 4.3: Influence on the participation factors as the four parameters of the current controller (CC) are varied. State variables of the current controller, PQ controller (PQC) and PLL are shown.

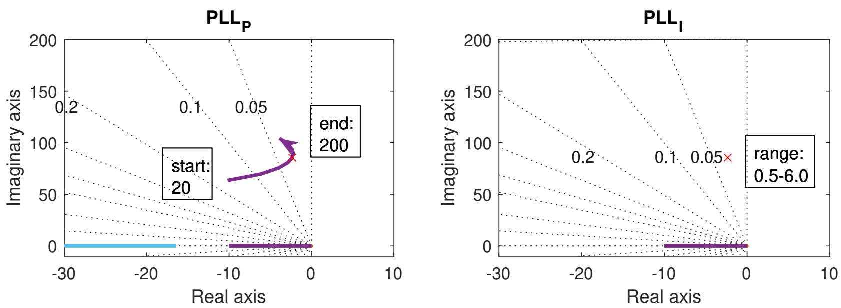

Figure 4.4: Eigenvalue mobility for varying the control parameters of the PLL. On the left, the proportional gain is shown. On the right, integration gain is shown. The arrows indicate the direction of increasing the parameter. The red cross indicates the nominal eigenvalue.

the proportional gains. As they increase, the participation also increases on that axis. This increase in participation is again mainly compensated by decreasing the participation in the perpendicular axis and "x2" of the PLL.
The participation of the PQ controller decreases slightly when the integration gains are increased. There is no significant difference between the two axes of the PQ controller.

4.2. Influence of Phase Locked Loop

The PLL uses an internal PI controller to keep track of the voltage angle. This voltage angle tracking is used in the current controller to perform a Park- and Clarke transform. These transform the current signals from a grid reference frame to a reference frame related to the voltage angle at the local bus. In the nominal operating point state, variable "x2" of the PLL significantly influences the sub-synchronous mode.
The nominal value of the proportional gain is 100 and is varied from 20 to 200. The integration gain nominal value is 3 and varies from 0.5 to 6. The influence of these parameters on the eigenvalue of the sub-synchronous mode is shown in figure 4.4.
It can be seen that as the proportional gain increases, also the frequency increases. The real part of the eigenvalue at first increases and then decreases again. This gives the least damping of the mode around the nominal operating point.
The integration gain is varied and leads to no significant change in the eigenvalue. Therefore, only the nominal operating point is shown as a red cross.

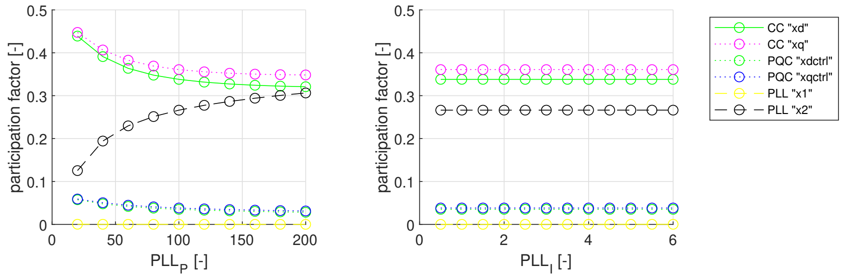

Figure 4.5: influence on the participation factors as the parameters of the PLL are varied. State variables of the current controller (CC), PQ controller (PQC) and PLL are shown.

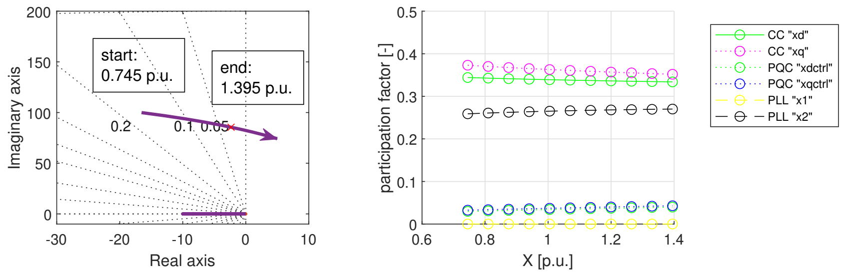

Figure 4.6: On the left, eigenvalue mobility for varying the line inductance of the radial connection. The arrow indicates the direction of increasing the line inductance. The red cross indicates the nominal eigenvalue. On the right, the influence on the participation factors as the line induction varies. State variables for the current controller (CC), PQ controller (PQC) and PLL are shown.

These results closely resemble the trajectory found in [55] for influencing the parameters of the PLL. In figure 4.5 influence on the participation factors by varying the PLL parameters is shown. It is shown that an increase of the proportional gain leads to a bigger participation factor for state variable ”x2” of the PLL. This is mainly compensated by the participation of the PI controllers of the current controller. Where the d-axis decreases more than the q-axis. Additionally, the PQ controller decreases a little bit in participation.
Just as in the eigenvalue, changing the integration gain has no significant influence on the participation factors of the control system.

4.3. Influence of Short Circuit Ratio

The total inductance determines the short circuit ratio of the system in the connection as formulated in equation 3.19. Therefore, the inductance is varied in this part. The nominal inductance of the connection is 1.07 p.u. and varies from 0.745 p.u. to 1.395 p.u. This results in a short circuit ratio ranging from 1.92 to 1.02. Note that an increased line inductance leads to a lower short circuit ratio. The results are shown in figure 4.6.
It can be seen that the increased line inductance leads to a lower frequency and a less damped system. This is compliant with the results found in [40]. In much other literature, it is also described how connections with a lower short circuit ratio are more prone to sub-synchronous oscillations [7, 16, 49, 52, 55, 63, 64].
The participation factors react slightly to the change line reactance. This is because the line reactance does not directly affect the control system of the WPP. The PLL participation increases slightly while the current controller's participation decreases on both axes as the line reactance increases.

4.4. Prony Analysis

In order to verify the eigenvalues, which are the result of small signal analysis, a Prony analysis is performed on a time signal of an unstable mode. The time simulation and the selected Prony window is shown in figure 4.7. The selected operation point is drawn from the experiment of increasing the

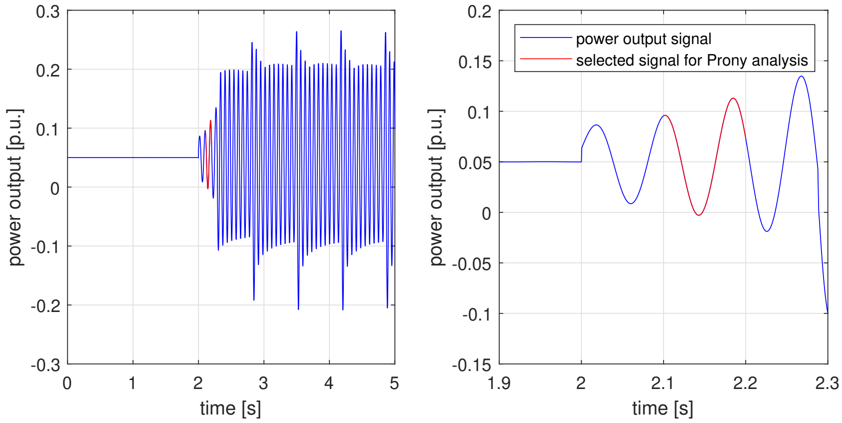

Figure 4.7: On the left, a power output signal of the WPP in an unstable operation. The control parameters have nominal values while the total inductance is X = 1.395. The same signal is shown on the right and focused on the Prony window.

Parameter	Small Signal Analysis	Prony Analysis	Units
damping σ	4.98	3.62	1/s
angular speed ω	74.2	74.7	rad/s
damping ratio ζ	-0.067	-0.049	
frequency f	11.8	11.9	Hz

Table 4.1: Comparison between small signal analysis results and Prony analysis results of an unstable operation.

line inductance. The line inductance is set to 1.395 p.u., which corresponds to the far right point of the trajectory depicted in figure 4.6. A Prony window between t = 2.1 s and t = 2.2 s is selected. The results of the eigenvalue determined by the small signal analysis and the Prony analysis are compared in table 4.1.

From these results, it can be seen that the frequency is closely matched. σ has a significant relative error contributing to an error in the damping ratio ζ. Still, the eigenvalue is in close proximity to each other in the imaginary plane. This result shows that the small signal analysis can indicate how sub-synchronous oscillations can grow in a power system.

4.5. Conclusions

In this step of the research, six parameters of the control systems and one grid parameter are investigated for their influence on the stability and frequency of sub-synchronous oscillations. These results are compared to literature. This comparison is made to verify if the used models are suitable for research on SSO.

In the current controller, the PI controller that controls the current on the d-axis is very similar to literature. The PI controller for the q-axis moves differently compared to that same literature [40]. The proportional gain has an opposite effect on the frequency, and the integration gain has the opposite effect on the damping, which is predicted by literature. In the literature, no exact definition of the nominal control parameters is given, which could explain the different behaviour.

The PLL also has a PI controller to track the voltage angle of the connection bus. It is found that the eigenvalue of the sub-synchronous mode is not sensitive to the integration gain of the PLL. The proportional gain shows the same trajectory of the eigenvalue as is shown in literature.

As a grid parameter, the line inductance is varied. This variation influences the SCR, a measure for grid strength. It is found that the weaker the connection becomes, the less damping will be present, and the system becomes more prone to SSO. This is in agreement with a lot of literature.

The instability of the system in one of the operational modes is shown using a time simulation. Using Prony analysis, the damping and frequency are compared to the eigenvalue found by small signal analysis of the same operational point. In the imaginary plane, these two points are close to each other.

To conclude, most results show that the used model behaves mostly similarly to models used in literature to study SSO. Therefore, this model can be used as a basis for the next two steps of this research. The results presented in this chapter contribute to answer research question 1 of the this thesis research.

5

Sub-Synchronous Oscillations in the IEEE-39 Bus System

This section investigates the propagation of SSO induced by a WPP in the IEEE-39 bus system. The results presented in this chapter formulate an answer to research question 2 of the thesis research. For this investigation, the same nominal operation point for the WPP will be used as in the previous step unless other specified.
First, a method described in [22] will be tested. This method describes how voltage changes in buses can be determined by using the rotor angles from the mode vector of any mode. These results are compared to time simulations of a SSO in the network. Additionally, the importance of the participation factors will be shown.
An overview of the method used in this chapter is given in figure 5.1.

5.1. Observability of Oscillations

In equations 3.8-3.17 a method of [22] to determine voltage changes in buses due to a mode oscillation is described. This method will be referred to as Vanfretties method. This method is tested by inducing a SSO by an unstable mode. Fourier transforms and Prony analysis of time signals of the bus voltages are compared to the results of Vanfretties method. Two different locations will be used to create an unstable mode. The WPP will be connected to buses 12 and 38. These locations are selected based on their positions in the grid. They are both on the grid's edge, resulting in a weaker connection. This makes fewer or non other modifications necessary to create an unstable operational point. This is one of the examples of how knowledge from the previous step is used in this research step.

5.1.1. Wind Power Plant at Bus 12

In order to create an unstable operation, some modifications to the network are made. The transformer connecting bus 12 to bus 11 is put out of service. This weakens the connection to the grid. Also the proportional gains in the current controller were decreased to $K_{d,p} = K_{q,p} = 0.1$. All other control parameters are the same as the nominal values used in the previous step. Small signal analysis yields a state space model which has a sub-synchronous mode of $\lambda_{SS} = 10.20 \pm j97.85$ at the initial conditions. Also, a time simulation of 10 seconds is performed. No events or triggers are used to induce a SSO. After about 2 seconds, a SSO becomes visible, which grows for about 1 second when a sustained oscillation is visible. The results of a time simulation of the voltage magnitudes V_i and voltage angles θ_i is shown in figure 5.2. A Prony analysis is performed on both the voltage magnitude and voltage angle of bus 12. Although all buses eventually have a sustained oscillation, Prony analysis is only performed on bus 12. It is found that each bus has a slightly different timing of the start of the growth of the oscillation. Therefore, it is difficult to determine a suitable Prony window for all signals. Using a Prony window between t = 2.15 s and t = 2.25 two pairs of eigenvalues are found. One for the voltage magnitude signal and one for the voltage angle signal. These values are $\lambda_{V_{12}} = 10.32 \pm j99.45$ corresponding the V_{12} and $\lambda_{\theta_{12}} = 9.67 \pm j100.34$ corresponding to θ_{12}. The Prony window of both signals is

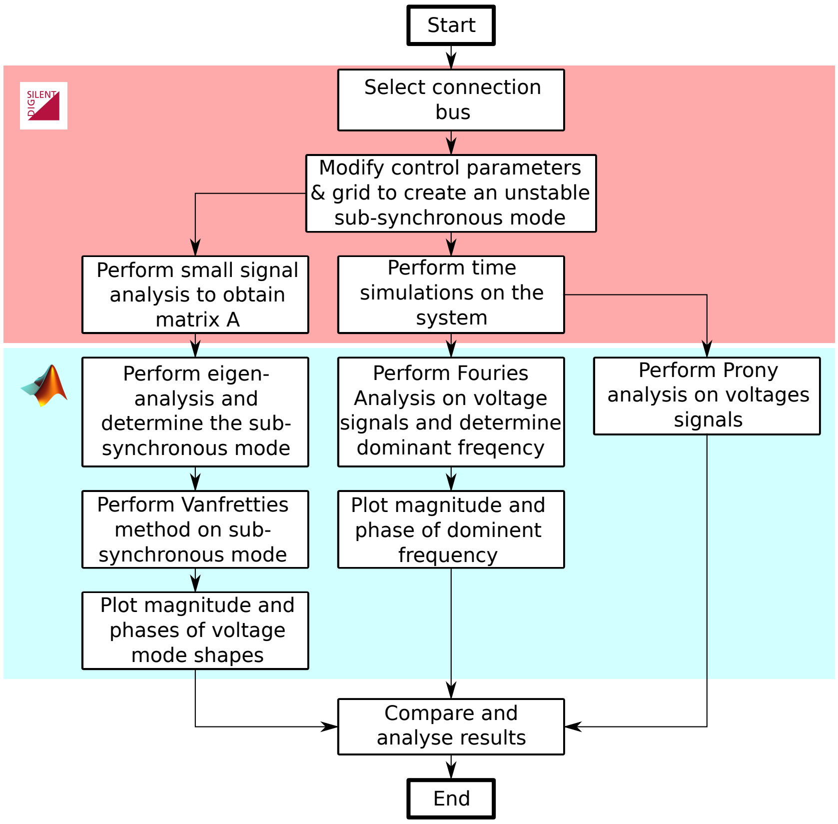

Figure 5.1: Flow diagram of used methods to obtain the results for this chapter.

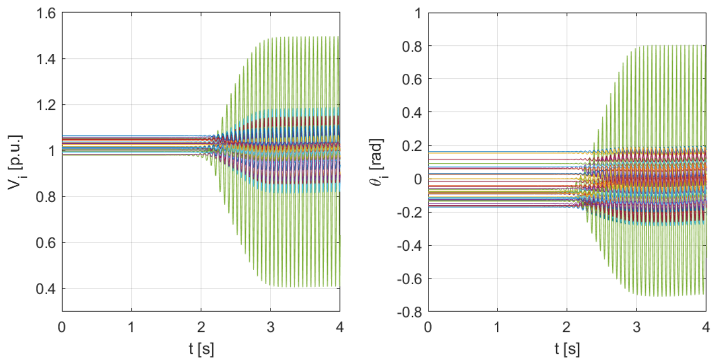

Figure 5.2: Results of time simulation between t = 1 s and t = 4 of unstable operation of a WPP connected to bus 12. Nominal control parameters are used except for $K_{d,p} = K_{q,p} = 0.1$. Additionally, transformer connecting bus 11 and 12 is disconnected. On the left, the voltage magnitudes V_i and voltage angles θ_i are shown on the right.

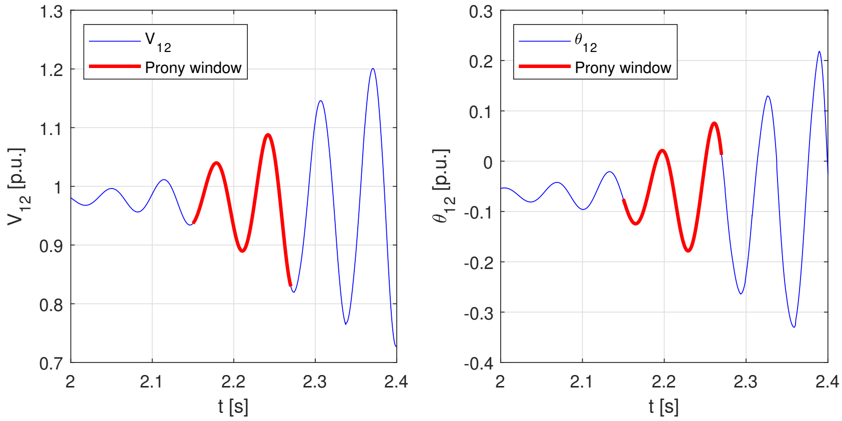

Figure 5.3: Prony window of unstable operation of a WPP connected to bus 12. Nominal control parameters are used except for $K_{d,p} = K_{q,p} = 0.1$. Additionally, transformer connecting bus 11 and 12 is disconnected. On the left voltage magnitude V_{12} and on the voltage angle θ_{12} is shown.

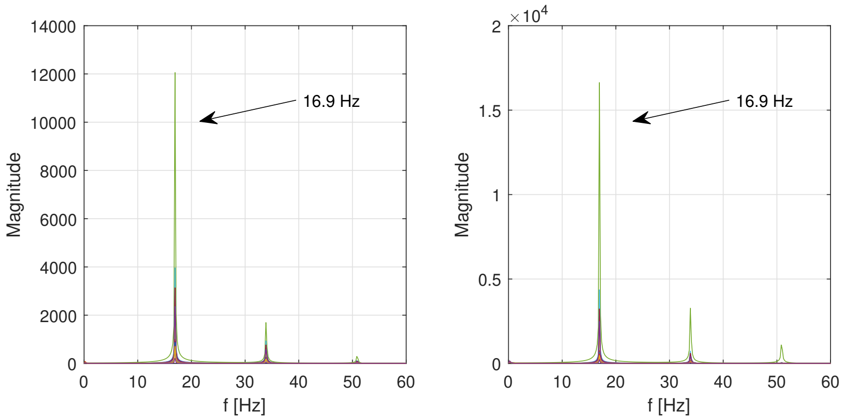

Figure 5.4: Results of Fourier analysis on the voltage signals V_i and θ_i during sustained oscillation between t = 4 s and t = 10 s.

shown in figure 5.3.

Additionally, a Fourier transform is taken from the time frame in which a sustained SSO is visible. This is between t = 4 s and t = 10 s. This is done for every bus in the system for both V_i and θ_i. The resulting resulting amplitudes for each frequency is shown in figure 5.4. It can be seen a the main frequency element is present at 16.9 Hz. Some smaller peaks are visible at 33.9 Hz and 50.8 Hz. These are exact multiples of the dominant frequency. These are present because the sinusoidal signals' shape is slightly skewed towards a saw tooth signal. This results in these other peak appearances in the spectrum. The results of the Fourier transform are compared to the results of Vanfretties method. The magnitude and phase of the peak frequency at 16.9 Hz are used for this comparison.

In order to implement Vanfretties method, all necessary data should be collected from the model. First, an admittance matrix $\mathbf{Y}_{nn}$ should be constructed. This is done by considering the current topology and loads of the network. In some places, the impedance should compensate for a tab change in some transformers. The resulting matrix can be verified by multiplying the matrix with a voltage vector $\mathbf{V}_n$ as described in equation 3.11. The results show only significant currents $\mathbf{I}_i$ in buses on which generators are connected. The extensions of the admittance matrix can then be determined using the transient reactances of the generators, which are described in [60]. The last inputs needed are bus voltages $\mathbf{V}_n$ and excitation voltages of the generators $\mathbf{E}_N$. These are obtained by exporting the results of the time simulation in PowerFactory. The values are taken as an average from the first 0.1 seconds of the simulation, during which no oscillations are present. This method is chosen because of the simplicity of exporting the data from PowerFactory. Note that these time signals do not represent a dynamic

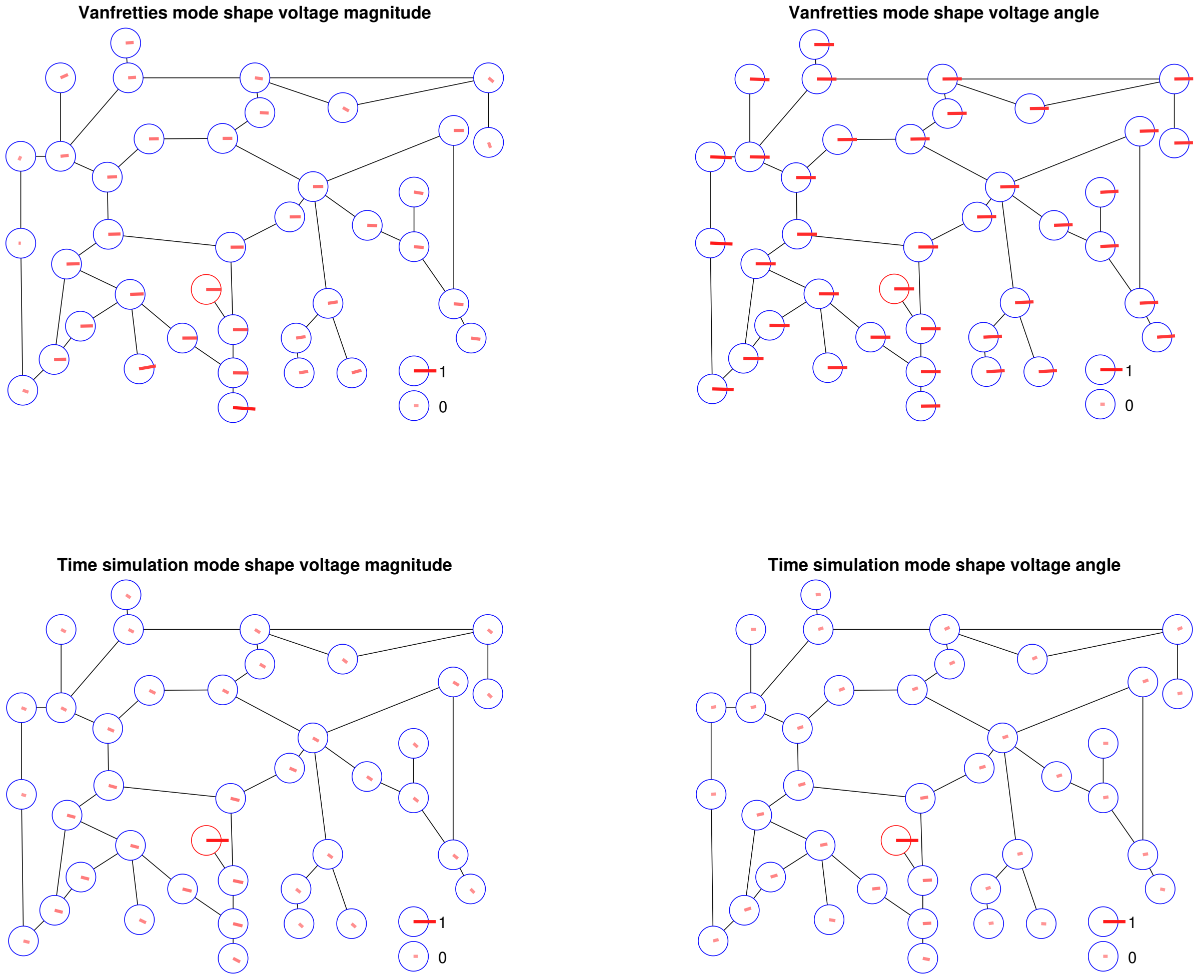

Figure 5.5: Comparison between normalised results of Vanfretties methods on the sub-synchronous mode and Fourier transform of voltages on the time simulation. On top, the results of Vanfrettis method are shown. On the bottom, the Fourier transform results are shown. On the left are the voltage magnitude oscillations ΔV_{12}. On the right are voltage angle oscillations $\Delta \theta_{12}$.. Bus 12 is marked with a red circle.

situation. At last, equations 3.15 and 3.16 are used to determine the sensitivities of the voltages to changes in the rotor angle. Matrices $\mathbf{C}_{V\delta}$ and $\mathbf{C}_{\theta\delta}$ can then be constructed. The mode shapes of the rotor angles can be used to find the oscillations $\Delta\mathbf{V}$ and $\Delta\boldsymbol{\theta}$. The mode shapes are found in the eigenvector of the sub-synchronous mode, which can be found using small signal analysis. The results of equations 3.8 and 3.10 give the mode shapes. These magnitude and phases are used to compare the results of the Fourier transform.

In figure 5.5, the results of Vanfretties method and the Fourier transform of the time simulations are compared. In this figure, the results for four result variables are shown. The results using Vanfretties method are used in the top for both the voltage magnitude oscillations as a phasor and voltage angle oscillation amplitude as a phasor. The bottom plots show the same results from the Fourier analysis of the sustained oscillations determined in the time simulations. In the four quadrants, the IEEE-39 bus system is drawn, with each bus represented as a circle. Inside each circle, a bar is shown. The length of the bar is related to the magnitude, and the angle represents the phase of that oscillation. These results are normalised for each result as the magnitude has great differences between the different methods. The phases are set in reference to bus 12. Therefore, magnitudes and phases can only be compared to buses of the same data set. Their overall differences can then be compared to the other networks.

It is seen that for Vanfretties method does not give the most significant amplitude at bus 12. The amplitudes are biggest at buses where generators are connected. For the voltage amplitude oscillation,

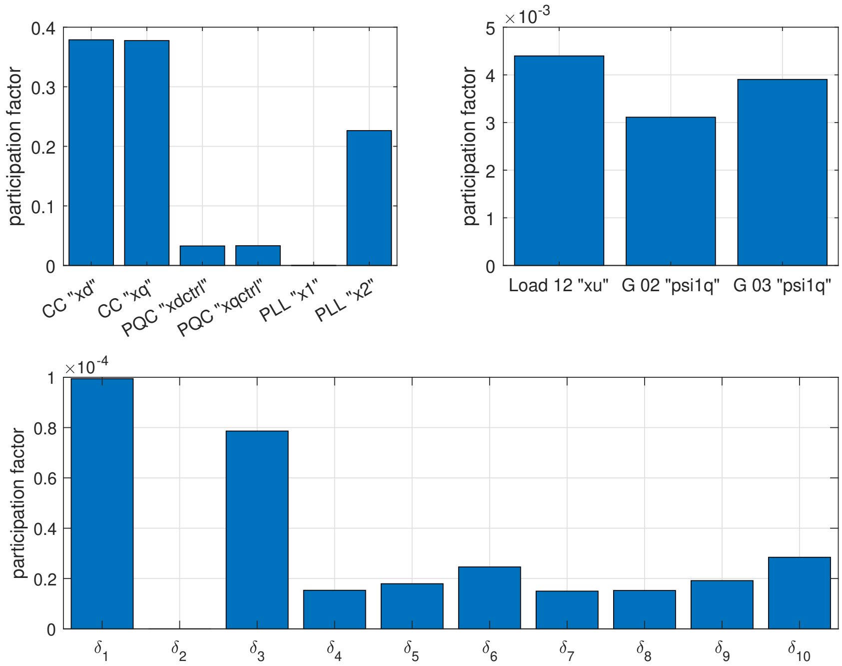

Figure 5.6: Participation factors of state variables in the sub-synchronous mode for WPP connected to bus 12. On the top left, the WPP control state variables are shown. On the top right other significant state variables are shown. On the bottom, the participation factors of all rotor angles of synchronous generators are shown.

the magnitude decreases much more over distance than the voltage angle oscillation. Close bus 12, the phases are relatively close to bus 12. However, on the edges of the network, some more extreme phases are present for the voltage magnitude oscillation. The voltage angle oscillations phases are not significantly different compared to bus 12.

The Fourier transform results show a clear decrease in amplitude further away from bus 12. This is valid for both the voltage magnitude and voltage angle oscillations. The phases of the voltage magnitude oscillations generally lag more as the distance from bus 12 increases. For the bus angle oscillation, the opposite is true.

In general, the results of Vanfretties method do not agree with the results based on a time simulation of this system. In order to understand these differences, the participation factors are investigated. The participation factors of the sub-synchronous mode are shown in figure 5.6.

It is important to note that the different bar plots have entirely different scales on the y-axis. The control system of the WPP shows similar participation factors as presented for the radial weak grid. Also, participation factors bigger than 0.001 are shown not to miss any essential state variables. These state variables are all related to grid elements in close proximity to the WPP. Lastly, the participation factors of the rotor angles δ_i of all connected SG are presented. First of all, it can be noted that the participation of δ_2 = 0 because this generator is the reference of the system. The maximum value of the participation factors is related to state variable δ_1, which is equal to 10^{-4}. As the rotor angles are an essential input of Vanfretties method, this could explain the results which do not comply with the time simulations.

The participation factors are a result of the small signal analysis of the system. Therefore it is important to also compare the results of the small signal analysis to the results of the Prony analysis and the Fourier transform results. The damping and oscillation frequency results are compared in table 5.1.

From the results in this table, it can be seen that the sub-synchronous mode identified from the small signal analysis is in general agreement with the time simulation results. The actual sub-synchronous frequencies are a bit higher. The damping determined from the Prony analysis is similar to the damping of the sub-synchronous mode.

Method	Frequency [Hz]	Damping [1/s]
Small Signal Analysis	15.6	10.2
Prony Analysis Voltage magnitude	15.8	10.3
Prony Analysis Voltage angle	16.0	9.7
Fourier transform Voltage magnitude	16.9	-
Fourier transform Voltage angle	16.9	-

Table 5.1: Comparison of frequency and damping results of different methods for an unstable WPP connected to bus 12.

Method	Frequency [Hz]	Damping [1/s]
Small Signal Analysis	10.6	4.8
Prony Analysis Voltage magnitude	11.3	2.3
Prony Analysis Voltage angle	11.4	2.1
Fourier transform Voltage magnitude	11.2	-
Fourier transform Voltage angle	11.2	-

Table 5.2: Comparison of frequency and damping results of different methods for an unstable WPP connected to bus 38.

5.1.2. Wind Power Plant at Bus 38

A WPP is connected to bus 38 of the IEEE-39 bus system. In order to create an unstable operation, line 28-29 is disconnected to create a weaker connection to the rest of the grid. Additionally, SG 9, also connected to bus 38, was out of service. This creates an unstable system. All control parameters were kept to the nominal values described in the previous step of the weak radial grid. Small signal analysis is performed to determine a sub-synchronous mode. This is used to execute Vanfretties method. Furthermore, time simulations are done to find oscillating bus voltages in the system. From these time simulations, Prony analysis is done on the voltage magnitude V_{38} and voltage angle θ_{38} signals of bus 38 in a time window where the oscillation is growing. A Fourier transform is taken from all buses for V_i and θ_i. The results of Vanfretties method and the Fourier transform are shown in figure 5.7.

In the results of Vanfretties method, the maximum amplitudes are on the bus of the closest SG. The amplitude in voltage magnitude oscillations ΔV_i decreases slightly at further distances from this generator. The phase of the oscillation does not change significantly. Similar results are visible for the magnitude of the oscillations for the voltage angle oscillation $\Delta\theta_i$. However, the phase of the oscillations both lags and leads in different parts of the grid. In the Fourier transform results, a significant decline in oscillation amplitude over distance away from bus 38 is visible. This is true for both voltage magnitude oscillation and voltage angle oscillation. The phases of the voltage magnitude oscillations lag significantly at further distances from bus 38. The voltage angle oscillations are slightly leading away from the WPP at bus 38.

Because of these big differences between Vanfretties method and the Fourier analysis in results, the participation factors are also further looked into. The participation factors of the sub-synchronous mode are shown in figure 5.8.

The bar plots have a completely different scale on the y-axis. The participation factors in the control system of the WPP are the most significant. The participation factors are very similar as presented for the weak radial grid. Some other participation factors of state variables with a value bigger than 0.001 are shown. Most of these relate to elements relatively close to the WPP. An exception on this is G 04 ”psi1q”, which is actually far away from bus 38. The participation factors of the rotor angles δ_i are all very small. The participation factor of δ_8 is the greatest with a value of $1.2{\cdot}10^{-4}$. As the mode shapes of these state variables are the input of Vanfretties method, this can explain low compliance to the time simulation results.

To verify the results of the small signal analysis, the eigenvalue of the sub-synchronous mode is compared to the results of the Prony analysis and Fourier transform. These are based on the time simulation of the system. The results are compared in table 5.2.

These results show that the eigenvalue frequency is slightly less than the frequency determined from the time simulation. The damping is slightly bigger compared to what is found in the Prony analysis. Although there are slight differences between the sub-synchronous eigenvalue from the small signal

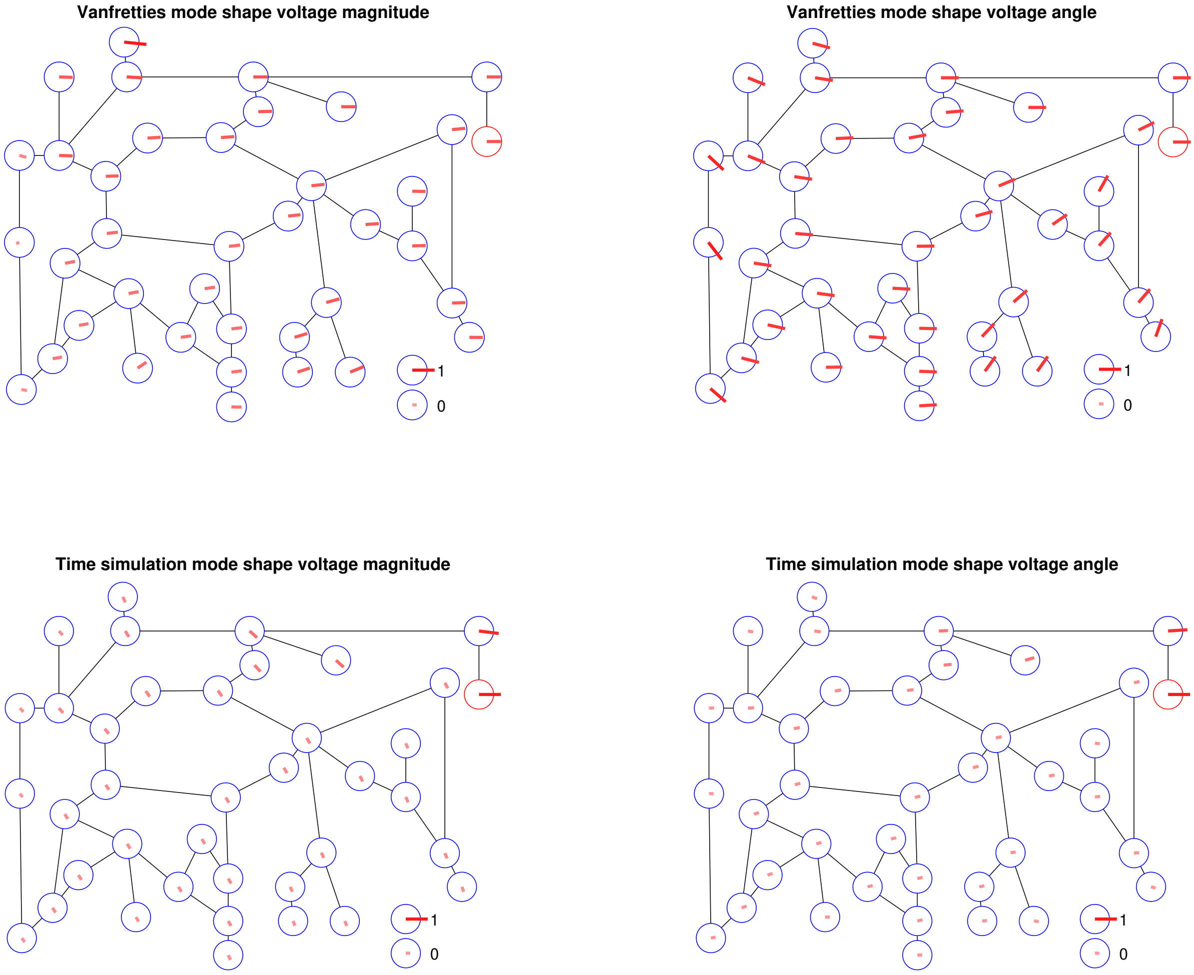

Figure 5.7: Comparison between normalised results of Vanfretties methods on the sub-synchronous mode and Fourier transform of voltages on the time simulation. On top Vanfrettis method is shown. On the bottom, the Fourier transform is shown. On the left are the voltage magnitude oscillations ΔV_{38}, and on the right are the voltage angle oscillations $\Delta \theta_{38}$.. Bus 38 is marked with a red circle.

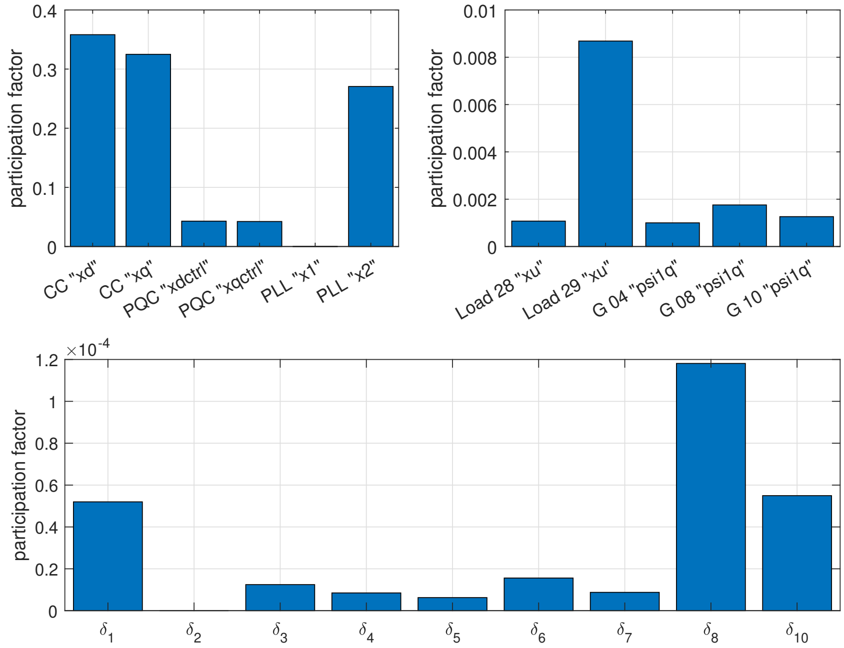

Figure 5.8: Participation factors of state variables in the sub-synchronous mode for WPP connected to bus 38. On the top left, the WPP control state variables are shown. On the top right other significant state variables are shown. On the bottom, the participation factors of all rotor angles of synchronous generators are shown.

analysis and the time simulation, the eigenvalue agrees with what happens in the time simulation.

5.2. Conclusions

The simulation results of two unstable systems are shown. Different methods to analyse the SSO are tested. Vanfretties method gives very different results than Fourier transform results. This can be explained because Vanfretties method uses the rotor angle mode shapes $\Delta\boldsymbol{\delta}_i$ as an input. However, it is shown that the participation of these rotor angles in the sub-synchronous mode is insignificant. Therefore, they are unsuitable for analysing SSO induced by type-4 wind turbines. This does not mean Vanfretties is unsuitable for all purposes. It could be used for modes with significant participation of the rotor angles. However, this is not tested in this research.

The eigenvalue related to the sub-synchronous mode is a good representation of the oscillations in time simulations. The damping was compared to the results of a Prony analysis during the growing phases of an oscillation. The frequency was compared to the results of the same Prony analysis as well as to the results of a Fourier transform of the results during the sustained oscillations.

Lastly, important insight is provided in the behaviour of SSO in the grid. It is found that the amplitude of the oscillations decreases strongly as the distance to the source increases. The voltage magnitude oscillation lags, moving further away from the source. The voltage angle oscillation leads as the distance to the source is increased.

The results presented in this chapter are used to formulate an answer to research question 2 of this thesis research.

6

Influence of Grid Operation on Sub-Synchronous Oscillations

This chapter will discuss the results of grid operation variation on sub-synchronous modes. This will give insight into what conditions can lead to an increased risk of SSO. It will also contribute to answering research question 1. First, the different variations performed on the IEEE-39 bus network are explained. This is followed by showing the results of the influence on sub-synchronous modes. At last, the conclusions from this research step are presented.

6.1. Grid Operation Variations

Different features of the IEEE-39 bus system and WPP will be varied. The varied features are the connection point of the WPP and topology, the grid loading and power output of the WPP. Each of these variations will first be further elaborated on.

6.1.1. Connection Point of Wind Power Plant and Grid Topology

Each bus in the network is stronger or weaker connected to the rest of the network. This depends on the number of connections and the strength of these connections. In chapter 4, it is shown that long radial connections are more prone to risks of SSO. In this research step, five buses are selected with different types of connections to the rest of the grid. These are buses 12, 16, 23, 26 and 38. In table 6.1 these buses are further elaborated on. Also, the connections which will separately be taken out of service are described. In the results, buses will be distinguished by the number of connections. They are distinguished between buses with two connections or fewer and buses with more connections. The less connection a bus has, the more essential each connection is.

6.1.2. Grid Loading

The influence on the sub-synchronous mode by grid loading is tested. The grid loading is defined as the power output of all generators and demand of the loads, weighted to the nominal demand and generation. Decreasing the network loading will decrease power flow through the lines. Three steps of loading are used: 100%, 75% and 50%. To create these scenarios, the demand and generation are modified accordingly.

6.1.3. Power Output of Wind Power Plant

The influence of the power output of the WPP on the sub-synchronous mode is investigated by setting different power output levels. The power output levels for a single WT are defined as 0.3 MW, 3.0 MW and 6.0 MW. This leads to a power output of the whole WPP of 52.5 MW, 525 MW and 1050 MW. In some cases, the maximum power output can not be tested in all scenarios. This is because this amount of power which needs to be transformed by the available connections, causes the Load Flow Calculation to be non-converging.

An overview of the methods used is shown in figure 6.1.

Bus	Number of Connections	Description
12	2	Low voltage bus connected by two transformers to 2 different buses. These transformers are tested to be out of service.
16	5	High voltage bus with the highest number of connections in the whole system. 1 connection are connected to 2 SGs. This connection will not be tested to be out of service as it would create an island in the network. 2 connections together form the connection to a small area which has both loads and SG. 2 other connections are connected to other larger parts of the system. For these last 4 connections, the influence on the sub-synchronous mode will be tested when they are taken out of service.
23	2	High voltage bus at the edge of the network. It is connected by two lines connecting it to the rest of the network. Taking any of these lines out of service will create a radial connection. Also, another line on this circle connection will be taken out of service. This results in a radial connection where WPP is halfway this connection.
26	4	High voltage bus which is has 2 connections which together form a radial connection to bus 38. 2 other connections are used to connected to other parts of the network.
38	1 (2 behind transformer)	Low voltage bus which is connected by one transformer to bus 29. This is the endpoint of a long radial connection to the rest of the grid. This radial connection is formed by two parallel connections consisting out of 3 lines. Taking any of these lines out of service will weaken the connection to the rest of the grid.

Table 6.1: Description of the positions of the buses connecting the WPP.

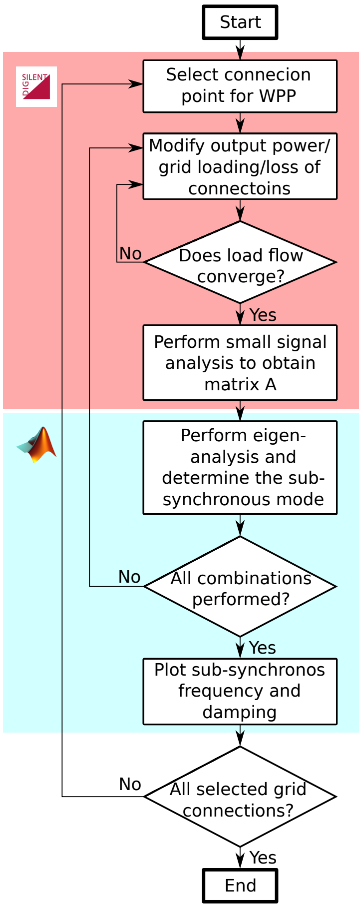

Figure 6.1: Flow diagram of used methods to obtain the results for this chapter.

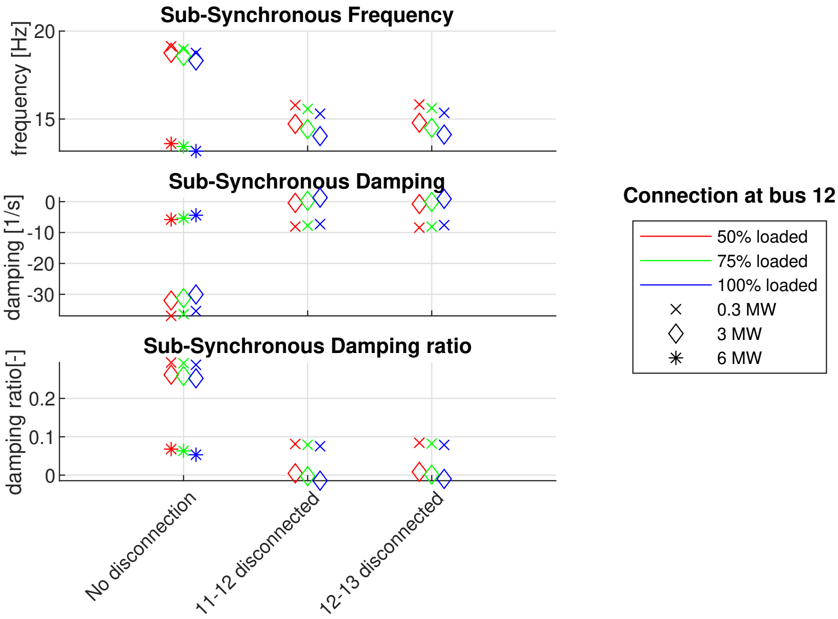

Figure 6.2: Mode results for operational variation for a WPP connected to bus 12.

6.2. Results

The results from this research step will be presented in two categories. First, the connection buses with 2 connections will be discussed. These are buses 12, 23 and 38. After this, the results of the buses with more than 2 connections will be discussed. These are buses 16 and 26.
The results for each connection will be presented in a separate figure. The results for the frequency, damping and damping ratio are shown in three plots. These are the results of the eigenvalue of the sub-synchronous mode. On the x-axis, the topology variation is shown. The colours represent the loading of the grid. Different markers represent the power output levels of the WTs.

6.2.1. Wind Power Plant with few connections

In figures 6.2, 6.3 and 6.4 the results for the WPP connected to bus 12, 23 and 38 are shown respectively. For these connections, it is visible that each connection lost to the rest of the grid has a negative impact on the damping. Furthermore, it will also decrease the sub-synchronous frequency. Similar results are present when the loading of the network is increased, or the power output of the WTs is increased. The results show some outliers in some cases for an increase of power output of the WPP. In these cases, the reduction in damping and frequency is more significant.

6.2.2. Wind Power Plant with multiple Connections

In figures 6.5 and 6.6 for the connection the WPP to bus 16 and 26 are shown respectively. For bus 16, it can be seen that the disconnection of 15-16 and 16-17 has a more significant influence on both the damping and frequency compared to the disconnection of 16-21 and 16-24. The function of these connections can explain the difference between the two pairs of connections. 16-21 and 16-24 are connected to a separate area which is less significant. The connections 15-16 and 16-17 are important for connecting to the rest of the grid. For the connection on bus 26, a similar situation is present. Connections 26-28 and 26-29 form a radial connection to a small network area. Disconnection of these lines has no significant influence on the sub-synchronous mode. The other connection for these two connection points has a more significant influence on the sub-synchronous eigenvalue. These connections are connected to a more significant part of the grid. The damping decreases in both cases. For the connection to bus 16, the frequency is increased, while for bus 26, the frequency decreases.
An increase in grid loading and power output of the WT both decrease damping and sub-synchronous frequency. The increase of power output leads to some out layers.

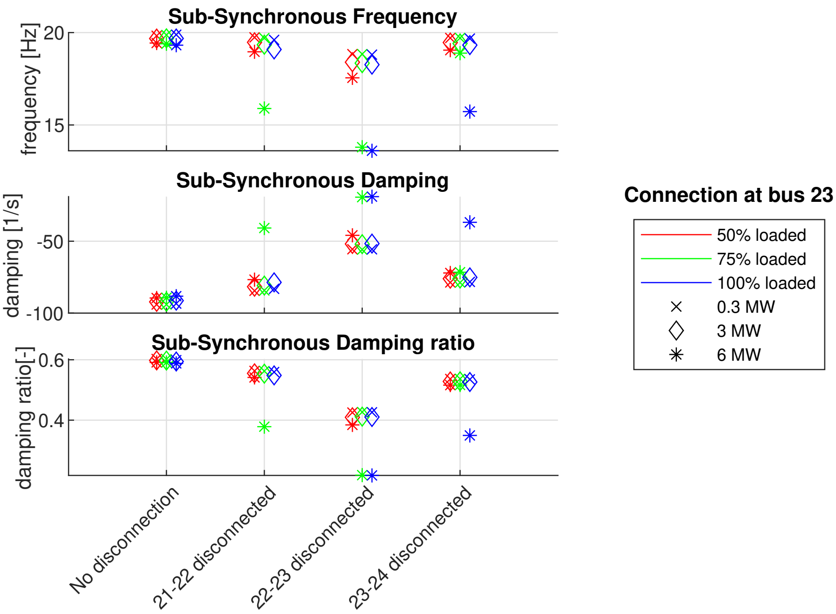

Figure 6.3: Mode results for operational variation for a WPP connected to bus 23.

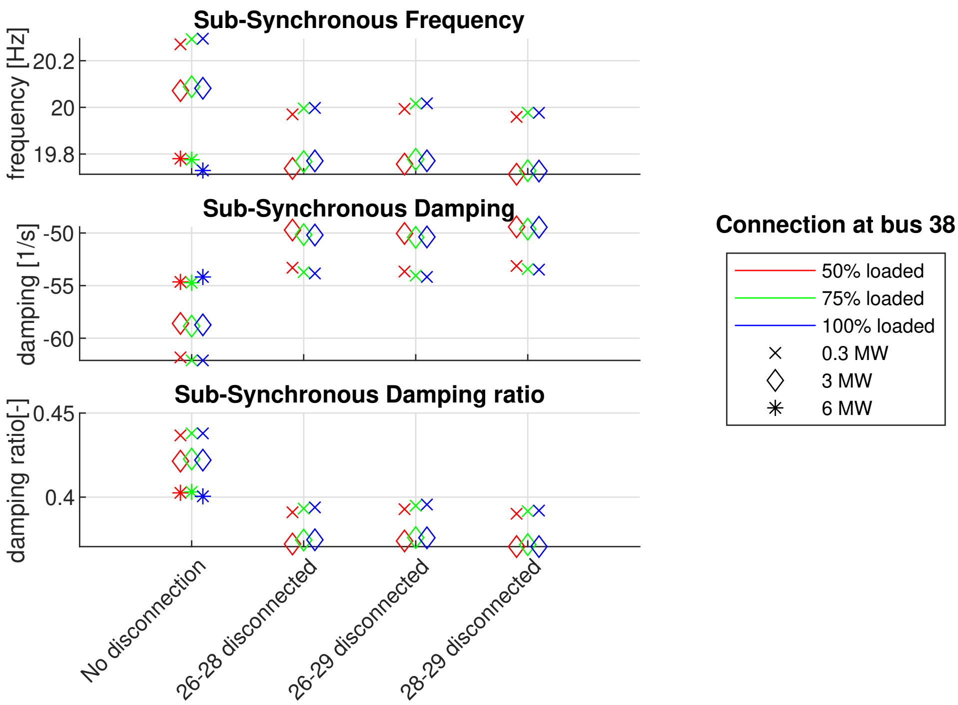

Figure 6.4: Mode results for operational variation for a WPP connected to bus 38.

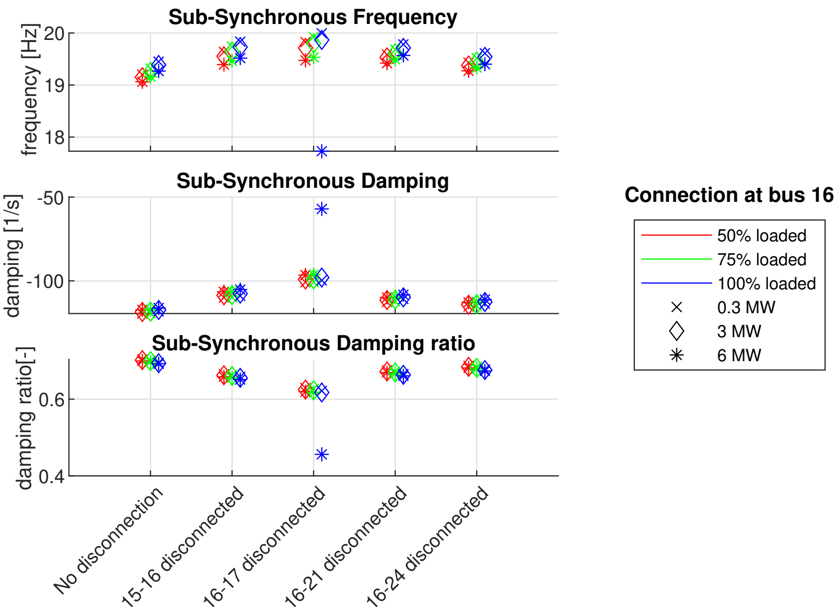

Figure 6.5: Mode results for operational variation for a WPP connected to bus 16.

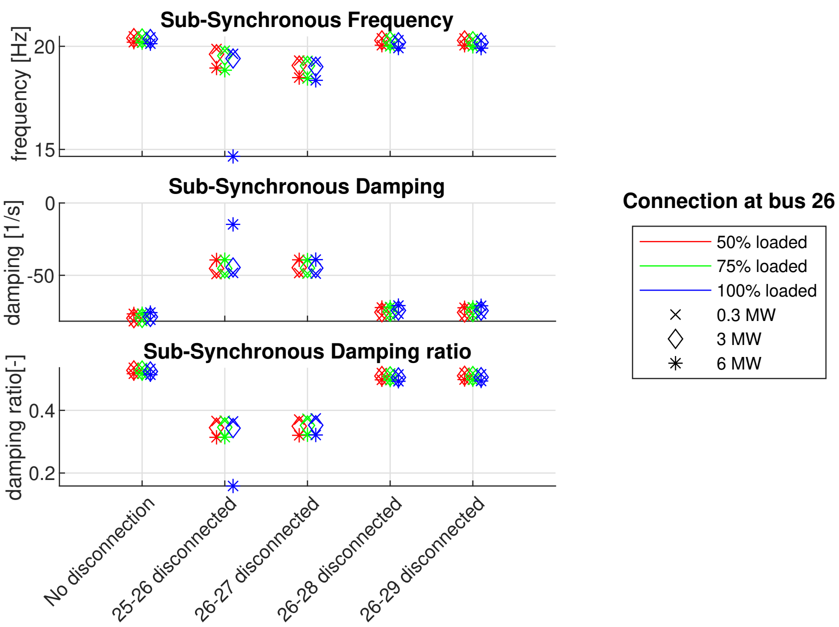

Figure 6.6: Mode results for operational variation for a WPP connected to bus 26.

6.3. Conclusions

Several conclusions can be made from the results of this research step on the influence of different grid operations on the sub-synchronous mode.
Firstly, an increase in loading of the network or power output of the WTs will always lead to less damping in the system and a decrease in the sub-synchronous frequency. In some cases, a sudden significant decrease in damping is shown in the results. There is no clear indication of why these outliers are present.
The significance of the influence of disconnecting a connection is strongly dependent on the importance of the connection. No significant change is observed if the connection is only connected to a small grid area. When the connection is connected to other a more significant areas of the grid, damping will decrease significantly. The frequency decreases in most cases. One case of an increase in frequency was observed when lines were disconnected.
The results presented in this chapter contribute to formulate an answer to research question 1 of this thesis research.

7

Implementation of Wide Area Monitoring and Control

This chapter discusses the implementation of a WAMC into the control system of a type-4 WT. First, the implementation itself will be introduced. This implementation is tested by comparing the time simulation results during the disconnection and reconnection of a transformer. Additional small signal analysis results support these results. At last, conclusions from this research step are presented. The results presented in this chapter give answers to research questions 3 and 4 of the thesis research.

7.1. Implementation into the Control System

This section introduces the implementation of the WAMC. First, the philosophy of this control system is explained. Then the modifications to the composite frame are discussed. After that, an additional model which collects the different signals is discussed. Also, the differential formulas which control this collector are explained.

The philosophy of this implementation of WAMC is based on the knowledge obtained from the previous chapters of this research. In chapter 5, it is concluded that the amplitude of SSO decreases strongly over distance. This is valid for both the oscillations in voltage magnitude and voltage angle. Therefore, a decision is made to feed information of an additional voltage angle of a remote bus. This can be implemented by adding a PLL block to the control system. In a real-world implementation, this data could be produced by a PMU. The signal of the PLL is used as a reference signal to the local PLL. The remote signal will determine how fast the local PLL signal can be changed. If the remote signal is also changing, this could indicate that the overall voltage angle in the system is changing due to outside circumstances. However, if only the local signal changes, this can amplify the SSO. The hypothesis is that this effect can be reduced by preventing the local PLL signals from adopting too quickly.

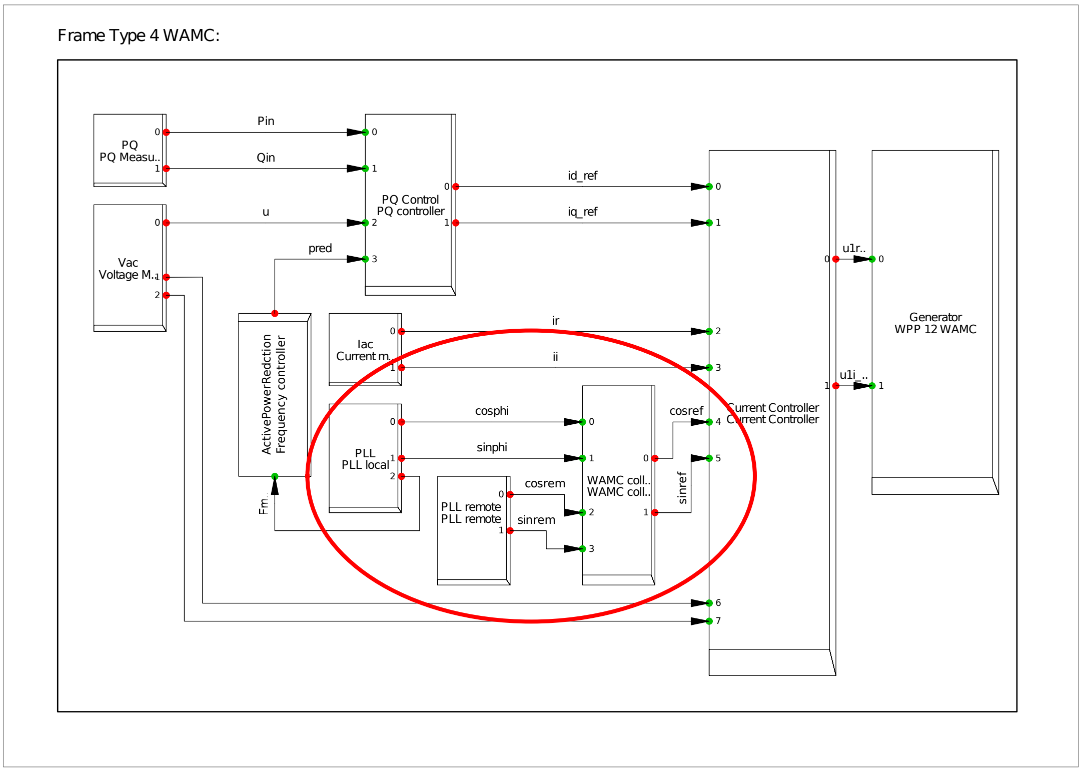

Figure 7.1: Composite frame of the implementation of WAMC. The red circle marks the modified blocks compared to the normal type-4 composite model.

In figure 7.1 the modified composite frame is shown. The red circle indicates the area in which elements have been added to the frame. An additional PLL is introduced for a remote bus. The signals of both the local PLL and the remote PLL are sent to a new model block which collects the signals and processes them. This block's output is then sent to the current controller's input. The current controller has no modification on how it handles these signals.

In figure 7.2 the collector model is shown. Three different types of blocks are present in the model. The remote signals are first fed into a delay block to model delays due to communication. The signals are also differentiated to calculate the rate of change of the angle in the collector block. The collector block receives the delayed and differentiated signals of the remote PLL as $dcos_{rem}$ and $dsin_{rem}$. The signals of the local PLL are fed directly to the collector as $cosphi_{in}$ and $sinphi_{in}$. These signals are normally directly fed to the current controller. In this control system rate of change of the local signals is limited by the remote signals.

In the collector block equations 7.1 to 7.6 are defined. These equations K_{loc} and K_{rem} are parameters used to weigh the local and remote signals. $d\theta_{rem}$ and $norm$ are used as internal variables. $cost$ and $sint$ are defined as state variables. This means these variables will be part of the small signal analysis. First, the angular speed $d\theta_{rem}$ of the remote voltage angle is calculated.

$$d\theta_{rem} = \sqrt{dcos_{rem}^2 + dsin_{rem}^2} \tag{7.1}$$

The differential of the state variables is calculated using the difference between the input of the local PLL and the output of the block. The differential is weighted to K_{loc} and the product of K_{rem} and $d\theta_{rem}$. This causes the rate of change of the output signal to be directly related to the rate of change measured on the remote PLL.

$$\frac{dcost}{dt} = (K_{loc} + K_{rem} d\theta_{rem})(cosphi_{in} - cosphi_{out}) \tag{7.2}$$

$$\frac{dsint}{dt} = (K_{loc} + K_{rem} d\theta_{rem})(sinphi_{in} - sinphi_{out}) \tag{7.3}$$

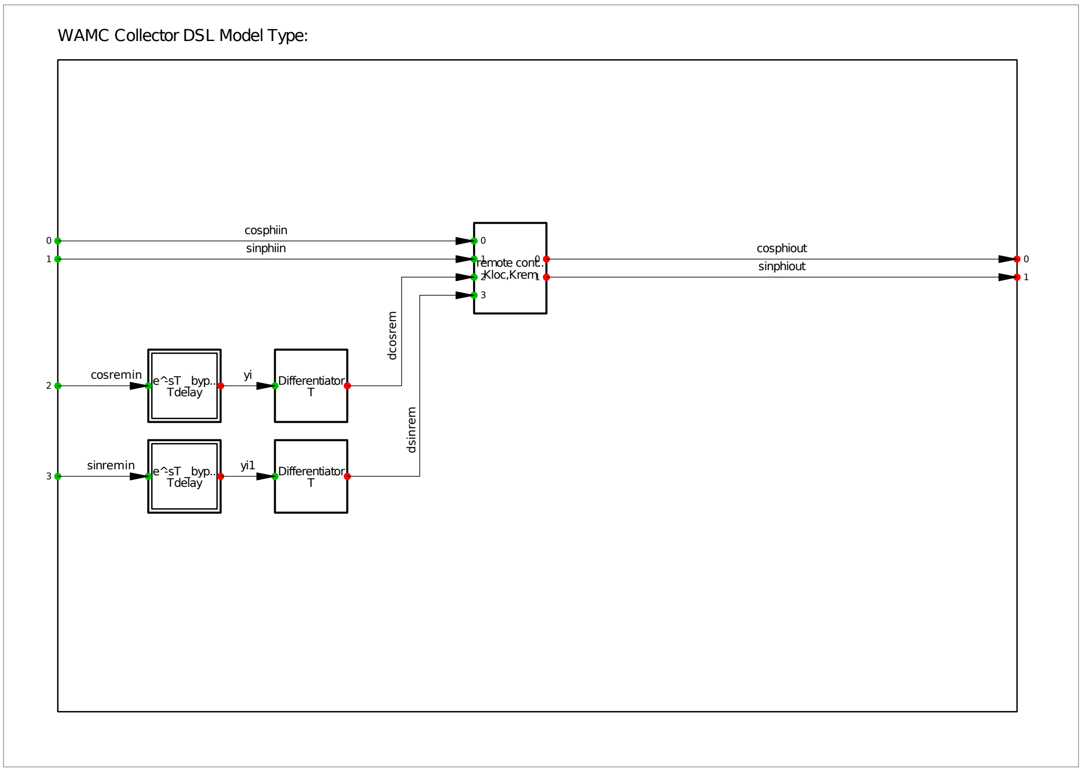

Figure 7.2: Block diagram of WAMC collector model.

Because equations 7.2 and 7.3 do not guarantee a normalised result the length is calculated as a normalising factor.

$$norm = \sqrt{cost^2 + sint^2} \tag{7.4}$$

The final output is then derived by the length to find a normalised result without altering the angle result.

$$cos_{out} = \frac{cost}{norm} \tag{7.5}$$

$$sin_{out} = \frac{sint}{norm} \tag{7.6}$$

7.2. Results of implementation of WAMC

This section will evaluate the improvements due to the implementation of WAMC. The behaviour of a WPP connected to bus 12 is analysed. The nominal settings of the current controller are used. The parameters of the WAMC collecter are set T_{delay} = 0.2 s, K_{loc} = 0.05 and K_{rem} = 1. Bus 6 is the remote bus for the PLL. The same nominal parameters are used for the remote PLL as for the local PLL.
A time simulation is performed in which one of the two transformers connecting it to the rest of the grid is disconnected at t = 1 s and reconnected at t = 3 s. The power output of the WPP is evaluated using Prony analysis. These results are compared to small signal analysis results for both the disconnected and connected situations of both WPPs. In figure 7.3 the results of the time simulation are shown for both WPPs.

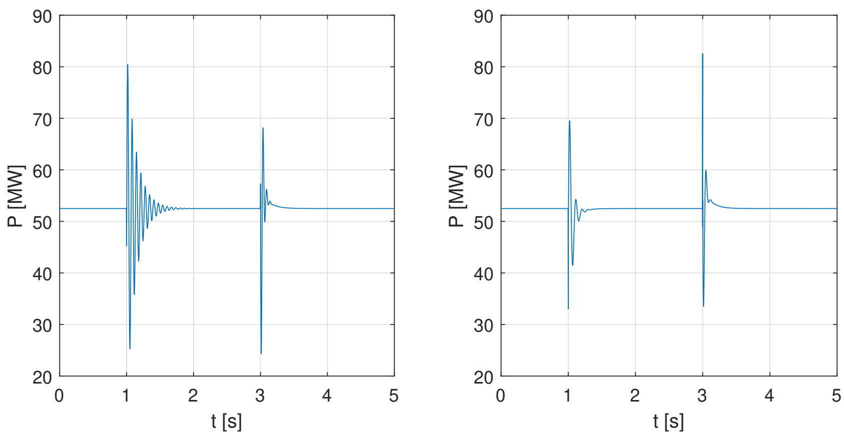

Figure 7.3: Comparison of power output oscillation for WPP without implementation of WAMC (left) and with the implementation of the WAMC. Nominal control parameters are used for the WPP. Transformation disconnection event at t = 1 s and reconnected at t = 3 s.

The oscillations without the WAMC take longer to stabilise. It can also be seen that the oscillations after reconnecting the transformer are more quickly damped. This is because, after the reconnection of the transformer, the WPP is stronger connected to the grid.
In figures 7.4 and 7.5 the Prony windows used are shown. Comparing the two figures shows that the first swing also has a smaller amplitude when the WAMC is implemented.

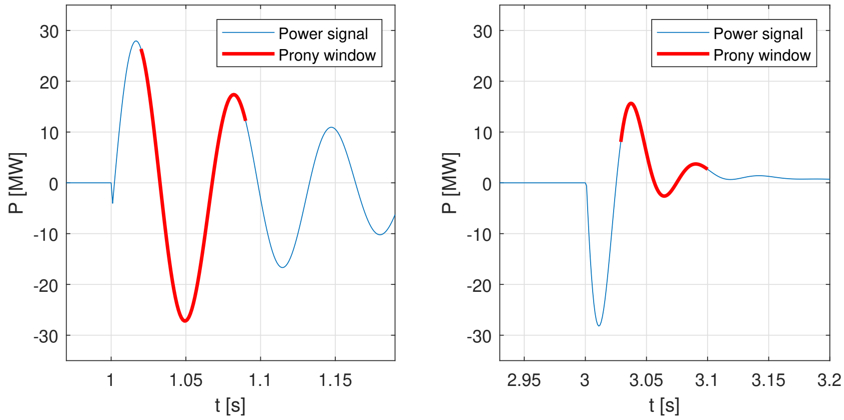

Figure 7.4: Prony analysis window after a switching event without WAMC implementation. Nominal control parameters are used for the WPP. On the left, the transformer is disconnected. On the right is the reconnection of the transformer.

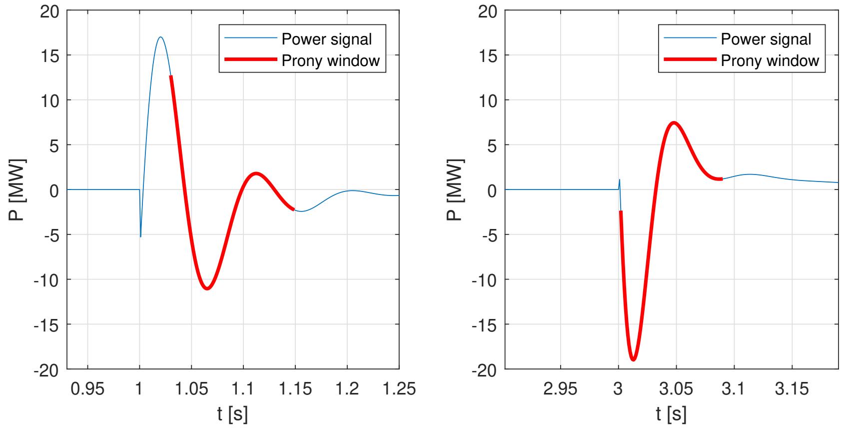

Figure 7.5: Prony analysis window after a switching event with WAMC implementation. Nominal control parameters are used for the WPP. On the left, the transformer is disconnected. On the right, the transformer is reconnected.

In table 7.1, the results of the Prony analysis and the small signal analysis are shown. From this, it can be seen that improved damping is achieved in all results. The sub-synchronous frequency decreases when WAMC is implemented. Together these changes also have a beneficial effect on the damping ratio. In figure 7.6, the significance of this eigenvalue change is illustrated in the imaginary plane. These are the results of the small signal analysis in the disconnected and reconnected transformer case.

	no WAMC			WAMC		
Transformer Connected	**Damping** σ **[1/s]**	**Frequency** f **[Hz]**	**Damping Ratio** ζ **[-]**	**Damping** σ **[1/s]**	**Frequency** f **[Hz]**	**Damping Ratio** ζ **[-]**
Prony Analysis	-38.3	16.2	0.35	-44.9	15.0	0.43
Small signal Analysis	-35.4	17.8	0.30	-45.5	13.8	0.46
Transformer Disconnected						
Prony Analysis	-5.7	15.1	0.06	-13.1	10.0	0.20
Small Signal Analysis	-7.3	15.3	0.08	-20.2	10.9	0.28

Table 7.1: Overview of results of Prony analysis and Small Signal Analysis of implementation of WAMC into the control systems of a type-4 WT.

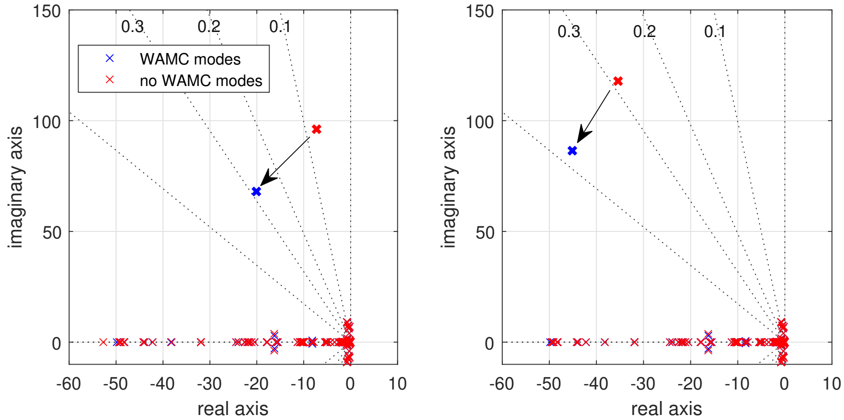

Figure 7.6: On left, change of sub-synchronous mode in the case of the disconnected transformer due to the implementation of WAMC. On the right, change of sub-synchronous mode due to implementation of WAMC, in the case all transformers connect

In figure 7.7, a comparison is made between the participation factor of the WAMC control systems and the classical control system. It can be seen that the participation of the (local) PLL is almost completely shifted to the already significant participation factors of the current controller. A small participation factor in state variable $sint$ of the WAMC is also visible.

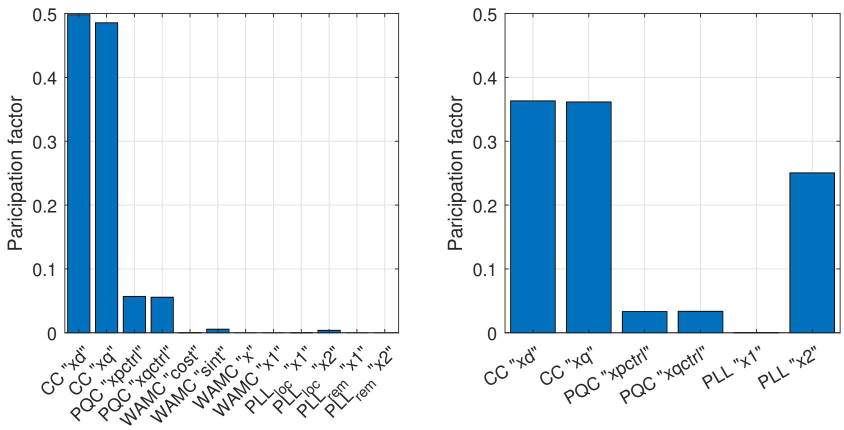

Figure 7.7: Comparison of participation factors of state variables in the control system of the WPP for a sub-synchronous mode. On the left, the results of WAMC implementation are shown. On the right, the results for a normal control system are shown.

7.3. Conclusions

In this chapter, an implementation of WAMC system was introduced for a type-4 wind turbine. A remote voltage angle is used to determine if the local voltage angle oscillations are local, possibly as SSO, or a wider oscillation. This implementation only requires a modification to this part of the control system. The used implementation significantly improved the damping of the sub-synchronous mode. Also, the sub-synchronous frequency is lowered, contributing to a lower damping ratio. Participation factors in the WAMC implementation system show that the participation of the local PLL has almost completely disappeared.

The results of this chapter give answers to research questions 3 and 4 of this thesis research.

8 Conclusion & Future work

This report presents the results of simulations performed to investigate SSOs behaviour induced by SSCI of type-4 WT. These results contribute to the scientific gap in the emerging phenomena due to the fast transition toward the power system of the future. In the power system of the future, more PEIG is integrated into the electrical grid.
During this research, a WT model is selected capable of modelling sub-synchronous behaviour. An aggregated WT model is used to model a WPP. Nominal parameters are selected and used as a base to observe behaviour changes. Six control parameters and one grid parameter are varied, and behaviour changes due to these variations are compared to literature. These simulations are performed in a small weak grid using a radial connection for the WPP. This enables the isolation of most behaviour from other influences of grid components. Although some differences exist in the behaviour compared to literature, there is enough confidence in the model to use it in further research steps.
In the following research steps, SSOs are modelled in the IEEE-39 bus system. This system is based on a real world system in New England, USA. The same base model is implemented in this grid model and can be connected to any bus in this system. In this model, unstable modes are created by minor modifications to the model parameters. This allows for observing the oscillation growth and frequency on all buses in the network. Using different methods, similar results are found. It is found that the SSO amplitudes decrease significantly over distance from WPP source. These results are then compared to results of Vanfretties method, which is found to be not valid for SSOs due to the low participation of SGs.
Grid operations are found to have a significant influence on the sub-synchronous mode. The connectivity to other significant parts of the grid is crucial for damping the sub-synchronous mode. Increased loading of the grid or power output of the WPP has a negative impact on the damping. In most cases, a decrease in damping goes hand in hand with a decrease in the frequency of the sub-synchronous.
Finally, a WAMC is integrated into the control system of the WPP. A remote voltage angle measurement determines voltage angle movements at the remote bus. This is used to dampen the measurement of the local voltage angle. In the case of a SSO, this helps to mitigate the oscillation. Small signal analysis and time simulations supported with Prony analysis are used to verify the desired outcome. It is found that damping is increased when wide area measurements are used.

8.1. Answers to research questions and discussion

1. **Which control- and grid parameters influence the frequency and damping ratio of SSOs?**
   In chapter 4, six control parameters are varied around the nominal values. These are four parameters of the current controller. It is found that increasing the proportional gains on both axes increases the damping and has little influence on the frequency of the sub-synchronous mode. The integration gains increase the damping and raise the frequency of the sub-synchronous mode. For the PLL, only the proportional gain influences the sub-synchronous mode. By increasing the proportional gain, the frequency is increased. The damping reached a minimum around the nominal value. The damping increases by increasing and decreasing the proportional gain from the nominal value.

In chapter 4, the SCR is varied to test the influence of the connection strength on the sub-synchronous mode. It found that weakening the connection strength will reduce the damping and the frequency of the sub-synchronous mode. This is supported by the results of chapter 6. When a line is disconnected, which is essential to connect the WPP to significant other parts of the grid, the damping and frequency both decrease.
Other results of chapter 6 show that an increase in grid loading and power output have similar results. Thus, the damping decreases, and the frequency decreases.

2. **How can the propagation of a SSO effectively be recognised through an AC transmission network?**
In chapter 5, results from all buses during a growing and sustained SSO are compared. These results include both the oscillations in voltage magnitude and voltage angle. Fourier analysis of these signals shows a clear spectral peak at the sub-synchronous frequency on all busses. The amplitude and phase of the oscillation at this frequency are compared for a sustained oscillation. The results show a clear decrease in sub-synchronous amplitude as the distance from the source increases. This is valid for both the voltage magnitude oscillations and the voltage angle oscillations. A difference between the two is shown in the phases. The voltage magnitude oscillation shows an increased lagging of the oscillation over increased distance. At the same time, the oscillation in the voltage angle shows a leading pattern over an increasing distance from the source. PMUs spread out through a network are able to detect both the oscillation in voltage magnitude and voltage angle. Using the accurate time stamping of the measurements the relative phases of the SSO can also be compared. This information can also be used to identify the source of the SSO.

3. **How to design a wide area controller to effectively out perform damping control that is exclusively based on local signals?**
From the results of chapter 5, it is concluded that the SSO amplitude decreases quite significantly over distance. At the same time, both literature and the participation factor results of chapters 4 and 5 indicate strong participation of the PLL on sub-synchronous modes. Therefore, the WAMC is implemented on the voltage angle measurement part of the control system. A remote PLL is introduced. In a real world implementation, this can be done by a data stream of a PMU. The movement of the remote voltage signal is used to determine the amount of damping on the local voltage angle measurement. A time delay is modelled to simulate any communication delays.
This implementation only requires modification on the parts handling the voltage angle measurements. All other model blocks of the control scheme are untouched. More comparisons can be made by using only a minimum amount of modification. Not only the effect on damping can be measured, but a comparison between participation factors can also be made. These comparisons are made in chapter 7.

4. **What is the effect of the implementation of WAMC based on PMU on SSO using minimal modifications?**
In chapter 7, the implementation of the WAMC on the voltage angle measurement is tested. This is done by comparing small signal analysis results and time simulation results. During the time simulation, one of two connections is disconnected and reconnected. The results from both methods show an improved damping ratio and lower sub-synchronous frequency when the WAMC is implemented. When the transformer is disconnected the damping ratio is increased from 0.08 to 0.30. Further tuning of the WAMC could improve the damping even more.

8.2. Scientific contributions

This thesis research makes two main contribution to scientific field of wind power integration into the electrical power grid. In previous work, the main focus is to explain past events and investigate the influence of control parameters and a little bit on grid strength.
This thesis research this is extended in the propagation of wind induced SSOs in an AC transmission network. The propagation is important to understand to estimate the danger of a sub-synchronous events. It is found that a SSO is quite a local event. Also the phase of the oscillation changes over distance. These results can form the basis to quickly identify the source of a SSO. The second contribution is an implementation WAMC in the control system of the type-4 WT. This implementation uses

a remote voltage angle measurement to enhance the damping of a sub-synchronous mode. These measurements can be provided using PMUs in the grid. An application to mitigate type-4 WT or other IBG induced SSOs using voltage angle measurements has not been previously been proposed. The implementation of the WAMC has been using small-signal analysis and time simulations. The results show a significant improvement in the damping ratio of the sub-synchronous mode.

8.3. Future Work

During this research, different phenomena and topics have been observed which do not fall within the scope of this research. Additionally, at some points in this research, assumptions of which the validity could be investigated.

- **Tuning of parameters in the WAMC system**
  In this research, little attention is given to tuning the parameters introduced in the newly designed system. In future work, attention can be given to this topic. An analytical analysis of the system could support this. Furthermore, the time delay considered for the PMU data stream is relatively long. This is done to ensure the minimum communication time. Investigation can be done on the minimum communication time and the influence of increasing or decreasing this delay. This time delay might even be a dynamic figure in a real world system as communication is disturbed.

- **Decrease of sub-synchronous oscillation amplitude over electrical distance**
  For the implementation of the WAMC, an assumption is made that the voltage angle oscillation amplitude at the remote bus is significantly smaller compared to local voltage angle oscillation in the case of a SSO. This is a qualitative result from chapter 5. However, more quantitative results can be obtained in future work. This could include a figure on how strongly the amplitude decreases over distance and which variables have a crucial influence. This can be line parameters, closely located loads or generators, or grid topology.

- **Impact of the utilisation of an aggregated model**
  This research uses an aggregated model of the WPP. The dynamic behaviour of only one WT is modelled and assumed to be the same for all WTs in the WPP. This is to improve computation times during simulations. Simulating every WT separately would still give them the same parameters. However, the interaction between the control systems of the different WTs could be monitored. At this moment, it is unknown what impact this has on the modelling of SSOs.

- **Influence of SGs stability of sub-synchronous modes**
  In chapter 5, SG 9 was disconnected for the case of the WPP connected to the same bus. This is done in order to create an unstable sub-synchronous mode. However, this research does not investigate the exact influence of SGs. As more RES are integrated into the grid, more fossil fuel power SG can be disconnected. It is therefore important to understand what implications this has on the stability in combination with more integration of large PEIG. In weak grids, SSOs have already caused significant events. As the push towards more PEIG is continued, even stronger grids could be impacted by SSO events induced by PE.

- **Influence of multiple WPPs connected in close proximity**
  In this research, only one WPP is used simultaneously during all simulations. Interesting questions can be asked about what would happen in case of multiple WPPs in close proximity of each other. Depending on the tuning of both WPPs, they could increase the risk of SSO events. However, the exact impact and critical parameters will need further investigation. As more WPPs are integrated into the grid, this becomes an increasingly important question for the stability of the grid. Moreover, as was stated in chapter 2, different types of PEIG have similar control systems resulting in similar behaviour.

A

NextGen GridOps Knowledge Framework

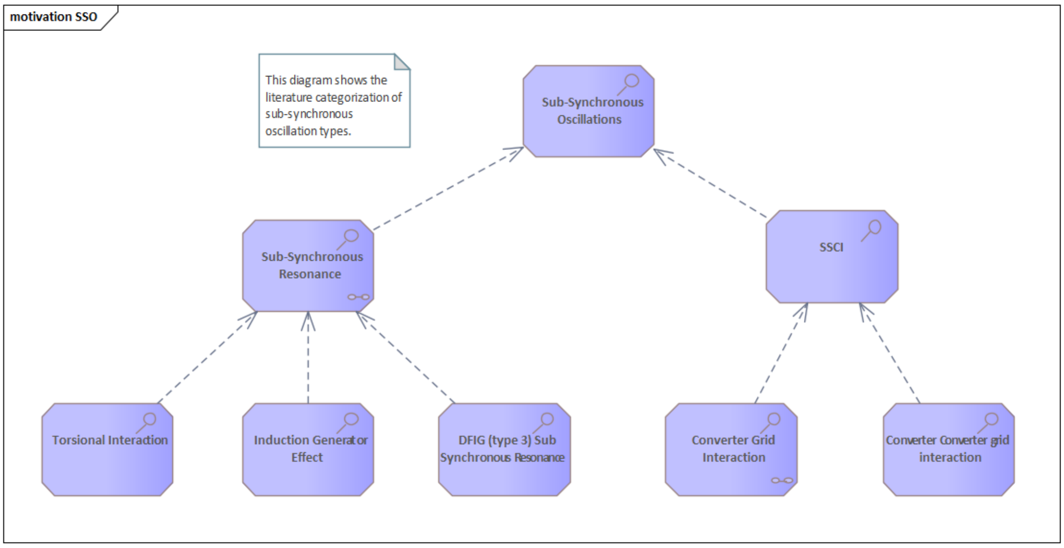

Figure A.1: Overview of sub-synchronous oscillation categorisation in the NextGen GridOps Framework.

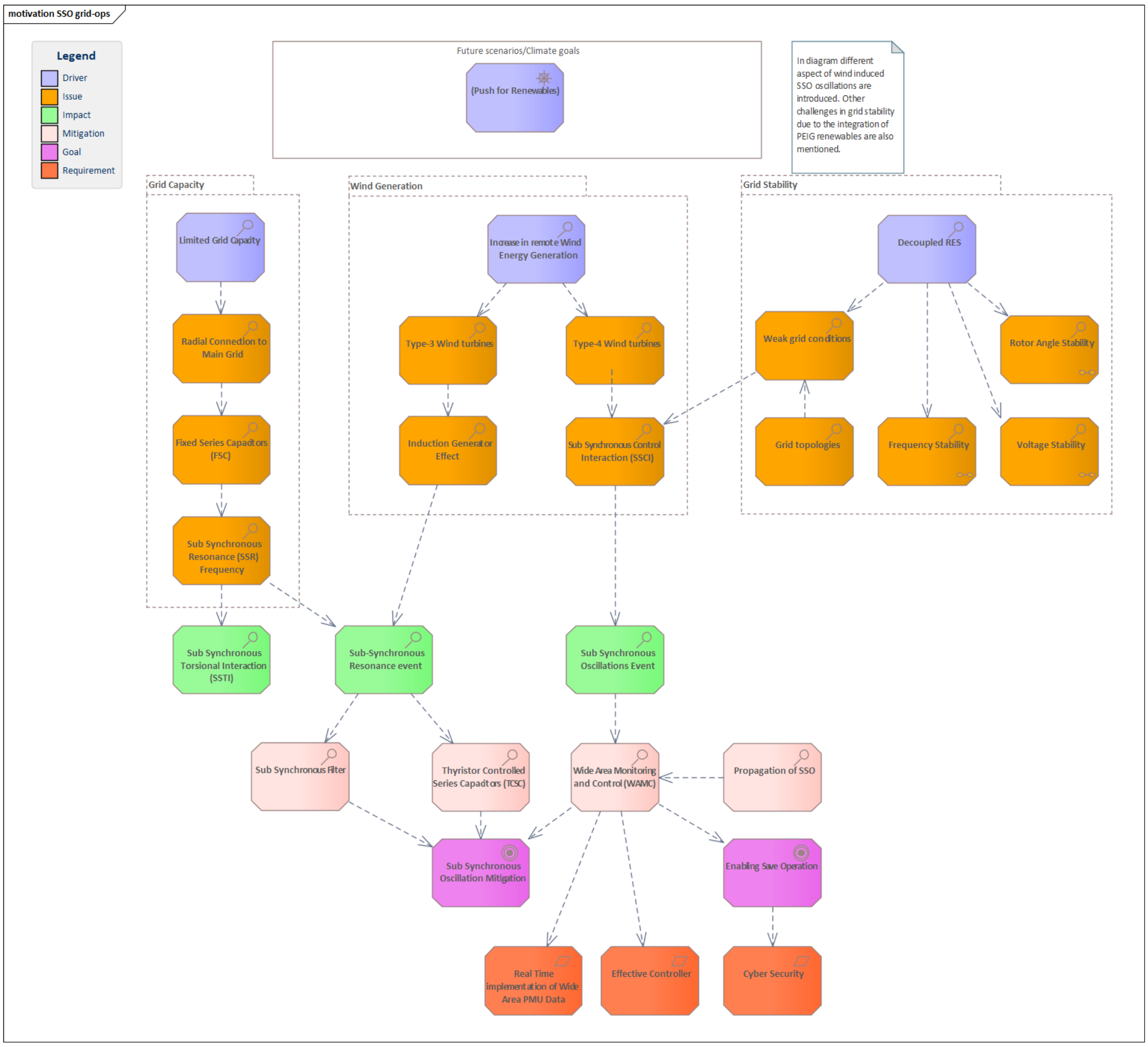

Figure A.2: Overview of sub-synchronous oscillation stability challenges in grid operations context modelled in the NextGen GridOps Framework.

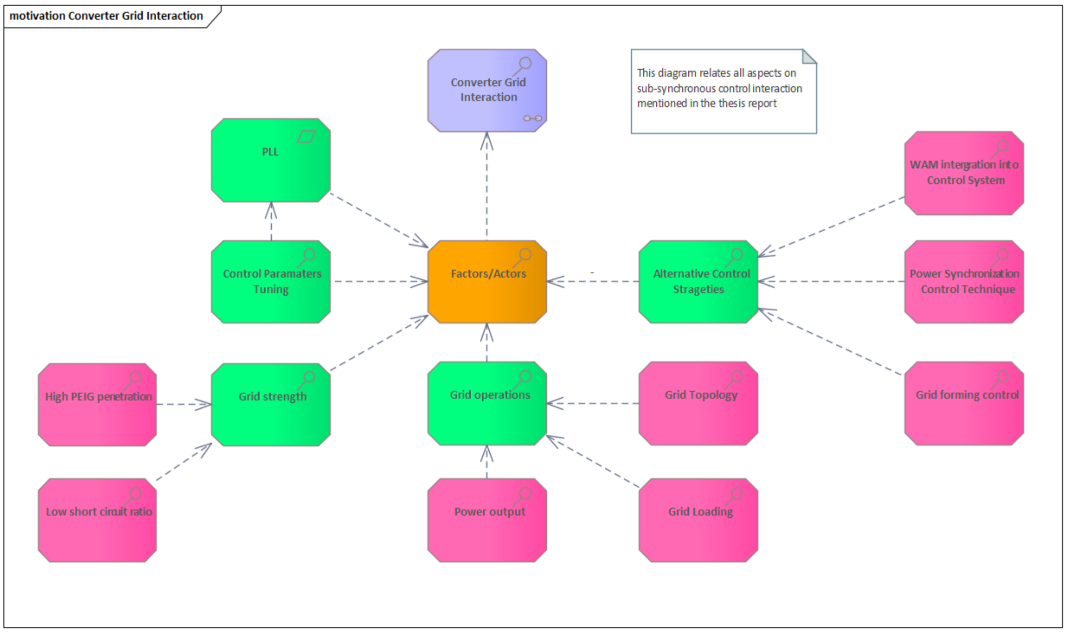

Figure A.3: Overview of facets related to sub-synchronous control interaction investigated in this thesis research modelled in the NextGen GridOps Framework.

B

Essential Grid Components

Type-3 Wind Turbines

Type-3 wind turbines use an induction machine to transform the mechanical power from the turbine shaft into electrical energy. The stator windings of the induction machine are directly coupled to the grid. The rotor windings are decoupled from the grid using AC-DC-AC converters. This topology is shown in figure B.1.

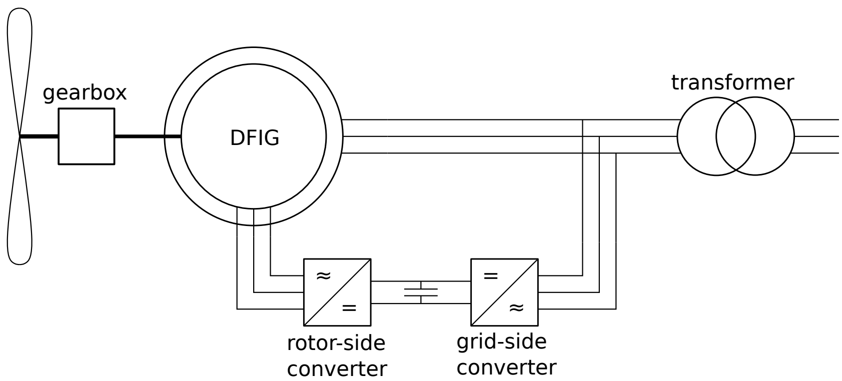

Figure B.1: Schematic of a type-3 WT using a doubly fed induction generator.

The power output of an induction machine is controlled by setting the slip of the machine. The slip is the relative rotational speed difference between the stator magnetic field and the rotor magnetic field. The stator magnetic field will rotate at a constant speed of the grid frequency. The rotor magnetic field rotates at the rotational speed of the rotor and frequency set by the RSC summed together. Because the frequency of the RSC is fully controllable, the slip s of the machine can be controlled. Since the slip controls the torque of the machine, this can be used to operate the WT at any speed. Controllability on the speed of the WT blades is essential to operate at the optimal aerodynamic point. One of the benefits of a DFIG is that the converters only need to be rated for a fraction of the total power output of the WT. Typically the converter is rated at around 30% of the rated power of the WT [65]. A downside to DFIG is the need for brush contacts to transfer the current to the rotor. These brushes will inevitably have wear and require maintenance.

Type-4 Wind Turbines

A type-4 WT uses a fully rated AC-DC-AC converter to control the speed of the WT. This FRC set-up is used to directly control the Permanent Magnet Synchronous Generator (PMSG) and blade speed. This allows it to always operate at the optimal aerodynamic operating point. A downside to a type-4 WT is the fully rated converter. From figure B.2, it can be seen how all power generated has to be converted.

This completely decouples the PMSG from the grid. This makes it easier to comply with grid codes on FRT requirements [65]. As RES are increasingly becoming significant in the grid, stricter grid codes are also required. Having this capability will make type-4 WTs more dominant in the future [66].

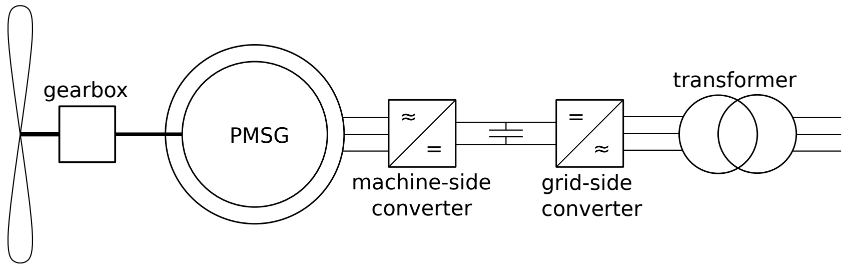

Figure B.2: Schematic of a type-4 WT using a permanent magnet synchronous generator.

Phasor Measurement Unit

Phasor Measurement Units are measuring devices in the power systems which are able to determine the phase voltage and current phase. This is done by matching the voltage and current measurement to accurate time measurement by Global Positioning System (GPS). Since GPS is available worldwide multiple PMU measurements in a system can be synchronised to the same timing system. This allows observing phase differences between different parts of the whole power grid. No other system allows for this type of application. Other measurement devices are usually only able to measure Root Mean Square (RMS) power flows or bus voltages and lack accurate time stamping. The rate of measurements of PMUs is also superior to other measuring options. Some PMU systems can take measurements at speeds up to 250 Hz. Data collected by multiple PMUs is collected by a Phasor Data Concentrator (PDC). From the PDC, all the data can be used by a WAMC and give operators helpful information from the system. Different latencies are present in the process of collecting PMU data. An overview is shown in figure B.3. First, a latency is present in taking a measurement referred to as the PMU latency. After this, the data is sent over a network to the PDC. Also, here a latency will be present. Lastly, it will take some time for the PDC to collect data of all different PMUs before it is available for application. The total latency until this point is referred to as the PDC reporting latency [67].

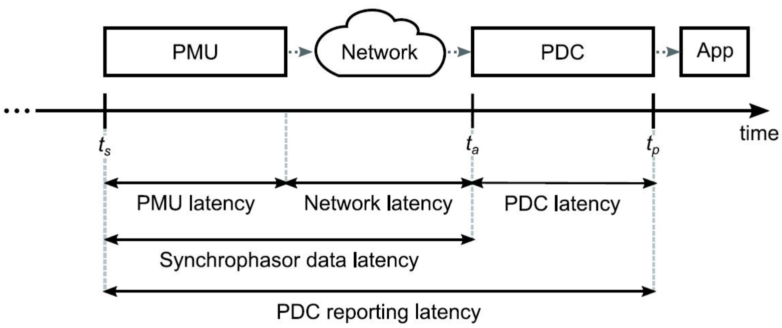

Figure B.3: Overview of different latencies in PMU data collection [67].

Voltage Source Converter

Voltage Source Converters are devices which can convert power from a DC link to an AC system or vice versa. To achieve this, the device uses PE components such as Insulated-Gate Bipolar Transistor (IGBT). VSC can be controlled as either to be grid following or grid forming. Also, VSCs can be self-commutating which means it has full control of the output voltage and current. Thus both the active and reactive power can be fully controlled. In this section, the topology and control system will be explained.

Topology

A simple representation of a two-level VSC is shown in figure B.4. In this topology, six switches can control the voltage on each phase of the AC system. By controlling the timing of each switch, the polarity of each output phase can be changed. Often Pulse Width Modulation (PWM) is used on the switch to virtually control the voltage more accurately. Still, filters are needed to create a proper sine wave and remove harmonics from the output signals.
A more sophisticated topology is a Multi Modular Converter (MMC). This type has arms (the connection between DC link and an AC phase) which can control the voltage in discrete voltage steps. This allows for the creation of waveforms which resembles a sine wave more closely. This leads to smaller and higher harmonics which are easier to filter. However, it creates a more complex control because each voltage step has a controllable switch. Another development is the addition of three more 60 ° shifted phases. A Y-Δ transformer shifts these phases. By increasing the number of phases, fewer harmonics will be present in the output voltages and currents of the VSC.

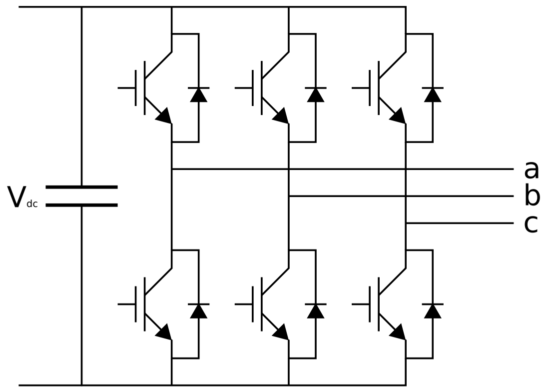

Figure B.4: Schematic of the topology of a two-level VSC.

Controller

In figure B.5 the control system of a VSC is represented. In this case, the active output power is controlled by the DC voltage and the reactive power is set by an arbitrary set point. This set point can be used to inject reactive power into the grid at the request of a grid operator. These components of the control system are referred to as the outer control loop or voltage loop. Both set points are filtered through a PI-controller and limiter to prevent rapid shifts in operating points. For these controllers the parameters $K_{p,dc}$ and $K_{i,dc}$ are introduced for the active power control and $K_{p,Q}$ and $K_{i,Q}$ for the reactive power control. These parameters are typically chosen such that the outer control loop has slower dynamics compared to the current control loop.
The inner control loop, or current control loop, controls the firing signals to each switch using the set points fed in by the outer control loop and the current state of the output signals. An essential component for the inner control loop is the PLL. The PLL tracks the voltage angle at the output terminal. This is used to transform the output current of the converter from an abc-frame to a dq-frame. In the abc-frame, the three phases each have a sinusoidal waveform separated by 120°. These signals are first transformed to an $\alpha\beta$-frame using a Clarke transform. In the $\alpha\beta$-frame, only two sinusoidal waveforms are shown, which are 90° separated. Both amplitudes of the signals represent the active and reactive components of the currents. These signals are then transformed to the dq-frame using the Park transformation. The dq-frame is a rotating frame at the system frequency on which the $\alpha\beta$-frame is projected. Because these signals are also periodic at the system frequency, the projection in the dq-frame leaves two DC signals representing the amount of active and reactive currents injected by the VSC. In this work, i_d refers to the active current, and i_q refers to the reactive current. The DC signal makes them very easy to use and manipulate in the control system. The PLL is essential for both the Clarke- and Park-Transform. The control system cannot operate correctly if the PLL is not properly locked to the terminal

voltage. The PLL is further explained below.
In B.5, it can be seen that the measured output currents are first transformed into a dq-frame. The measured i_d and i_q signals are first compared to the reference signals from the outer control loop. These difference signals are then filtered by a PI-controller to be converted to an output voltage v_d and v_q. For the filters the control parameters $K_{p,dS}$ and $K_{i,dS}$ are introduced for i_d and $K_{p,qS}$ and $K_{i,qS}$ for i_q. The resulting signals are then compared to the actual values and compensated for the line inductance. Then they are transformed using the inverse Park- and Clark-Transform to be fed into the firing signals of the switches.

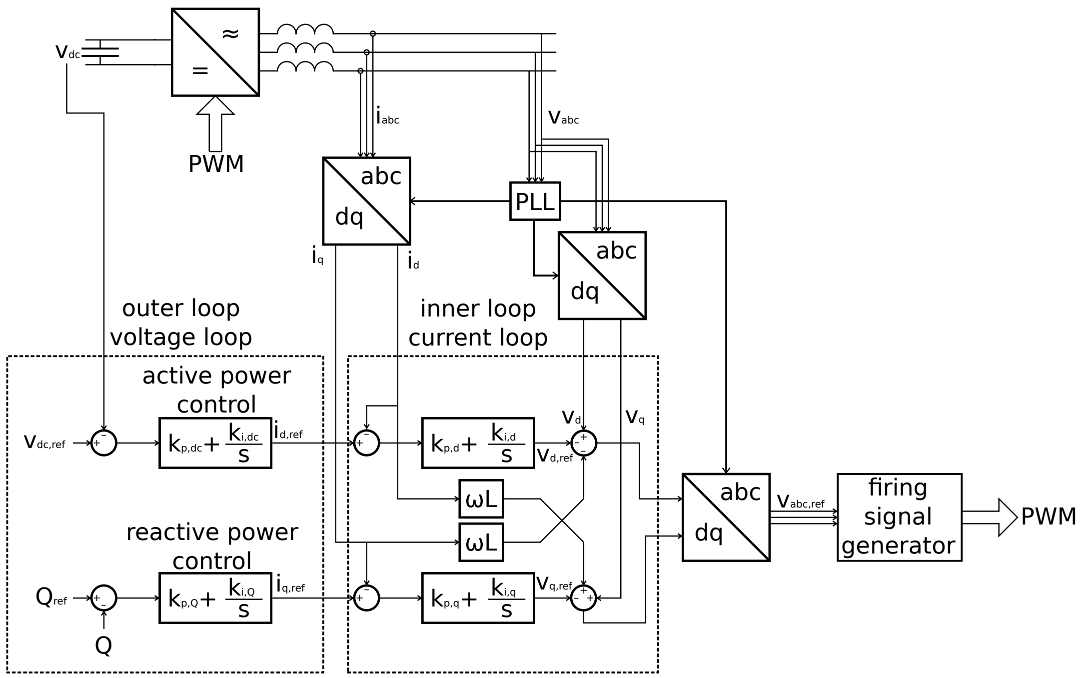

Figure B.5: Schematic of a general GSC control system used in back-to-back converters.

Phase Locked Loop

The PLL is an essential element in the control system of a grid following inverter. The PLL will keep track of the voltage angle θ at the connection point. In this research a Synchronous Reference Frame (SRF) PLL is used. This is the most widely used PLL in inverter applications [68]. This type of PLL uses the output voltage angle to obtain d- and q-components of the measured three-phase voltages. The PLL tries to keep the q-axis equal to zero. This is done by feeding the result through a PI-controller, which can alter the output voltage angle θ. A schematic of the control of the PLL is shown in figure B.6.
In PowerFactory, the PLL element has a cosine and sine output signal of the voltage angle. This prevents edge cases where the voltage angle can jump by 2π.

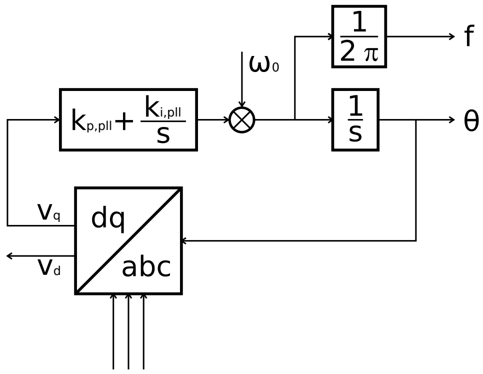

Figure B.6: Schematic of the control system of a SRF PLL [68].

Synchronous Generator

Synchronous generators are the most often used type of generators for large scale power plants. By their magnetic coupling of the rotating mass or inertia to the electrical system, they play an essential role in the frequency stability of the grid. An unbalance in power generation and demand will lead to a speed change in the rotating masses in the machines. The more inertia in the system, the lower this acceleration will be. This gives operators or automatic speed governors more time to react by changing the power output of a generator.

Magnetic coupling and rotor angle

The magnetic coupling of the synchronous generator couples the electrical and mechanical parts of the system. To explain this coupling, a schematic of a synchronous generator is shown in figure B.7.

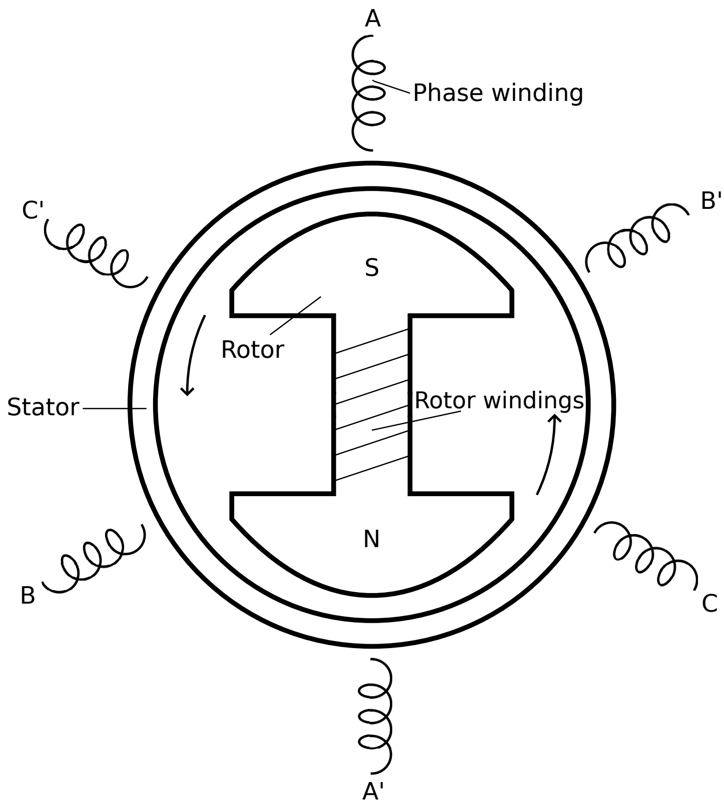

Figure B.7: Schematic of simple synchronous machine.

The synchronous machine is directly connected to the three-phase grid. Each phase has two coils connected in parallel. When a current flows through a coil of one phase, a magnetic field between the two coils will be induced. In a three phase system, these currents will flow consecutively through each phase. This results in a rotating magnetic field on the inside of the stator. The stator is the fixed part of the machine. Inside this void, the rotor is placed. The rotor will be magnetised by either a permanent magnet or by an electromagnet using a rotor winding. It can be derived that the energy in this system is minimised when the rotor magnetic field and rotating magnetic field line up. Angle δ is defined as the angle between the rotor and the rotating magnetic field. A torque force can be derived as a function of this angle δ [69].

$$T = T_{max} \sin \delta \tag{B.1}$$

In practice, this means the rotor will lead the rotating field when the machine generates electrical power. The rotor lags to the magnetic field if the machine is used as a motor and extracts electrical power. It can be imagined as if the rotor pulls or is pulled by the magnetic field.
Around the rotor angle δ equation B.1 can be linearised. This yields a spring equation. Around the actual rotor angle, the rotor will behave as a spring. If it is excited, it will start oscillating around the equilibrium. Control systems of the generator, if badly tuned, amplify this oscillation. In a system with multiple generators, different generators or groups of generators can oscillate against each other. This can lead to low frequency power oscillations in the power system.
These oscillations can lead to rotor angle instability. Below a rotor angle δ of 90°, the rotor angle is stable. Until this limit, an increase in δ leads to bigger torque forcing the magnetic field and rotor angle to line up. After the limit of 90°, the torque will start decreasing. Therefore, it will no longer be a stable system. Rotor angle stability is an essential aspect of electrical power systems.

C

PowerFactory Models

Weak Grid Model

In figure C.1 the grid PowerFactory model is shown. The impedances match the values given in table 3.1. In PowerFactory, the impedances are specified per unit length. Therefore, all lines are set to have a length of 100 km. Their resistance and reactance per unit length are shown in table C.1. The reactance of the transformers can be set as per unit values in PowerFactory. These values correspond with the values in 3.1.
Other components in the model is the 175 6 MW Fully Rated Wind Turbine, which is further elaborated on in a separate section. Also, an external grid component is connected to absorb all active and reactive power generated by the WPP. A SG is also placed in the model. However, this SG is not used in the simulations.

Line	Length [km]	Voltage [kV]	Resistance [mΩ/km]	Reactance [mΩ/km]
1	100	110	1.613	9.68
2	100	220	16.13	209.733
3	100	220	0	25.813

Table C.1: Line parameters in PowerFactory model for the weak grid.

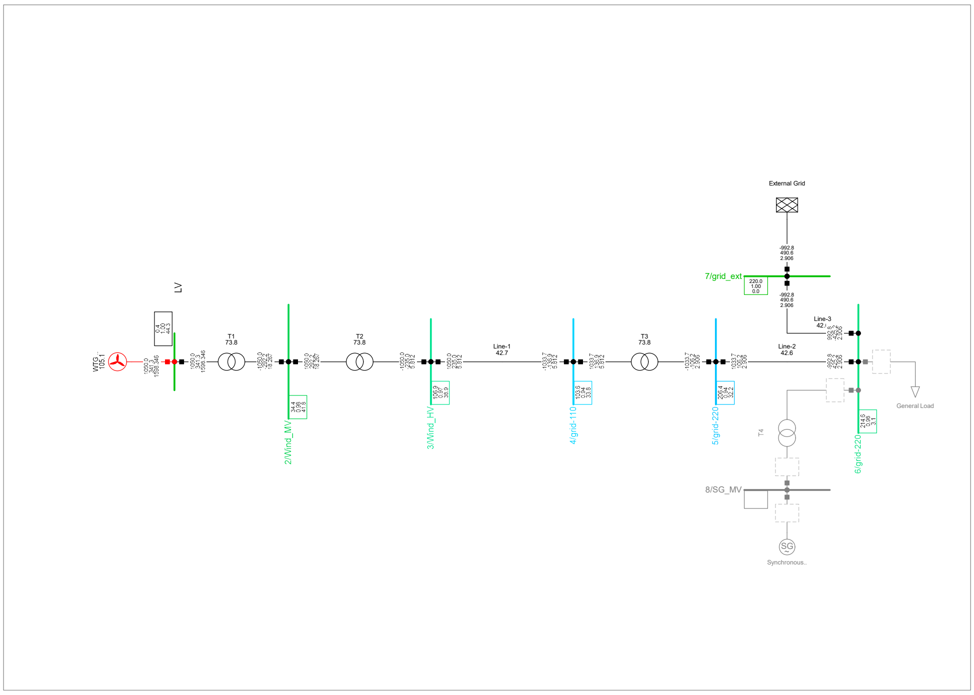

Figure C.1: Weak grid model in Powerfactory

IEEE-39 Bus System Model

The IEEE-39 Bus system is a standard system used regularly in research. It was first used in 1970 [70]. It is a well known reference system among researchers and is often used for research and publications. In this section, the system and the model in PowerFactory are described. It is based on the transmission network of New England, USA. It operates at 60 Hz and consists of 39 buses, 10 generators, 19 loads, 34 lines and 12 transformers. The exact system parameters can be found in [60].

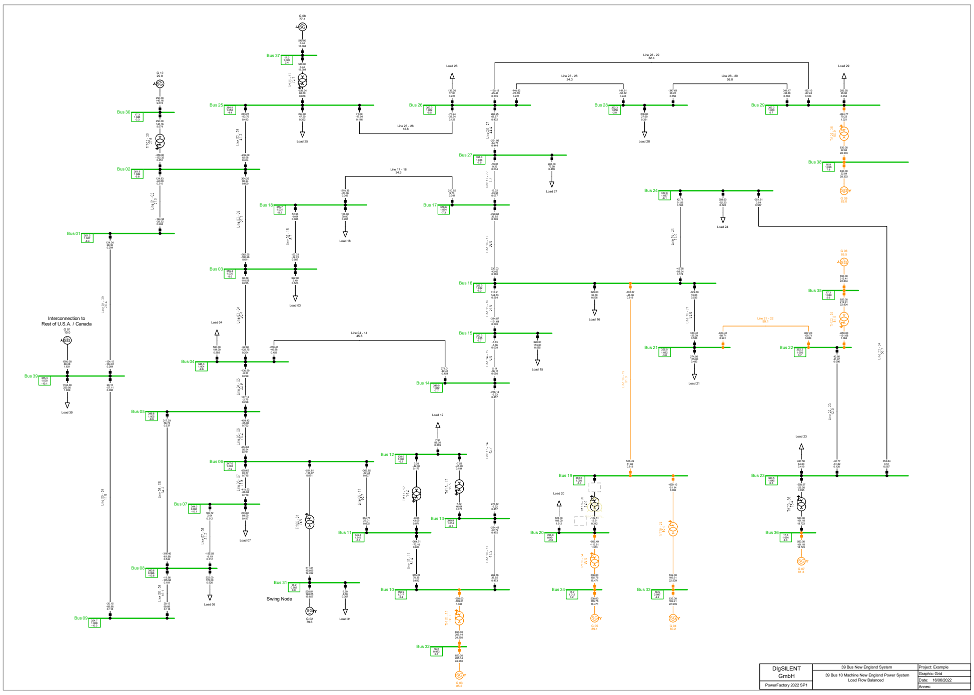

Figure C.2: IEEE-39 Bus system load flow results in nominal conditions.

Fully Rated Converter Model

The DIgSILENT PowerFactory FullyRatedConverter WTG 0.4kV 6MW is a template model available in the PowerFactory Software. [54]. It describes the grid side converter of a wind turbine and does not include and machine side converter. This is sufficient in this research since the rotor and grid speed are decoupled by the back-to-back converters. The composite model frame is depicted in figure C.3. It consists of three sub-models, four measurement blocks and the static generator element, which are further elaborated on below.

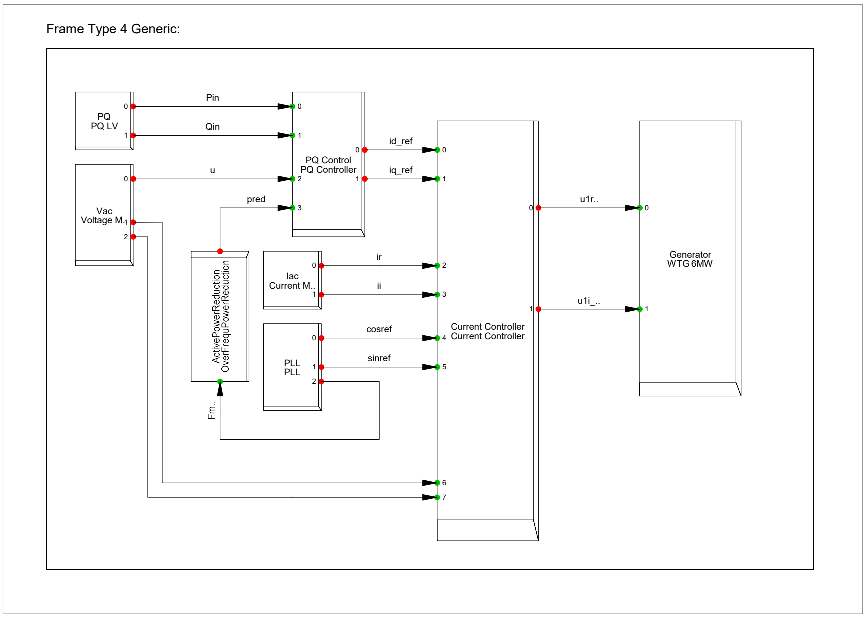

Figure C.3: Compostie Frame of the DIgSILENT FullyRatedConverter WTG 6.0MW 50Hz template.

- **OverFrequPowerReduction.ElmDsl**
  This element is triggered in the event of over frequency in the grid. A certain threshold can be set to trigger power reduction. This trigger is expected not to be activated during this research since frequency variations are not in the scope.

- **PQ Controller.ElmDsl**
  This element controls the active and reactive power set points. The actual power output of the wind farm is compared to the set point and fed through a PI controller. This signal is then sent to the current controller model.

- **Current Controller.ElmDsL**
  The current controller converts the power set points to current signals fed to the generator element. The measured current signals are transformed to a d-q frame using the voltage angle data measured by the PLL. The d-q current signals are compared to the power set points and fed to a PI controller. The signals are then converted back to the grid reference frame. These signals are fed to the generator element. The PI controller contains the parameters $K_{d,p}$,T_d,$K_{q,p}$ and T_q. The time constants are converted to integration gain parameters $K_{d,i}$ and $K_{q,i}$ to make it more compatible with existing literature. This conversion is explained down below.

Measurement units are:

- **PQ LV.staPqmea**
  This element measures the active and reactive power output of the WPP. These signals are fed to the PQ Controller.

- **Voltage Measurement.StaVmea**
  The voltage is measured at the bus where the WPP is connected. These measurements are in a real part and an imaginary part in the reference frame of the grid.

- **Current Measurement.StaImea**
  The current measurement is the current which is flowing from the WPP to the grid. Two signals are fed to the current controller. This is a real and imaginary part of the current in the reference frame of the grid.

- **PLL.ElmPhi_pll**
  The PLL measures the relative voltage angle of the bus the WPP is connected to. It is a single reference frame PLL. This is the most commonly used type of PLL [68, 71]. The PLL is not just a simple measurement device as the other elements. It has an internal PI controller, which can have dynamic behaviour interaction with the system. The exact model explained in [59]. This element has three output signals. The first two are a cosine and a sine value of the voltage angle at the bus. Together they define the voltage angle without discontinuity challenges of a single angle signal in radians. Additionally, the frequency signal is measured.

The generator element receives a real and imaginary signal from the current controller in the reference frame of the grid. This means this signal should already have taken into account the voltage angle at the connected bus.

Conversion of T_d and T_q to $K_{d,i}$ and $K_{q,i}$

In the PowerFactory model, the following equations are defined for the PI control for both the d-axis and q-axis. In these equations, the d-axis is taken as an example, but the q-axis operates in the same way. In the following equations, di_d is the difference between the d-axis reference signal and the actual d-axis current. x_d is a state variable.

$$\frac{dx_d(t)}{dt} = \frac{K_{d,p}}{T_d} di_d(t) \tag{C.1}$$

$$i_d(t) = K_{d,p} di_d(t) + x_d(t) \tag{C.2}$$

By substituting C.1 into C.2 results in:

$$i_d(t) = K_{d,p} di_d(t) + \frac{K_{d,p}}{T_d} \int di_d(t) \tag{C.3}$$

In this form, it can be seen that $K_{d,i}$ and $K_{q,i}$ are defined as follows.

$$K_{d,i} = \frac{K_{d,p}}{T_d} \tag{C.4}$$

$$K_{q,i} = \frac{K_{q,p}}{T_q} \tag{C.5}$$

Bibliography

1. Shivakumar, A. *et al.* Valuing blackouts and lost leisure: Estimating electricity interruption costs for households across the European Union. *Energy Research & Social Science* **34,** 39–48. ISSN: 2214-6296 (Dec. 2017).
2. Frequency response of PV inverters towards high renewable penetrated distribution networks. *CSEE Journal of Power and Energy Systems.* ISSN: 20960042 (2022).
3. Yuan, M., Thellufsen, J. Z., Lund, H. & Liang, Y. The electrification of transportation in energy transition. *Energy* **236,** 121564. ISSN: 0360-5442 (Dec. 2021).
4. White, P. R., Rhodes, J. D., Wilson, E. J. & Webber, M. E. Quantifying the impact of residential space heating electrification on the Texas electric grid. *Applied Energy* **298,** 117113. ISSN: 0306-2619 (Sept. 2021).
5. Lechtenböhmer, S., Nilsson, L. J., Åhman, M. & Schneider, C. Decarbonising the energy intensive basic materials industry through electrification – Implications for future EU electricity demand. *Energy* **115,** 1623–1631. ISSN: 0360-5442 (Nov. 2016).
6. Mehigan, L., Deane, J. P., Gallachóir, B. P. & Bertsch, V. A review of the role of distributed generation (DG) in future electricity systems. *Energy* **163,** 822–836. ISSN: 0360-5442 (Nov. 2018).
7. Sewdien, V., Wang, X., Torres, J. R. & Van Der Meijden, M. *Critical review of mitigation solutions for SSO in modern transmission grids* July 2020.
8. Adams, J., Carter, C. & Huang, S. H. ERCOT experience with Sub-synchronous Control Interaction and proposed remediation. *Proceedings of the IEEE Power Engineering Society Transmission and Distribution Conference.* ISSN: 21608555 (2012).
9. Yunhong, L., Hui, L., Xiaowei, C., Jing, H. & Ul I, Y. Impact of PMSG on SSR of DFIGs connected to series-compensated lines based on the impedance characteristics. *The Journal of Engineering* (2017).
10. Narendra, K. *et al.* New microprocessor based relay to monitor and protect power systems against sub-harmonics. *2011 IEEE Electrical Power and Energy Conference, EPEC 2011,* 438–443 (2011).
11. Wang, L. *et al.* Investigation of SSR in Practical DFIG-Based Wind Farms Connected to a Series-Compensated Power System. *IEEE Transactions on Power Systems* **30,** 2772–2779. ISSN: 08858950 (Sept. 2015).
12. Xie, X. *et al.* Characteristic Analysis of Subsynchronous Resonance in Practical Wind Farms Connected to Series-Compensated Transmissions. *IEEE Transactions on Energy Conversion* **32,** 1117–1126. ISSN: 08858969 (Sept. 2017).
13. Xu, Y. & Cao, Y. Sub-synchronous oscillation in PMSGs based wind farms caused by amplification effect of GSC controller and PLL to harmonics. *IET Renewable Power Generation* **12,** 844–850. ISSN: 17521424 (May 2018).
14. Li, Y., Fan, L. & Miao, Z. Replicating Real-World Wind Farm SSR Events. *IEEE Transactions on Power Delivery* **35,** 339–348. ISSN: 19374208 (Feb. 2020).
15. Xu, Y., Zhao, S., Cao, Y. & Sun, K. Understanding Subsynchronous Oscillations in DFIG-Based Wind Farms Without Series Compensation. *IEEE Access* **7,** 107201–107210. ISSN: 21693536 (2019).
16. National Grid ESO. *Technical Report on the events of 9 August 2019* tech. rep. (2019).
17. *European Green Deal* tech. rep. (European Commission, Brussels, Dec. 2019).
18. Agrawal, V. K. & Agarwal, P. K. Application of PMU Based Information in Improving the Performance of Indian Electricity Grid (2012).

19. Novosel, D., Madani, V., Bhargava, B., Vu, K. & Cole, J. Dawn of the grid synchronization. *IEEE Power and Energy Magazine* **6,** 49–60. ISSN: 15407977 (2008).
20. Appasani, B., Jha, A. V., Mishra, S. K. & Ghazali, A. N. Communication infrastructure for situational awareness enhancement in WAMS with optimal PMU placement. *Protection and Control of Modern Power Systems* **6,** 1–12. ISSN: 23670983 (Dec. 2021).
21. Mao, A., Yu, J. & Guo, Z. PMU placement and data processing in WAMS that complements SCADA. *2005 IEEE Power Engineering Society General Meeting* **1,** 780–783 (2005).
22. Vanfretti, L. & Chow, J. H. Analysis of power system oscillations for developing synchrophasor data applications. *2010 IREP Symposium - Bulk Power System Dynamics and Control - VIII, IREP2010* (2010).
23. Ushakov, V. Y. From the History of Electrical Power Engineering. *Green Energy and Technology* **0,** 13–21. ISSN: 18653537 (2018).
24. Kundur, P. *Power System Stability and Control* (McGraw Hill, 1994).
25. Mantzaris, J. C., Metsiou, A. & Vournas, C. D. Analysis of interarea oscillations including governor effects and stabilizer design in South-Eastern Europe. *IEEE Transactions on Power Systems* **28,** 4948–4956. ISSN: 08858950 (2013).
26. Lehner, J., Kaufhold, M., Treuer, M. & Weissbach, T. Monitoring of inter-area oscillations within the European interconnected network based on a wide area measuring system. *2010 IEEE PES Transmission and Distribution Conference and Exposition: Smart Solutions for a Changing World* (2010).
27. Unfccc. ADOPTION OF THE PARIS AGREEMENT - Paris Agreement text English.
28. Alatrash, H., Mensah, A., Mark, E., Haddad, G. & Enslin, J. Generator emulation controls for photovoltaic inverters. *IEEE Transactions on Smart Grid* **3,** 996–1011 (2012).
29. Gonzalez-Longatt, F. M. *Activation schemes of synthetic inertia controller on full converter wind turbine (type 4)* in *2015 IEEE Power & Energy Society General Meeting* (2015), 1–5.
30. Ramtharan, G., Jenkins, N., Anaya-Lara, O. & Bossanyi, E. Influence of rotor structural dynamics representations on the electrical transient performance of FSIG and DFIG wind turbines. *Wind Energy: An International Journal for Progress and Applications in Wind Power Conversion Technology* **10,** 293–301 (2007).
31. Morren, J., De Haan, S. W., Kling, W. L. & Ferreira, J. Wind turbines emulating inertia and supporting primary frequency control. *IEEE Transactions on power systems* **21,** 433–434 (2006).
32. Yingcheng, X. & Nengling, T. Review of contribution to frequency control through variable speed wind turbine. *Renewable energy* **36,** 1671–1677 (2011).
33. Nguyen, D. & Negnevitsky, M. A review of fault ride through strategies for different wind turbine systems | IEEE Conference Publication | IEEE Xplore. *IEEE* (Dec. 2010).
34. Frigo, G., Pegoraro, P. A. & Toscani, S. Low-latency, three-phase pmu algorithms: Review and performance comparison. *Applied Sciences (Switzerland)* **11,** 1–34. ISSN: 20763417 (Mar. 2021).
35. Li, C., Sun, Y. & Chen, X. *Analysis of the blackout in Europe on November 4, 2006 | IEEE Conference Publication | IEEE Xplore* 2007.
36. *Interim Report – Continental Europe Synchronous Area Separation on 8 January 2021* tech. rep. (ENTSO-E, Feb. 2021).
37. Wilson, D. H., Al-Ashwal, N., Halldorsson, H. & Boroczky, S. Discrete control for transient stability and oscillations: Applications and case studies. *IEEE Power and Energy Society General Meeting.* ISSN: 19449925 (2013).
38. Fairley, P. Utilities roll out real-time grid controls: Synchrophasor tech enables rapid response to broken power lines and other emergencies. *IEEE Spectrum* **55,** 9–10. ISSN: 19399340 (Oct. 2018).
39. *Lesson Learned - Sub-Synchronous Interaction between Series-Compensated Transmission Lines and Generation* tech. rep. (NERC, 2011).

40. Liu, H. *et al.* Subsynchronous Interaction between Direct-Drive PMSG Based Wind Farms and Weak AC Networks. *IEEE Transactions on Power Systems* **32,** 4708–4720. ISSN: 08858950 (Nov. 2017).

41. Hodges, D. A., Bowler, C. E. & Jackson, R. L. Results of subsynchronous resonance test at mohave. *IEEE Transactions on Power Apparatus and Systems* **94,** 1878–1889. ISSN: 00189510 (1975).

42. *Subsynchronous Oscillation Risks of Wind Power Plants Connecting to Finnish Series Compensated Network* tech. rep. (Fingrid, Oct. 2020).

43. *Specific study requirements for power park modules connected in vicinity of Fingrid's series compensated network* tech. rep. (Fingrid, Jan. 2021).

44. Goldberg, S. Subsynchronous resonance in series compensated transmission lines. *IEEE Transactions on Power Apparatus and Systems* **PAS-92,** 1649–1658. ISSN: 00189510 (1973).

45. Zhao, M., Yuan, X., Hu, J. & Yan, Y. Voltage Dynamics of Current Control Time-Scale in a VSC-Connected Weak Grid. *IEEE Transactions on Power Systems* **31,** 2925–2937. ISSN: 08858950 (July 2016).

46. Papavasiliou, A., Papathanassiou, S. A., Manias, S. N. & Demetriadis, G. Current control of a voltage source inverter connected to the grid via LCL filter. *PESC Record - IEEE Annual Power Electronics Specialists Conference,* 2379–2384. ISSN: 02759306 (2007).

47. Shah, R., Sánchez, J. C., Preece, R. & Barnes, M. Stability and control of mixed AC–DC systems with VSC-HVDC: a review. *IET Generation, Transmission & Distribution* **12,** 2207–2219. ISSN: 1751-8695 (May 2018).

48. Analysis of the Cyber Attack on the Ukrainian Power Grid Defense Use Case (2016).

49. Fan, L. Modeling Type-4 Wind in Weak Grids. *IEEE Transactions on Sustainable Energy* **10,** 853–864. ISSN: 19493029 (Apr. 2019).

50. Bayo-Salas, A., Beerten, J., Rimez, J. & Van Hertem, D. Analysis of control interactions in multi-infeed VSC HVDC connections. *IET Generation, Transmission & Distribution* **10,** 1336–1344. ISSN: 1751-8695 (Apr. 2016).

51. Shah, R., Mithulananthan, N., Bansal, R. C. & Ramachandaramurthy, V. K. A review of key power system stability challenges for large-scale PV integration. *Renewable and Sustainable Energy Reviews* **41,** 1423–1436. ISSN: 1364-0321 (Jan. 2015).

52. Sainz, L., Monjo, L., Cheah-Mane, M. & Liang, J. Assessment of subsynchronous oscillations in AC grid-connected VSC systems with type-4 wind turbines. *IET Renewable Power Generation* **13,** 3088–3096. ISSN: 1752-1424 (Dec. 2019).

53. Badrzadeh, B. *Electromagnetic transient simulation models for large-scale system impact studies in power systems having a high penetration of inverter-connected generation* ISBN: 9782858735860 (2022).

54. PowerFactory DIgSILENT. *Technical Reference DIgSILENT Fully Rated Converter Wind Turbine Templates* tech. rep. (2022).

55. Du, W., Wang, X. & Wang, H. Sub-synchronous interactions caused by the PLL in the grid-connected PMSG for the wind power generation. *International Journal of Electrical Power and Energy Systems* **98,** 331–341. ISSN: 01420615 (June 2018).

56. Adib, A., Mirafzal, B., Wang, X. & Blaabjerg, R. On stability of voltage source inverters in weak grids. *IEEE Access* **6,** 4427–4439. ISSN: 21693536 (Dec. 2017).

57. Yan, G., Wan, Q., Jia, Q. & Liu, J. Analysis of SSO Characteristics of D-PMSGs Based Wind Farm under Weak AC System. *2nd IEEE Conference on Energy Internet and Energy System Integration, EI2 2018 - Proceedings* (Dec. 2018).

58. Li, Y., Fan, L. & Miao, Z. Wind in Weak Grids: Low-Frequency Oscillations, Subsynchronous Oscillations, and Torsional Interactions. *IEEE Transactions on Power Systems* **35,** 109–118. ISSN: 15580679 (Jan. 2020).

59. PowerFactory DIgSILENT. *Technical Reference Phase Measurement Device ElmPhi pll* tech. rep. (2022).
60. Powerfactory, D. *39 Bus New England System* tech. rep. (DIgSILENT PowerFactory GmbH, Gomaringen, Germany, 2020).
61. Ranjbar, S., Aghamohammadi, M. R. & Haghjoo, F. Damping inter-area oscillation in power system by using global control signals based on PSS devices. *2017 25th Iranian Conference on Electrical Engineering, ICEE 2017,* 1330–1335 (July 2017).
62. Gonzalez-Longatt, F. & Torres, J. L. R. *Modelling and Simulation of Power Electronic Converter Dominated Power Systems in PowerFactory* (Springer Nature, 2021).
63. Shair, J. *et al.* Overview of emerging subsynchronous oscillations in practical wind power systems. *Renewable and Sustainable Energy Reviews* **99,** 159–168. ISSN: 1364-0321 (Jan. 2019).
64. Huang, Y. & Wang, D. Effect of Control-Loops Interactions on Power Stability Limits of VSC Integrated to AC System. *IEEE Transactions on Power Delivery* **33,** 301–310. ISSN: 08858977 (Feb. 2018).
65. Molina, M. G. & Mercado, P. E. in *Wind turbines* (In Tech, 2011).
66. Blaabjerg, F. & Ma, K. Future on power electronics for wind turbine systems. *IEEE Journal of Emerging and Selected Topics in Power Electronics* **1,** 139–152. ISSN: 21686785 (Sept. 2013).
67. Derviskadic, A., Romano, P., Pignati, M. & Paolone, M. Architecture and Experimental Validation of a Low-Latency Phasor Data Concentrator. *IEEE Transactions on Smart Grid* **9,** 2885–2893. ISSN: 19493053 (July 2018).
68. Guo, X.-Q., Wu, W.-Y. & Gu, H.-R. Phase locked loop and synchronization methods for grid-interfaced converters: a review. ISSN: 0033-2097.
69. Sen, P. C. *Principles of electric machines and power electronics* (John Wiley & Sons, 2007).
70. Bills, G. W. On-line stability analysis study, RP 90-1 (Oct. 1970).
71. Golestan, S., Monfared, M. & Freijedo, F. D. Design-oriented study of advanced synchronous reference frame phase-locked loops. *IEEE Transactions on Power Electronics* **28,** 765–778. ISSN: 08858993 (2013).